

A Survey of CN and CH Variations in Galactic Globular Clusters from SDSS Spectroscopy

Jason P. Smolinski

Department of Physics & Astronomy and JINA: Joint Institute for Nuclear Astrophysics,
Michigan State University, East Lansing, MI 48824, USA

`smolin19@msu.edu`

Sarah L. Martell

Astronomisches Rechen-Institut, Zentrum für Astronomie der Universität Heidelberg,
69120 Heidelberg, Germany

`martell@ari.uni-heidelberg.de`

Timothy C. Beers, Young Sun Lee

Department of Physics & Astronomy and JINA: Joint Institute for Nuclear Astrophysics,
Michigan State University, East Lansing, MI 48824, USA

`beers@pa.msu.edu, lee@pa.msu.edu`

Received _____; accepted _____

ABSTRACT

We present a homogeneous survey of the CN and CH bandstrengths in eight Galactic globular clusters observed during the course of the Sloan Extension for Galactic Understanding and Exploration (SEGUE) sub-survey of the SDSS. We confirm the existence of a bimodal CN distribution among RGB stars in all of the clusters with metallicity greater than $[\text{Fe}/\text{H}] = -1.7$; the lowest metallicity cluster with an observed CN bimodality is M53, with $[\text{Fe}/\text{H}] \simeq -2.1$. There is also some evidence for individual CN groups on the subgiant branches of M92, M2, and M13, and on the red giant branches of M92 and NGC 5053. Finally, we quantify the correlation between overall cluster metallicity and the slope of the CN bandstrength-luminosity plot as a means of further demonstrating the level of CN-enrichment in cluster giants. Our results agree well with previous studies reported in the literature.

Subject headings: Globular clusters: individual (M2, M3, M13, M15, M53, M71, M92, NGC 5053) - Stars: abundances - Stars: evolution

1. Introduction

Standard models for the formation of Galactic globular clusters (GCs) have long held that they should display little star-to-star variations in their observed atmospheric elemental abundances. However, observations over the past forty years (beginning with Osborn 1971) have repeatedly shown this expectation is not fully met, with variations in carbon and nitrogen abundance being commonly studied through the strengths of the 3883 Å CN and 4320 Å CH absorption bands. For clusters of moderate to high metallicity ($[\text{Fe}/\text{H}] > -2.0$), significant scatter in light-element abundances has been observed on the red giant branch (RGB; e.g. Norris & Freeman 1979; Suntzeff 1981), and in some cases even down to the main sequence (MS; e.g. Cannon et al. 1998; Harbeck et al. 2003a; Briley et al. 2004).

The observed variations in carbon and nitrogen abundance are part of a larger light-element pattern that involves enrichment in N, Na, and Mg along with depletion in C, O, and Al, and is often studied in correlated or anticorrelated abundance pairs (C-N, O-N, Mg-Al, Na-O, etc.). Gratton et al. (2004) reviews a number of these studies, and Carretta et al. (2009b) dramatically increased the number of cluster stars surveyed for these variations. There are two independent modes of variation in globular cluster light-element abundances: a steady decline in $[\text{C}/\text{Fe}]$ and increase in $[\text{N}/\text{Fe}]$ as stars evolve along the RGB, and star-to-star variations in the light-element abundances at a fixed luminosity, at all evolutionary phases.

Several hypotheses have been proposed to explain these observed anomalies. The progressive abundance changes on the RGB are believed to be the result of deep mixing within individual stars (Sweigart & Mengel 1979; Charbonnel 1994; Denissenkov & Vandenberg 2003), beginning at the “bump” in the RGB luminosity function (Fusi Pecci et al. 1990; Shetrone 2003). The hydrogen-burning shell proceeds outward as a star evolves along the RGB, eventually (for all stars with $M < 2.5M_{\odot}$; Gilroy 1989) encountering the

molecular-weight discontinuity left behind by the inward reach of the convective envelope during first dredge-up (Thomas 1967; Iben 1968). When this occurs, the shell’s progress is delayed as its fusion rate adjusts to the new chemical abundances, causing a loop in the star’s evolution along the RGB. In a population of coeval stars, this produces an enhancement in the differential luminosity function. Once the shell begins to proceed outward again, the molecular-weight gradient it experiences is lower, and the process of deep mixing (Denissenkov & Vandenberg 2003) begins to operate, transporting material between the hydrogen-burning shell and the surface and continuously adjusting surface carbon and nitrogen abundances.

Early studies of star-to-star light-element abundance variations (e.g. Suntzeff 1981; Langer 1985) suggested that deep mixing might be responsible for the C-N variations at fixed luminosity as well as the progressive abundance changes along the RGB. However, variations in sodium, magnesium and aluminum are difficult to explain as a result of mixing within RGB stars since they require higher temperatures than are reached in the hydrogen-burning shell. Internal mixing is also not a good explanation for light-element abundance variations in main-sequence stars, since they do not have the ability to conduct either high-temperature fusion or mass transport between their cores and surfaces.

The presence of these abundance variations at all evolutionary phases implies some form of unexpected enrichment within individual clusters prior to, or shortly after, their formation. Some researchers have suggested that the primordial gas cloud from which a given cluster formed may have initially been chemically inhomogeneous (e.g. Cohen 1978; Peterson 1980). A variation on this hypothesis appeals to cluster “self-enrichment.” Rather than assuming all stars in a given cluster are co-*eval*, it is assumed that an additional population(s) of stars formed, with compositions affected by the gas expelled by supernovae and/or strong stellar winds from intermediate-mass asymptotic giant branch (AGB) stars.

While each hypothesis has its merits and weaknesses (see Gratton et al. 2004, for a complete review), no single model accounts for the full set of observed light-element abundance variations in GCs – it remains possible that each may play a role (e.g. Martell et al. 2008c; Decressin et al. 2009).

One of the strongest constraints on the proposed scenarios is the fact that, in the majority of moderate- to high-metallicity GCs, the CN abundance distribution is bimodal. The self-enrichment scenario accommodates this observation most naturally, with the CN-weak and CN-strong groups representing the first and second populations of stars to have formed in the cluster, respectively. This idea has received increasing recent support, as improved photometric measurements have revealed the presence of multiple subgiant branches (SGBs) and main sequences in many GCs (Bedin et al. 2004; Piotto et al. 2007). Spectroscopic abundance analyses have also begun to reveal distinct sequences on the RGBs of some clusters (Marino et al. 2008; Lardo et al. 2011). In addition, studies of the spatial distributions of stars in clusters with accurate photometry have revealed the presence of correlated differences in $U - B$ colors (Carretta et al. 2010; Kravtsov et al. 2011), which suggests variations in chemical compositions within the cluster.

In this paper we use available photometric and spectroscopic data from Data Release 7 (DR7; Abazajian et al. 2009) of the Sloan Digital Sky Survey (SDSS; York et al. 2000) to examine the CN and CH bandstrength distributions for stars in eight GCs, including stars from the upper RGB to, in some cases, 1–2 magnitudes below the main sequence turnoff (MSTO). We show that there exists a clear bimodal distribution in CN bandstrengths for clusters with $[\text{Fe}/\text{H}] \geq -2.0$. Other interesting CN bandstrength variations are suggested to exist among the three clusters in our sample with $[\text{Fe}/\text{H}] < -2.0$.

This paper is organized as follows. In Section 2 we briefly describe our data and the cluster membership selection process. In Section 3 we define the adopted CN and CH

indices for stars in various stages of evolution. We then compare the derived CN and CH distributions in Section 4. In Section 5 we search for any correlations between these distributions with the global cluster parameters. Finally, our results and implications are discussed in Section 6.

2. Observational Data

The SDSS and its extensions have acquired *ugriz* photometry for several hundred million stars; the most recent public release is DR8 (Aihara et al. 2011). The Sloan Extension for Galactic Understanding and Exploration (SEGUE; Yanny et al. 2009), one of three sub-surveys that together formed SDSS-II, extended the *ugriz* imaging footprint of SDSS-I (Fukugita et al. 1996; Gunn et al. 1998; York et al. 2000; Gunn et al. 2006; Stoughton et al. 2002; Abazajian et al. 2003, 2004, 2005, 2009; Pier et al. 2003; Adelman-McCarthy et al. 2006, 2007, 2008) by approximately 3500 deg², and also obtained $R \simeq 2000$ spectroscopy for approximately 240,000 stars over a wavelength range of 3800–9200 Å. This included spectra for a collection of Galactic globular and open clusters, which served as calibrators for the T_{eff} , $\log g$, and [Fe/H] scales for all stars observed by SDSS/SEGUE, as processed by the SEGUE Stellar Parameter Pipeline (SSPP; Lee et al. 2008a,b; Allende Prieto et al. 2008). Tables 1 and 2 list the photometric, spectroscopic, and physical properties of the eight GCs in our sample. The SSPP produces estimates of T_{eff} , $\log g$, [Fe/H], and radial velocities (RVs), along with the equivalent widths and/or line indices for 85 atomic and molecular absorption lines, by processing the calibrated spectra generated by the standard SDSS spectroscopic reduction pipeline (Stoughton et al. 2002). See Lee et al. (2008a) for a detailed discussion of the approaches used by the SSPP; Smolinski et al. (2011) provides details on the most recent updates to this pipeline, along with additional validations.

Membership selection for the clusters is based on the color-magnitude diagram (CMD) mask algorithm described by Grillmair et al. (1995). Details on the application of this method to our specific clusters are described by Lee et al. (2008b) and Smolinski et al. (2011), and will only be briefly summarized here. The procedure involves a series of cuts, reducing the overall sample to include only those stars for which one can reasonably claim true membership. First, all stars within the tidal radius of the GC are selected. Stars with available spectra but with $\langle S/N \rangle < 10$ (averaged over the entire spectrum), or that lacked estimates of $[Fe/H]$ or RV, are excluded. A CMD is then constructed of the remaining stars, along with a CMD of stars in a concentric annulus designated to represent the field. A measure of the effective signal-to-noise in regions of the CMD is obtained, where the “signal” in this case constitutes those stars within the tidal radius and the “noise” constitutes those stars within the field region. Cluster-region stars within segments of the CMD above a threshold signal-to-noise are then selected. Finally, Gaussian fits to the highest peaks in the $[Fe/H]$ and RV distributions of those stars (expected to represent the cluster) are obtained, and stars within 2σ of the mean in both $[Fe/H]$ and RV are considered true member stars. This procedure results in the following numbers of true member stars: M92 (58), M15 (98), NGC 5053 (16), M53 (19), M2 (71), M13 (293), M3 (77), and M71 (8). Figures 1 and 2 show the final CMDs for these eight globular clusters.

Membership selection for M71 was complicated due to difficulties encountered with the photometry values available for this cluster at the time of our analysis (see An et al. 2008; Smolinski et al. 2011). This made the CMD mask algorithm less reliable for selecting likely spectroscopic members. Therefore, stars inside the tidal radius were selected and passed on to the final $[Fe/H]$ and RV cuts, with those stars that had questionable photometry excluded from consideration. As a result, only eight stars with available spectroscopy made it through the final cut for this cluster.

3. CN Bandstrength Distribution

A common approach for investigation of the star-to-star light element abundance variations within GCs is measurement of the 3883 Å CN molecular absorption band (Norris & Freeman 1979; Norris et al. 1981; Smith et al. 1996; Harbeck et al. 2003a,b; Pancino et al. 2010). This measurement does not require high-resolution spectroscopy, making it ideal for low-resolution spectroscopic surveys such as SDSS. The feature is typically measured using a spectral index defined as the magnitude difference between the integrated flux within a wavelength window containing the absorption band and the integrated flux within a sideband representing the continuum. However, the precise definition of this spectral index is often varied according to the luminosity class of the stars under consideration, due to the presence of other temperature-dependent absorption lines, such as H ζ at 3889 Å, that can potentially interfere with the adopted continuum window. In this section, we describe the CN spectral indices used for each region of the CMD and their observed distributions.

3.1. CN Absorption on the Red Giant Branch

We measured the strength of the CN absorption band at 3883 Å in RGB stars using the spectral index $S(3839)$ defined by Norris et al. (1981):

$$S(3839)_N = -2.5 \log \frac{\int_{3846}^{3883} I_\lambda d\lambda}{\int_{3883}^{3916} I_\lambda d\lambda}, \quad (1)$$

where I_λ is the measured intensity, and the subscript N indicates it is from the Norris et al. (1981) definition. Figure 3 shows the blue regions of SDSS spectra for two RGB stars in M3. The line-band and comparison-band windows are indicated. These two stars were selected because they have similar effective temperatures and apparent g -band magnitudes

(indicating similar luminosities on the RGB), as well as nearly identical Ca II and CH G-band strengths (indicating similar metallicities and carbon abundances). Despite these similarities, they exhibit clear differences in their CN 3883 Å absorption strengths.

The formation efficiency of the CN molecule is temperature dependent, where cooler effective temperatures allow increased molecular formation. When one looks at a population of stars, one therefore sees an increased ability for molecular formation moving up the CMD. While the majority of MS stars (aside from the coolest ones) have effective temperatures too high for significant molecular formation, the ability for this molecule to form on the SGB and RGB increases with luminosity as the star expands and its surface temperature drops. The result of this is that, all things being equal, we expect to see increased CN absorption on the RGB when compared to the SGB and this effect must be accounted for in the analysis prior to inferring any abundance differences. Furthermore, for clusters of moderate metallicity, when the CN absorption strengths are plotted as a function of luminosity or temperature, two groups generally appear – one CN-weak (sometimes referred to as CN-normal), the other CN-strong (enriched). A linear relationship is then fit to the CN-weak locus, and the vertical difference in $S(3839)_N$ between each point and the baseline is measured, as illustrated for M3 in the bottom-left panel of Figure 4. This vertical difference is denoted as $\delta S(3839)_N$, and is taken to be a temperature-corrected measure of CN absorption. The other panels in this figure are generalized histograms of this temperature-corrected index for our sample of clusters, discussed in detail below. The raw and corrected values are listed for each cluster in Table 3.

The slope of the relationship between CN bandstrength and luminosity is metallicity dependent, so each cluster must be corrected individually prior to constructing comparisons across the sample. Figure 5 shows this relationship between the CN slope and $[Fe/H]$, obtained by dividing our entire sample into 0.1-dex wide metallicity bins and fitting a line

to the CN-weak locus of each bin. Note the trend of decreasing CN slope with decreasing $[\text{Fe}/\text{H}]$, which is similar to the trend for field giants from DR7 reported by Martell & Grebel (2010). When the slope of each panel in their Figure 6 is plotted as a function of metallicity, we obtain a linear relationship for field giants:

$$\text{CN Slope}_{\text{field}} = -0.17 - 0.08[\text{Fe}/\text{H}]. \quad (2)$$

The expression obtained for our sample of cluster RGB stars is:

$$\text{CN Slope}_{\text{cluster}} = -0.18 - 0.07[\text{Fe}/\text{H}], \quad (3)$$

and is statistically equivalent to the field giant relationship ($\sigma_{\text{slope}} = 0.04, \sigma_{\text{intercept}} = 0.07$). The data point corresponding to $[\text{Fe}/\text{H}] = -1.40$ has been omitted from this linear fit as an outlier.

It is difficult to draw a direct comparison between the two samples due to their differing mass functions. The cluster giants are all exclusively old and span a relatively small range in mass at any given value of M_g , whereas the field giants from the Martell & Grebel (2010) sample potentially span a much broader range of mass and age.¹ Similarities between these relationships may hint at a common origin (see Martell & Grebel 2010, for further discussion).

Figure 6 shows the distribution of $\delta\text{S}(3839)_N$ as a function of absolute g -magnitude.

¹Figure 6 in Martell & Grebel (2010) plots CN versus absolute M_r , whereas we use absolute M_g . Because these are all RGB stars with the same $(g-r)_0 \sim 0.5$, converting M_r to M_g should only produce an essentially uniform shift of all stars in each plot, not affecting the slopes significantly.

Values for both RGB and SGB stars are shown, calculated using the CN index definition of Norris et al. (1981). Blue triangles represent SGB stars, while red circles represent RGB stars, with filled and open symbols indicating CN-strong and CN-weak stars, respectively. While a small amount of scatter exists for the most metal-poor clusters (M92, M15, and NGC 5053), no separation that would indicate a bimodal distribution is obvious, consistent with Figure 4. For the remaining five clusters at higher metallicity, starting with M53 at a metallicity of $[\text{Fe}/\text{H}] = -2.06$, two distinct populations of stars in $\delta\text{S}(3839)_{\text{N}}$ -space are apparent.

For M3, a small number of possible AGB stars are noted in the figure with black symbols. The majority of these stars appear CN-weak, with only one CN-strong AGB star. This result is similar to the observations reported by Campbell et al. (2010), who found that, in a sample of nine Galactic GCs, all showed either a total lack of CN-strong AGB stars or a significant depletion of CN-strong AGB stars compared to those present on the RGB. These authors noted that no current explanation exists in standard stellar evolution theory as to why stars on the AGB should have reduced CN abundances compared to the RGB, particularly because the low effective temperatures should be suitable for similarly efficient molecular CN formation. In principle, increased mixing both on the RGB and at the beginning of AGB ascent should contribute more N (and thus stronger CN) to the stellar envelope, which should be apparent in surface abundance measurements. Such a discrepancy has been noted for a long time; two possible explanations were proposed by Norris et al. (1981). First, if two chemically distinct populations in the cluster existed after star formation ceased, one of which was helium-rich and evolved to populate the blue end of the horizontal branch (HB), but never ascended to the AGB, this might lead to the deficiency of CN-strong stars. The second explanation hypothesized that increased mixing in some stars produced increased CN abundances, but also led to increased mass loss at the RGB tip, producing stars populating the blue end of the HB that never ascended the AGB.

The problem remains unsolved, and requires additional work.

Adopting the corrected values obtained from the above procedure, we produced a generalized histogram of the $\delta S(3839)_N$ distribution for each cluster, shown in Figure 4. This was accomplished by representing each point as a Gaussian, centered on $\delta S(3839)_N$ with a FWHM equal to the uncertainty of that particular $\delta S(3839)_N$ measurement, and then adding the individual Gaussians together. The uncertainty for each $S(3839)_N$ measurement was determined as in Martell & Grebel (2010), using a Monte Carlo approach. Each pixel in the error vector produced by the SDSS spectroscopic reduction pipeline was multiplied by a factor between 0 and 1, drawn from a normalized distribution. This new vector was then added to the data vector and the indices were remeasured. This process was repeated 100 times and the standard deviation was taken to be the uncertainty. Naturally, the resultant uncertainties are related to the S/N of the spectra; uncertainties for the high-S/N spectra were much lower than the typical uncertainties found in the literature. For this reason, recent studies have sometimes smoothed their histograms to make them more directly comparable to past studies. Smoothing the histogram also helps eliminate any artificial substructure in the distribution created by small number statistics, while additionally accounting for unidentified sources of uncertainty.

In Figure 4, the clusters are arranged in order of increasing metallicity, from left to right, top to bottom, and represent the $\delta S(3839)_N$ distribution on the RGB for each cluster. Many of these clusters have been studied previously, so comparisons can be made with our present observations. Suntzeff (1981) reported a bimodal distribution in CN indices in M3 and M13 on the upper RGB (stars more luminous than the HB). This observation for M3 was confirmed on the upper RGB by Smith et al. (1996) and Lee (1999), and on the lower RGB of M3 by Norris & Smith (1984). Smith et al. (1996) also report CN bimodality among M13 RGB stars, and the proportions of CN-strong stars we observe in

these two clusters agree well with those reported by Suntzeff (1981). M2 was studied by Smith & Mateo (1990) and shown to have a bimodal CN distribution, also matching in proportion to that seen in our data.

Studies of M71 by Smith & Norris (1982), Lee (2005), and Alves-Brito et al. (2008) all report CN bimodality on the RGB. Evidence for bimodality is found in our data as well, at the same level as observed for 47 Tuc (Norris & Freeman 1979), which is of comparable metallicity to M71. It is interesting that Alves-Brito et al. (2008) have claimed the existence of CN-strong AGB stars in their sample. As mentioned above, nearly all CN observations of AGB stars have demonstrated a depletion in CN, which makes their observation unique. It is possible that M71 is so metal-rich compared to other GCs studied to date that this encourages additional CN enrichment on the AGB, in spite of whatever mechanism might be causing the depletions in other cluster AGB stars. However, if this were the case, one might expect some manifestation on the RGB as well, in the form of a higher ratio of CN-strong to CN-weak stars. Yet, in the Alves-Brito et al. (2008) sample the ratio is only ~ 0.3 . Further investigation of AGB stars in M71 would be of interest to determine whether their observations are representative of the cluster. Note that Mallia (1978) reported a large fraction of CN-strong AGB stars in 47 Tuc, so we might expect to find a similar fraction in M71.

Moving to the $[\text{Fe}/\text{H}] \leq -2.0$ regime, M53 has not been extensively studied. Martell et al. (2008b) reported a broad but not strongly bimodal distribution of CN absorption strengths in their sample of upper RGB stars (brighter than the RGB bump), where deep mixing is expected to have altered the stellar surface abundances. Their Figure 6 shows a generalized histogram for M53 that is similar to ours in Figure 4, but theirs appears slightly narrower and smoother (though in fact our histogram has been smoothed by a larger factor than their distribution). When our $\delta\text{S}(3839)_{\text{N}}$ values are combined with

theirs, producing a sample spanning nearly the entire RGB, a KMM test (Ashman et al. 1994) indicates that the hypothesis that the observations are drawn from a single Gaussian parent population can be rejected at high statistical confidence ($p = 0.05$). The generalized histogram for this combined data set is shown in Figure 7, where the individual data sets are also indicated. The distribution clearly indicates the presence of a CN-strong component, with a ratio of CN-strong to CN-weak stars of 0.61, suggesting a population of CN-strong stars in the cluster with a range of enrichment levels.

We now consider the other very metal-poor clusters in our sample: M92, M15, and NGC 5053. Carbon et al. (1982) studied carbon and nitrogen abundances in M92 from the SGB to the AGB, and reported a general decrease in C abundances moving to higher luminosities, but no correlation or anticorrelation between the C and N abundances. Instead, they determined that the total number of C+N atoms varies from star to star within the cluster, an observation at odds with predictions that the sum ought to remain constant. Similar conclusions were reached by Trefzger et al. (1983) regarding M15 – C abundance drops as one moves up the RGB, but N abundance remains on average the same, although with some uncorrelated star-to-star variations. A more recent study of M15 by Lee (2000) also failed to detect reliable evidence of CN bimodality, although they confirmed the existence of a very small number of CN-enriched stars, also reported by Langer et al. (1992).

A recent study by Shetrone et al. (2010) of NGC 5466 ($[\text{Fe}/\text{H}] \simeq -2.2$) suggested the possible presence of two CN groups, with a small mean separation of only 0.055. They noted that the generalized histogram of their RGB stars was not well-described by a single Gaussian fit. In a similar fashion, we examined the generalized histograms for RGB stars in the very metal-poor clusters M92, M15, and NGC 5053. Figure 8 shows the histograms for these clusters, as well as that of NGC 5466 from Shetrone et al. (2010), fit with a single

Gaussian; residuals are plotted in the insets in each panel. The residuals from the fits to our three very metal-poor clusters are clearly larger than those of NGC 5466, suggesting that our data also may not be well-described by a single Gaussian population. However, a KMM test for each cluster (including NGC 5466) cannot reject the null hypothesis that a single population well-describes the observed data, indicating that hints of the non-Gaussian distributions in our data may simply be due to small- n statistics. If these clusters possess multiple CN behaviors, they may not be discernible within the present measurement uncertainties. Due to the fact that double-metal molecules like CN are particularly difficult to observe at low $[\text{Fe}/\text{H}]$, this problem could be solved by measuring individual element abundances rather than molecular bandstrengths.

3.2. CN Absorption on the Subgiant Branch and Main Sequence

Perhaps the most intriguing observations of the CN bimodality phenomenon are to be found among stars in the relatively unevolved regions of cluster CMDs. Contrary to predictions of standard stellar evolutionary models, significant variations in CN bandstrengths have been reported for stars prior to their undergoing first dredge-up (eg. Briley et al. 2002; Cohen et al. 2002), even down to the main sequence in 47 Tuc (Cannon et al. 1998; Harbeck et al. 2003a). However, searches within other cluster MS stars have produced mixed results. Cohen (1999a) reported no significant CN variation for MS/MSTO stars belonging to M13, although the CN features in their spectra were shown to be too weak for reliable measurement (Briley & Cohen 2001). Carbon and nitrogen abundance analyses of these stars by Briley et al. (2004) showed that this was likely due to the fact that there is very little change in bandstrength for a given change in abundance at luminosities near the turnoff, where effective temperatures are relatively high compared to MS and giant stars (see their Figure 2). Main sequence stars in M71 have been claimed

to exhibit CN bimodality at a level larger than the measurement uncertainty, as well as an anticorrelation between CN and CH (Cohen 1999b). Follow-up analysis of this data further showed that the variation is at the same level as that observed for RGB stars in that cluster, leading the authors to claim that no significant mixing is occurring on the RGB (although this could also simply mean that first dredge-up did not significantly affect the surface carbon and nitrogen abundances), and that the abundance variations were in place at the time the stars formed (Briley & Cohen 2001). In their sample of eight GCs, Kayser et al. (2008) found no statistically significant variation in CN abundance for stars on the MS and SGB, but they again attributed that to low S/N spectra producing relatively large measurement uncertainties. Finally, Pancino et al. (2010) reported CN bimodality for MS stars in four of their most metal-rich clusters among a sample of 12 clusters. Clearly, minimizing measurement uncertainty plays a vital role in addressing the question of CN abundance variations on the MS, and further observations of larger samples of MS stars are needed for improved statistical certainty. In this section, we report on the MS/SGB stars observed for four clusters in our sample.

We measured the strength of the CN absorption band at 3883 Å on the main sequence using the spectral index $S(3839)$ defined by Harbeck et al. (2003a) for MS stars:

$$S(3839)_H = -2.5 \log \frac{\int_{3861}^{3884} I_\lambda d\lambda}{\int_{3894}^{3910} I_\lambda d\lambda}. \quad (4)$$

Uncertainties and $\delta S(3839)_H$ values were calculated the same way as described in Section 3.1. Figure 9 shows the distribution of $\delta S(3839)_H$ values for the four clusters that have SEGUE spectra for stars on the MS – M92, M15, M2, and M13 (in order of increasing [Fe/H]). A large amount of scatter is apparent, but not when compared to the typical uncertainty indicated by the error bars shown in the upper right corner of each panel. Furthermore, inset in each panel is the distribution of $\delta S(3839)_H$ as a function of $\langle S/N \rangle$,

which shows that the source of this scatter may lie in the relatively low S/N of the spectra for these faint stars. The decrease in CN strength near $M_g \approx 4$ is not unexpected, since this corresponds to the turnoff where the effective temperatures are the highest (and thus CN molecular formation is at its lowest), but one would expect that CN bandstrengths should essentially all increase for luminosities below this point again, as it does for luminosities higher than this point, rather than simply increasing in dispersion. Generalized histograms of the $\delta S(3839)_H$ values for these four clusters are shown in Figure 10. No indications of bimodality are seen, suggesting that when the relatively larger uncertainties are taken into account, nothing statistically significant stands out. Although the residuals (see inset panels) are asymmetric and, in the cases of M92 and M13, double-peaked, we see nothing indicating the presence of two populations of stars. It seems more likely that the asymmetries in the figures are simply due to finite sampling from a single Gaussian distribution. A KMM test fails to reject the hypothesis that these data were drawn from a single Gaussian parent population. Further observations with smaller uncertainties are needed to determine whether the observed distributions’ asymmetries are due to the presence of two distinct populations or not.

The Norris et al. (1981) definition for the CN index was used for stars located on the SGB, although the Harbeck et al. (2003a) definition is also valid. Figure 11 shows the distributions of $\delta S(3839)_N$ abundances on the SGB for the same four clusters as in Figure 10. The histograms for M92, M2, and M13 appear to provide evidence of independent CN groups. The solid blue lines and dashed black lines are as before, while the red dotted curves provide the generalized histograms for the proposed CN groups on the SGBs of each cluster. Insets in each panel again show the differences between the data and the superposed single Gaussian curve. Cohen (1999a) looked for CN variations on the upper MS/MSTO region of M13 and reported nothing significant; however it appears that our data does indicate the presence of CN variation on the SGB of this cluster. These observations indicate that, for

very metal-poor clusters such as M92, as well as for clusters with moderate metallicity such as M2 and M13, there appear to be signs of enhanced N enrichment well before the point of first dredge-up. These issues are explored further below.

3.3. Hidden Substructure in Generalized Histograms

While generalized histograms are a more natural representation of the distribution of data than binned histograms, it is important to consider the impact of any adopted smoothing factors. Smoothing factors are sometimes used to produce a histogram that more closely resembles those of past studies by multiplying the uncertainties of each data point by some appropriate factor. This is also done to account for any sources of uncertainty that may have been overlooked. One may choose to adopt a smoothing factor which produces a distribution that is comparable to past studies, but choosing a smoothing factor that is too high may wash out important details in the data.

To study the potential impact of smoothing on the generalized histograms of our clusters, we divided up the CMDs for the four GCs with full CMD coverage into several regions – RGB above the bump (where the RGB bump was identified), RGB, SGB/MSTO, and MS. We then looked at the $\delta S(3839)$ indices for stars in each region and produced two generalized histograms, one smoothed to match the observational uncertainties of previous studies (solid black line) and one unsmoothed (dashed red line), shown in Figures 12 – 15. Because measurement errors from previous studies are typically ~ 0.05 , when our typical Monte Carlo-calculated uncertainties were smaller than this they were amplified (smoothed) by an integer factor (shown in each panel) to approximate the errors from previous studies.

Naturally, the unsmoothed lines exhibit more potential substructure, but one must still determine what level of substructure is meaningful. This can be qualitatively estimated as

a function of the number of stars used in the bin and the relative peak sizes. For example, while the RGB of M92 (Figure 12) appears to exhibit substructure in the unsmoothed histogram, the paucity of stars in this region of the CMD obviates this claim (the CN-strong peak only has one star). As mentioned above, for very metal-poor clusters such as M92 and M15, it is expected that the difference between CN-strong and CN-weak groups should be smaller when measuring the S(3839) index. At the metallicity of M92, this difference is expected to be on the order of 0.1, suggesting that if more data were available we might be able to determine whether the apparent substructure is real or merely an artifact of small number statistics.

From inspection of the RGB of M15 (Figure 13), we again see possible asymmetries in the upper regions that may be associated with substructure. However, a KMM test for this portion is again unable to reject a single Gaussian parent population.

At more moderate metallicities, M2 (Figure 14) and M13 (Figure 15) exhibit very clear signs of CN variation on the RGB. The uppermost region of M13 is at a luminosity above the RGB bump, suggesting that the increase in CN is likely due at least in part to the deep mixing thought to occur at that point. Figure 15 depicts the expected appearance of stronger CN bandstrengths as stars evolve up the RGB, although a group of CN-weak stars always remains present. It is also worth noting that initial variations first appear on the SGB, as seen in the right-hand panel (c).

4. CH Bandstrength Distribution

While investigation of CN bandstrengths can provide some insight into possible chemical inhomogeneities within cluster stars, CH absorption strength is also typically considered as a means of distinguishing between nitrogen abundance behavior and carbon

abundance behavior. This is generally done by measuring the absorption strength of the 4300 Å CH G-band and comparing with the CN bandstrengths. Previous studies of cluster giants have shown that, at a given luminosity, the CN-strong stars tend to have weak CH G-bands, implying nitrogen enhancement. Additionally, Gratton et al. (2000) demonstrated that the general behavior in clusters is that the CH bandstrength decreases with increasing luminosity, while the summed ratio $[(C+N)/Fe]$ remains constant – again indicating the presence of nitrogen enhancement as stars move up the RGB. However, these abundances are not predicted by standard stellar evolution models to change significantly along the RGB between first dredge-up and helium flash (Iben 1964), at least without the assumption of additional mixing.

Many definitions of indices that measure the CH G-band have been employed (Norris et al. 1981; Trefzger et al. 1983; Briley & Smith 1993; Lee 1999; Harbeck et al. 2003a,b; Martell et al. 2008b) and proposed (Martell et al. 2008a) in the past; these differ primarily because they were developed for use with stars of specific metallicity or luminosity ranges. Figure 16 shows the linebands and sidebands used by four common definitions. While the use of different CH bandstrength indices complicates quantitative comparison with literature studies, qualitative comparisons can still be useful. Inspection of Figure 16 reveals the presence of the H_γ and H_δ Balmer lines that can interfere with the continuum sidebands in the Norris et al. (1981) and Martell et al. (2008b) index definitions. These two definitions were developed using samples of the most luminous, and therefore the coolest, red giants in their clusters of interest, where Balmer absorption has minimal impact. Of the two that remain, the Briley & Smith (1993) definition only includes the blue side of the continuum, which can potentially cause artificially depressed values for cooler stars where the continuum is more strongly sloped. Therefore, the Lee (1999) definition was adopted for this study:

$$CH(4300)_L = -2.5 \log \frac{\int_{4270}^{4320} I_\lambda d\lambda}{\frac{1}{2} \left(\int_{4230}^{4260} I_\lambda d\lambda + \int_{4390}^{4420} I_\lambda d\lambda \right)}. \quad (5)$$

This definition has the advantage that it has been used for clusters covering a broad range of metallicities, from M15 (-2.33 ; Lee 2000) to M71 (-0.82 ; Lee 2005), and it also avoids the influence of Balmer lines that appear in hotter stars. In addition, it samples the continuum on both sides of the CH G-band, thus providing a more accurate representation of the “expected” continuum at the location of the line band, regardless of the slope of the continuum in this region. The resulting indices are also tabulated in Table 3.

Figure 17 shows the CH index versus $\delta S(3839)_N$ for our cluster sample, ordered from low to high metallicity. From inspection of this figure, CN-weak stars are typically also CH-strong, while those stars that are CN-strong are typically CH-weak, with a few exceptions. Figure 18 is a similar set of plots, but here the CH-index is plotted against absolute g -magnitude. The RGB stars within each cluster exhibit the strongest CH absorption when they are CN-weak, and vice versa. SGB stars are included as well for the two clusters in our study where they are also available. Our results are consistent with previous studies of giants in M2 (Smith & Mateo 1990), M13 (Suntzeff 1981; Briley & Smith 1993; Smith et al. 1996), M3 (Suntzeff 1981; Smith et al. 1996), and M71 (Smith & Norris 1982; Lee 2005; Alves-Brito et al. 2008). Interestingly, M53 does not exhibit this anticorrelation in our sample or that of Martell et al. (2008b).

4.1. CH Behavior at Low Metallicity

Examination of the CH-CN anticorrelation for low-metallicity clusters is challenging, due in part to the decreased abundances of all metals in the stellar atmospheres. This phenomenon has been demonstrated before with synthetic spectra spanning a range

of N abundances at low metallicity (Martell et al. 2008b). This suggests a possible low-metallicity observational cutoff, below which bimodality is either too difficult to detect with data of the quality we were able to obtain or too difficult to measure due to the low levels of CN present.

Shetrone et al. (2010) predict that abundance variations should exist at all metallicities, even though bandstrength variations will become impossible to see at sufficiently low values of $[\text{Fe}/\text{H}]$. To investigate this, we now consider whether the CN-CH anticorrelation is observable in the very metal-poor clusters M92, M15, and NGC 5053. Following the approach of Shetrone et al. (2010), we fit a line to the raw $S(3839)_N$ values as a function of g -magnitude, then label those above the line as CN-strong and those below the line as CN-weak. The results of this exercise for M92, M15, and NGC 5053 are shown in Figure 19, plotted against absolute g -magnitude for direct comparison. For the remainder of this paper these two groups will be used to distinguish those stars with slightly higher and slightly lower CN bandstrengths. At the lowest point on the RGB (still above the SGB), there is little difference in the CH bandstrengths between the CN-strong and CN-weak stars. However, as one moves up the RGB, an apparent anticorrelation sets in for RGB stars in M92 at $M_g \approx 1.5$. Similar behavior is not seen in M15 and NGC 5053, possibly due to the limited sampling.

If CN abundance variations are in place prior to a star’s evolution up the RGB, one might expect to see an anticorrelation between CN and CH on the SGB and MS. Although more difficult to observe, since higher temperatures would tend to break up the molecules, such anticorrelations have been reported previously for MS stars (Cannon et al. 1998; Cohen 1999b; Harbeck et al. 2003a; Pancino et al. 2010). Figure 20 shows the relationship between CH and CN indices for MS and SGB stars in M92, M15, M2, and M13, with the CN indices derived using the Harbeck et al. (2003a) definition. As in Fig. 9, we see a minimum in CH

bandstrength for M13 at $M_g \approx 4$, corresponding to the higher effective temperatures of the turnoff point (see Figure 2 from Briley et al. 2004). While an anticorrelation may exist on the upper SGBs of M2 and M13, which would be consistent with the signs of CN bimodality on the SGB of these clusters and consistent with Figure 18, no other anticorrelations are clearly seen. While further study is needed, we are confident that follow-up observations of MS stars in these clusters will reveal the same types of bandstrength variations as reported in previous studies.

5. Correlations with Cluster Parameters

The possibility that CN enrichment is linked in some way with various physical parameters of the parent cluster has been examined extensively in previous studies. For example, Norris (1987) identified a possible correlation between CN bandstrength and the apparent ellipticity of the cluster using data from 12 Galactic GCs. This suggested correlation was confirmed by Smith & Mateo (1990), who combined their observations of M2 with the set from Norris (1987), but was not seen by Kayser et al. (2008) using data from eight clusters (of which three were in common between the two studies). They concluded that the correlation with ellipticity is not as significant as initially believed. Smith & Mateo (1990) also reported a correlation between CN enrichment and cluster central velocity dispersion, which was again disputed by Kayser et al. (2008). The Smith & Mateo (1990) claim of a CN enrichment correlation with integrated cluster luminosity received moderate support from the observations of Kayser et al. (2008).

Figure 21 shows the number ratio of CN-strong to CN-weak RGB stars for the clusters in our sample, denoted by r , plotted against various cluster parameters drawn from the

Harris (1996) catalog.² These values are tabulated in Table 4. The number ratio is useful because it reveals the relative population sizes of the individual CN groups, and provides a constraint on the chemical evolution of the cluster.

M92 and M15 were treated differently because they do not possess CN-strong stars, at least by the conventional definition, and hence would have an r value of zero. However, Figures 12 and 13 suggest the presence of stars that might be identified as CN-strong (relative to the rest of the cluster). Furthermore, an alternative method for adopting relatively CN-strong and CN-weak stars was described in Section 4.1 for M92, M15, and NGC 5053. Using this approach, we determined alternative r values for M92, M15, and NGC 5053, which are plotted in Figure 21 as open triangles. Spearman rank correlation coefficients were calculated for the distributions and are provided in the upper-left corner of each panel; the top and bottom numbers correspond to the sample with and without the second r quantity included, respectively, for M92, M15, and NGC 5053.

Supporting the claims of Norris (1987) and Smith & Mateo (1990), we observe a moderate correlation between CN enrichment and cluster ellipticity. We also note a moderate correlation between CN enrichment and central velocity dispersion (Figure 22), in the same sense as Smith & Mateo (1990), with a Spearman coefficient of 0.52 when using the ratios for the proposed CN divisions in M92, M15, and NGC 5053, though no such correlation in our data is observed with cluster luminosity (see Figure 21). However, the range of cluster luminosities in our sample is not very broad. Only two clusters with absolute V -magnitude brighter than -8.0 were observed, one of which is metal-poor with no solidly identified CN-strong stars and the other having fewer than 10 stars with reliable spectroscopy. When we combine our data with that of Kayser et al. (2008) and

²All references to Harris (1996) refer to the 2010 update on his web page: <http://www.physics.mcmaster.ca/~harris/mwgc.dat>.

Smith & Mateo (1990), also shown in Figure 22, the overall trends become clearer; the largest fraction of CN-strong stars are found in the most luminous and massive clusters. This result is consistent with expectations from the self-enrichment scenario – the most massive clusters possess the deepest gravitational potentials, allowing them to retain the largest amount of chemically enriched gas expelled from evolving stars.

While studies to date typically quote an average value of the r parameter from the clusters in their samples, it is not clear that this quantity is meaningful. Comparing the values directly is complicated by the fact that some studies only use RGB stars, while others include subgiants, dwarfs, and even AGB stars as well. Since dwarfs, with their hotter atmospheres, are less likely to show significant CN absorption, their inclusion may bias the value downward. The same holds true for the inclusion of AGB stars, since they are nearly always CN-weak (see Campbell et al. 2010, for further discussion). The study by Pancino et al. (2010), comprised entirely of MS dwarfs, reported an average of $r = 0.82 \pm 0.29$, while the average of the r values reported by Kayser et al. (2008) for the giants in their sample is 0.61. Together, these results indicate that for the clusters in their samples, both of which span a large range of $[\text{Fe}/\text{H}]$ and luminosity, the CN-strong stars are in the minority. However, studies of Na and O abundances in cluster giants by Carretta et al. (2009b,c) suggest that the ratio is much higher, with enriched stars comprising 50–70% of the total ($r > 1$). The compilation by Smith & Mateo (1990) of giants from 16 clusters gives an average ratio of 1.72, which agrees well with Carretta et al. (2009b,c). While it is puzzling that two samples of cluster giants would yield such discrepant results, this may result from a bias toward more luminous clusters, since their inclusion would artificially inflate the fraction of CN-strong stars in the sample. Table 5 lists the mean r values alongside the mean M_V values for our sample and the three GCs from the literature. The increase in $\langle r \rangle$ with $\langle M_V \rangle$ is apparent, indicating that conclusions drawn based upon the CN ratio must account for any potential biases from including or excluding

massive GCs in the sample.

6. Conclusions and Discussion

We have used low-resolution SEGUE spectra to confirm the presence of a bimodality in the CN distributions for stars in GCs with $[\text{Fe}/\text{H}] > -2$. In addition, we extend the metallicity limit for which CN bimodality has been observed to at least $[\text{Fe}/\text{H}] \sim -2.1$, by adding M53 to the collection. Furthermore, we have presented evidence suggesting the presence of a much smaller division between CN-strong and CN-weak groups on the RGB of M92, down to luminosities corresponding to $M_V \sim 1.8$, which is in quantitative agreement with earlier studies suggesting carbon depletion setting in below the RGB bump. Evidence for two CN groups on the RGB of M15, with a similar metallicity as M92, also exists. Previous CN abundance studies of M92 and M15 have not shown strong evidence for bimodality in either cluster. We also confirm an overall anticorrelation between CN and CH bandstrengths on the RGB for M2, M13, and M3, for luminosities beyond the point of first dredge-up, while offering evidence that M92 may also display the same anticorrelation. Our samples for M53 and M71 are too small to make strong claims for anticorrelations, although M53 appears to have CN and CH bandstrengths that are uncorrelated. Despite its chemical similarity to M92, no apparent CN-CH anticorrelation is present among M15 giants. Finally, NGC 5053 exhibits a remarkably uniform CH bandstrength along the RGB, in spite of the fact that our sample of stars straddles the RGB bump, where deep mixing is predicted to set in.

Our observations support a scenario in which evolved stars disperse enriched gas throughout the cluster that ultimately forms a second generation of stars. This results in two chemically disparate populations of stars. Such abundance variations are not observed among even the oldest and most massive open clusters (Jacobson et al. 2008;

Martell & Smith 2009), presumably due to their significantly lower gravitational potentials preventing them from retaining enriched gas from evolved stars. Furthermore, current theoretical models of the origin of light-element abundance variations rely heavily on the high density environments of proto-globular clusters to facilitate enrichment of subsequent stellar populations. Since these chemically enriched stellar populations appear to form preferentially in GCs, this motivates the argument that the presence of CN-strong stars in the Galactic halo may have been stripped from GCs into the field, rather than being the result of *in situ* formation (Martell & Grebel 2010). Additional studies of halo GCs should provide an opportunity to explore and quantify this contribution directly.

J.P.S., T.C.B., and Y.S.L. acknowledge partial funding of this work from grants PHY 02-16783 and PHY 08-22648: Physics Frontiers Center/Joint Institute for Nuclear Astrophysics (JINA), awarded by the US National Science Foundation.

Funding for the SDSS and SDSS-II has been provided by the Alfred P. Sloan Foundation, the Participating Institutions, the National Science Foundation, the U.S. Department of Energy, the National Aeronautics and Space Administration, the Japanese Monbukagakusho, the Max Planck Society, and the Higher Education Funding Council for England. The SDSS Web Site is <http://www.sdss.org/>.

The SDSS is managed by the Astrophysical Research Consortium for the Participating Institutions. The Participating Institutions are the American Museum of Natural History, Astrophysical Institute Potsdam, University of Basel, University of Cambridge, Case Western Reserve University, University of Chicago, Drexel University, Fermilab, the Institute for Advanced Study, the Japan Participation Group, Johns Hopkins University, the Joint Institute for Nuclear Astrophysics, the Kavli Institute for Particle Astrophysics and Cosmology, the Korean Scientist Group, the Chinese Academy of Sciences (LAMOST), Los Alamos National Laboratory, the Max-Planck-Institute for Astronomy (MPIA), the

Max-Planck-Institute for Astrophysics (MPA), New Mexico State University, Ohio State University, University of Pittsburgh, University of Portsmouth, Princeton University, the United States Naval Observatory, and the University of Washington.

REFERENCES

- Abazajian, K. N., et al. 2009, *ApJS*, 182, 543
- . 2004, *AJ*, 128, 502
- . 2005, *AJ*, 129, 1755
- . 2003, *AJ*, 126, 2081
- Adelman-McCarthy, J. K., et al. 2008, *ApJS*, 175, 297
- . 2007, *ApJS*, 172, 634
- . 2006, *ApJS*, 162, 38
- Aihara, H., et al. 2011, *ApJS*, 193, 29
- Allende Prieto, C., et al. 2008, *AJ*, 136, 2070
- Alves-Brito, A., Schiavon, R. P., Castilho, B., & Barbuy, B. 2008, *A&A*, 486, 941
- An, D., et al. 2008, *ApJS*, 179, 326
- Ashman, K. M., Bird, C. M., & Zepf, S. E. 1994, *AJ*, 108, 2348
- Bedin, L. R., Piotto, G., Anderson, J., King, I. R., Cassisi, S., & Momany, Y. 2004, *Memorie della Societa Astronomica Italiana Supplementi*, 5, 105
- Briley, M. M., & Cohen, J. G. 2001, *AJ*, 122, 242
- Briley, M. M., Cohen, J. G., & Stetson, P. B. 2002, *ApJ*, 579, L17
- . 2004, *AJ*, 127, 1579
- Briley, M. M., & Smith, G. H. 1993, *PASP*, 105, 1260

- Campbell, S. W., Yong, D., Wylie-de Boer, E. C., Stancliffe, R. J., Lattanzio, J. C., Angelou, G. C., Grundahl, F., & Sneden, C. 2010, *Mem. Soc. Astron. Italiana*, 81, 1004
- Cannon, R. D., Croke, B. F. W., Bell, R. A., Hesser, J. E., & Stathakis, R. A. 1998, *MNRAS*, 298, 601
- Carbon, D. F., Romanishin, W., Langer, G. E., Butler, D., Kemper, E., Trefzger, C. F., Kraft, R. P., & Suntzeff, N. B. 1982, *ApJS*, 49, 207
- Carretta, E., Bragaglia, A., D’Orazi, V., Lucatello, S., & Gratton, R. G. 2010, *A&A*, 519, A71+
- Carretta, E., Bragaglia, A., Gratton, R., D’Orazi, V., & Lucatello, S. 2009a, *A&A*, 508, 695
- Carretta, E., Bragaglia, A., Gratton, R., & Lucatello, S. 2009b, *A&A*, 505, 139
- Carretta, E., et al. 2009c, *A&A*, 505, 117
- Charbonnel, C. 1994, *A&A*, 282, 811
- Cohen, J. G. 1978, *ApJ*, 223, 487
- . 1999a, *AJ*, 117, 2428
- . 1999b, *AJ*, 117, 2434
- Cohen, J. G., Briley, M. M., & Stetson, P. B. 2002, *AJ*, 123, 2525
- Decressin, T., Charbonnel, C., Siess, L., Palacios, A., Meynet, G., & Georgy, C. 2009, *A&A*, 505, 727
- Denissenkov, P. A., & Vandenberg, D. A. 2003, *ApJ*, 593, 509

- Fukugita, M., Ichikawa, T., Gunn, J. E., Doi, M., Shimasaku, K., & Schneider, D. P. 1996, *AJ*, 111, 1748
- Fusi Pecci, F., Ferraro, F. R., Crocker, D. A., Rood, R. T., & Buonanno, R. 1990, *A&A*, 238, 95
- Gilroy, K. K. 1989, *ApJ*, 347, 835
- Gratton, R., Sneden, C., & Carretta, E. 2004, *ARA&A*, 42, 385
- Gratton, R. G., Sneden, C., Carretta, E., & Bragaglia, A. 2000, *A&A*, 354, 169
- Grillmair, C. J., Freeman, K. C., Irwin, M., & Quinn, P. J. 1995, *AJ*, 109, 2553
- Grundahl, F., Stetson, P. B., & Andersen, M. I. 2002, *A&A*, 395, 481
- Gunn, J. E., et al. 1998, *AJ*, 116, 3040
- . 2006, *AJ*, 131, 2332
- Harbeck, D., Smith, G. H., & Grebel, E. K. 2003a, *AJ*, 125, 197
- . 2003b, *A&A*, 409, 553
- Harris, W. E. 1996, *AJ*, 112, 1487
- Iben, Jr., I. 1964, *ApJ*, 140, 1630
- . 1968, *ApJ*, 154, 581
- Jacobson, H. R., Friel, E. D., & Pilachowski, C. A. 2008, *AJ*, 135, 2341
- Kayser, A., Hilker, M., Grebel, E. K., & Willemsen, P. G. 2008, *A&A*, 486, 437
- Kravtsov, V., Alcaïno, G., Marconi, G., & Alvarado, F. 2011, ArXiv e-prints

Langer, G. E. 1985, *PASP*, 97, 382

Langer, G. E., Suntzeff, N. B., & Kraft, R. P. 1992, *PASP*, 104, 523

Lardo, C., Bellazzini, M., Pancino, E., Carretta, E., Bragaglia, A., & Dalessandro, E. 2011, *A&A*, 525, A114+

Lee, S. 1999, *AJ*, 118, 920

—. 2005, *Journal of Korean Astronomical Society*, 38, 23

Lee, S. G. 2000, *Journal of Korean Astronomical Society*, 33, 137

Lee, Y. S., et al. 2008a, *AJ*, 136, 2022

—. 2008b, *AJ*, 136, 2050

Mallia, E. A. 1978, *A&A*, 70, 115

Mandushev, G., Staneva, A., & Spasova, N. 1991, *A&A*, 252, 94

Marino, A. F., Villanova, S., Piotto, G., Milone, A. P., Momany, Y., Bedin, L. R., & Medling, A. M. 2008, *A&A*, 490, 625

Martell, S. L., & Grebel, E. K. 2010, *A&A*, 519, A14+

Martell, S. L., & Smith, G. H. 2009, *PASP*, 121, 577

Martell, S. L., Smith, G. H., & Briley, M. M. 2008a, *PASP*, 120, 839

—. 2008b, *PASP*, 120, 7

—. 2008c, *AJ*, 136, 2522

McLaughlin, D. E., & van der Marel, R. P. 2005, *ApJS*, 161, 304

- Norris, J. 1987, *ApJ*, 313, L65
- Norris, J., Cottrell, P. L., Freeman, K. C., & Da Costa, G. S. 1981, *ApJ*, 244, 205
- Norris, J., & Freeman, K. C. 1979, *ApJ*, 230, L179
- Norris, J., & Smith, G. H. 1984, *ApJ*, 287, 255
- Osborn, W. 1971, *The Observatory*, 91, 223
- Pancino, E., Rejkuba, M., Zoccali, M., & Carrera, R. 2010, *A&A*, 524, A44+
- Peterson, R. C. 1980, *ApJ*, 237, L87
- Pier, J. R., Munn, J. A., Hindsley, R. B., Hennessy, G. S., Kent, S. M., Lupton, R. H., & Ivezić, Ž. 2003, *AJ*, 125, 1559
- Piotto, G., et al. 2007, *ApJ*, 661, L53
- Schlegel, D. J., Finkbeiner, D. P., & Davis, M. 1998, *ApJ*, 500, 525
- Shetrone, M., Martell, S. L., Wilkerson, R., Adams, J., Siegel, M. H., Smith, G. H., & Bond, H. E. 2010, *AJ*, 140, 1119
- Shetrone, M. D. 2003, *ApJ*, 585, L45
- Smith, G. H., & Mateo, M. 1990, *ApJ*, 353, 533
- Smith, G. H., & Norris, J. 1982, *ApJ*, 254, 149
- Smith, G. H., Shetrone, M. D., Bell, R. A., Churchill, C. W., & Briley, M. M. 1996, *AJ*, 112, 1511
- Smolinski, J. P., et al. 2011, *AJ*, 141, 89
- Stoughton, C., et al. 2002, *AJ*, 123, 485

Suntzeff, N. B. 1981, ApJS, 47, 1

Sweigart, A. V., & Mengel, J. G. 1979, ApJ, 229, 624

Thomas, H. 1967, ZAp, 67, 420

Trefzger, D. V., Langer, G. E., Carbon, D. F., Suntzeff, N. B., & Kraft, R. P. 1983, ApJ,
266, 144

Yanny, B., et al. 2009, AJ, 137, 4377

York, D. G., et al. 2000, AJ, 120, 1579

Table 1. Globular Cluster Photometric Properties

| Cluster | | RA (J2000) | Dec (J2000) | (l, b) | $(m - M)_0^a$ | $E(B - V)^b$ | r_t^a (arcmin) |
|----------|-----|-------------|-------------|----------------|---------------|--------------------|---------------------|
| NGC 6341 | M92 | 17:17:07.39 | +43:08:09.4 | (68.3, +34.9) | 14.64 | 0.023 | 15.17 |
| NGC 7078 | M15 | 21:29:58.33 | +12:10:01.2 | (65.0, -27.3) | 15.37 | 0.110 | 21.50 |
| NGC 5053 | | 13:16:27.09 | +17:42:00.9 | (335.7, +78.9) | 16.12 | 0.017 | 13.67 |
| NGC 5024 | M53 | 13:12:55.25 | +18:10:05.4 | (333.0, +79.8) | 16.25 | 0.021 | 21.75 |
| NGC 7089 | M2 | 21:33:27.02 | -00:49:23.7 | (58.4, -35.8) | 15.49 | 0.045 | 21.45 |
| NGC 6205 | M13 | 16:41:41.24 | +36:27:35.5 | (59.0, +40.9) | 14.48 | 0.017 | 25.18 |
| NGC 5272 | M3 | 13:42:11.62 | +28:22:38.2 | (42.2, +78.7) | 14.95 | 0.013 | 38.19 |
| NGC 6838 | M71 | 19:53:46.49 | +18:46:45.1 | (56.7, -4.6) | 12.86 | 0.275 ^c | 8.96 |

Note. — Photometric properties of the globular clusters in our sample as drawn from the literature. The parameter r_t is the tidal radius in arcminutes. The listed distance modulus $(m - M)_0$ is extinction corrected. Note that the Harris values have been updated from <http://www.physics.mcmaster.ca/~harris/mwgc.dat>. References: ^a Harris (1996); ^b Schlegel et al. (1998); ^c Grundahl et al. (2002).

Table 2. Globular Cluster Spectroscopic and Physical Properties

| Cluster | [Fe/H] ^a | [Fe/H] _C | V_r^a (km s ⁻¹) | $\log(\frac{M}{M_\odot})$ (dex) | R_{gc}^a (kpc) | C^a | σ^a (km s ⁻¹) | ε^a |
|----------|---------------------|---------------------|----------------------------------|------------------------------------|---------------------|-------|-------------------------------------|-----------------|
| M92 | -2.31 | -2.35 | -120.0 | 5.43 ^b | 9.6 | 1.68 | 6.0 | 0.10 |
| M15 | -2.37 | -2.33 | -107.0 | 5.84 ^c | 10.4 | 2.28 | 13.5 | 0.05 |
| NGC 5053 | -2.27 | -2.30 | +44.0 | 4.80 ^b | 17.8 | 0.74 | 1.4 | 0.21 |
| M53 | -2.10 | -2.06 | -62.9 | 5.65 ^b | 18.4 | 1.72 | 4.4 | 0.01 |
| M2 | -1.65 | -1.66 | -5.3 | 5.84 ^b | 10.4 | 1.59 | 8.2 | 0.11 |
| M13 | -1.53 | -1.58 | -244.2 | 5.57 ^b | 8.4 | 1.53 | 7.1 | 0.11 |
| M3 | -1.50 | -1.50 | -147.6 | 5.58 ^b | 12.0 | 1.89 | 5.5 | 0.04 |
| M71 | -0.78 | -0.82 | -22.8 | 4.29 ^c | 6.7 | 1.15 | 2.3 | 0.00 |

Note. — Spectroscopic and physical properties of the globular clusters in our sample as drawn from the literature. The parameter [Fe/H]_C is from the recalibrated globular cluster metallicity scale of Carretta et al. (2009a). Distance from Galactic center R_{gc} calculated assuming $R_0 = 8.0$ kpc. Central concentration C derived from a King model where $C = \log(r_t/r_c)$. ^c Mandushev et al. (1991). Note that the Harris values have been updated from <http://www.physics.mcmaster.ca/~harris/mwgc.dat>.

References: ^a Harris (1996); ^b McLaughlin & van der Marel (2005);

Table 3. Line Indices of Adopted True Member Stars

| spSpec name | $(g-r)_0$ | g | σ_g | S(3839) | $\sigma_{S(3839)}$ | $\delta S(3839)$ | CH(4300) _L | $\sigma_{CH(4300)}$ | Type |
|----------------|-----------|--------|------------|---------|--------------------|------------------|-----------------------|---------------------|------|
| (1) | (2) | (3) | (4) | (5) | (6) | (7) | (8) | (9) | (10) |
| M92 | | | | | | | | | |
| 2247-54169-362 | 0.441 | 17.343 | 0.011 | -0.172 | 0.031 | 0.022 | -0.489 | 0.013 | RGB |
| 2247-54169-364 | 0.456 | 16.533 | 0.015 | -0.196 | 0.015 | -0.020 | -0.466 | 0.008 | RGB |
| 2247-54169-367 | 0.439 | 16.519 | 0.009 | -0.169 | 0.018 | 0.006 | -0.460 | 0.008 | RGB |
| 2247-54169-380 | 0.484 | 16.093 | 0.010 | -0.187 | 0.016 | -0.021 | -0.450 | 0.008 | RGB |
| 2247-54169-404 | 0.455 | 16.503 | 0.010 | -0.165 | 0.016 | 0.010 | -0.504 | 0.009 | RGB |
| 2247-54169-444 | 0.467 | 16.006 | 0.011 | -0.184 | 0.010 | -0.020 | -0.453 | 0.006 | RGB |
| 2247-54169-451 | 0.472 | 16.188 | 0.008 | -0.133 | 0.013 | 0.035 | -0.479 | 0.007 | RGB |
| 2247-54169-452 | 0.480 | 15.985 | 0.009 | -0.142 | 0.014 | 0.021 | -0.497 | 0.006 | RGB |
| 2247-54169-529 | 0.440 | 17.182 | 0.008 | -0.176 | 0.028 | 0.015 | -0.483 | 0.010 | RGB |
| 2247-54169-531 | 0.443 | 16.488 | 0.007 | -0.170 | 0.019 | 0.005 | -0.459 | 0.008 | RGB |
| 2247-54169-546 | 0.408 | 17.107 | 0.007 | -0.076 | 0.025 | 0.113 | -0.492 | 0.011 | RGB |
| 2247-54169-561 | 0.479 | 16.490 | 0.010 | -0.194 | 0.020 | -0.020 | -0.456 | 0.007 | RGB |
| 2247-54169-573 | 0.447 | 16.016 | 0.013 | -0.189 | 0.012 | -0.025 | -0.441 | 0.006 | RGB |
| 2247-54169-581 | 0.457 | 16.373 | 0.007 | -0.178 | 0.018 | -0.006 | -0.490 | 0.009 | RGB |
| 2247-54169-589 | 0.457 | 17.007 | 0.010 | -0.200 | 0.025 | -0.014 | -0.478 | 0.012 | RGB |
| 2247-54169-620 | 0.405 | 17.503 | 0.005 | -0.179 | 0.033 | 0.019 | -0.494 | 0.013 | RGB |
| 2247-54169-408 | 0.521 | 15.333 | 0.010 | -0.132 | 0.009 | 0.016 | -0.473 | 0.005 | RGB |
| 2247-54169-418 | 0.527 | 15.524 | 0.008 | -0.199 | 0.009 | -0.046 | -0.428 | 0.004 | RGB |
| 2247-54169-449 | 0.479 | 15.490 | 0.006 | -0.111 | 0.010 | 0.040 | -0.478 | 0.006 | RGB |
| 2247-54169-484 | 0.601 | 15.117 | 0.011 | -0.117 | 0.008 | 0.026 | -0.428 | 0.005 | RGB |
| 2247-54169-504 | 0.518 | 15.125 | 0.011 | -0.134 | 0.010 | 0.009 | -0.452 | 0.005 | RGB |
| 2247-54169-563 | 0.533 | 15.492 | 0.007 | -0.148 | 0.009 | 0.003 | -0.436 | 0.005 | RGB |
| 2247-54169-608 | 0.531 | 15.383 | 0.003 | -0.215 | 0.011 | -0.066 | -0.421 | 0.006 | RGB |
| 2247-54169-610 | 0.538 | 15.198 | 0.004 | -0.143 | 0.009 | 0.002 | -0.417 | 0.005 | RGB |
| 2247-54169-379 | 0.189 | 17.638 | 0.011 | -0.254 | 0.033 | -0.053 | -0.511 | 0.013 | SGB |
| 2247-54169-458 | 0.365 | 17.845 | 0.010 | -0.209 | 0.035 | -0.003 | -0.494 | 0.016 | SGB |
| 2247-54169-514 | 0.372 | 17.645 | 0.021 | -0.073 | 0.029 | 0.128 | -0.507 | 0.013 | SGB |
| 2247-54169-516 | 0.363 | 17.860 | 0.016 | -0.165 | 0.033 | 0.041 | -0.523 | 0.015 | SGB |
| 2247-54169-519 | 0.379 | 17.809 | 0.018 | -0.164 | 0.043 | 0.040 | -0.465 | 0.018 | SGB |
| 2247-54169-538 | 0.306 | 17.966 | 0.007 | -0.135 | 0.044 | 0.074 | -0.521 | 0.021 | SGB |

Table 3—Continued

| spSpec name | $(g-r)_0$ | g | σ_g | S(3839) | $\sigma_{S(3839)}$ | $\delta S(3839)$ | CH(4300) _L | $\sigma_{CH(4300)}$ | Type |
|----------------|-----------|--------|------------|---------|--------------------|------------------|-----------------------|---------------------|------|
| (1) | (2) | (3) | (4) | (5) | (6) | (7) | (8) | (9) | (10) |
| 2247-54169-541 | 0.387 | 17.691 | 0.009 | -0.121 | 0.035 | 0.081 | -0.514 | 0.016 | SGB |
| 2247-54169-575 | 0.360 | 17.882 | 0.006 | -0.248 | 0.047 | -0.042 | -0.496 | 0.021 | SGB |
| 2247-54169-584 | 0.367 | 17.789 | 0.006 | -0.275 | 0.043 | -0.071 | -0.529 | 0.016 | SGB |
| 2247-54169-616 | 0.366 | 17.890 | 0.008 | -0.263 | 0.040 | -0.057 | -0.521 | 0.016 | SGB |
| 2256-53859-513 | 0.372 | 17.645 | 0.021 | -0.142 | 0.021 | 0.059 | -0.517 | 0.011 | SGB |
| 2256-53859-522 | 0.270 | 18.084 | 0.012 | -0.228 | 0.031 | -0.017 | -0.550 | 0.014 | SGB |
| 2256-53859-535 | 0.204 | 18.349 | 0.009 | -0.270 | 0.032 | -0.053 | -0.549 | 0.014 | SGB |
| 2256-53859-536 | 0.225 | 18.395 | 0.013 | -0.255 | 0.027 | -0.036 | -0.531 | 0.015 | SGB |
| 2256-53859-538 | 0.386 | 17.762 | 0.006 | -0.187 | 0.022 | 0.017 | -0.490 | 0.011 | SGB |
| 2247-54169-409 | 0.314 | 20.443 | 0.022 | -0.282 | 0.045 | -0.016 | -0.561 | 0.022 | MS |
| 2256-53859-411 | 0.240 | 18.413 | 0.012 | -0.285 | 0.037 | -0.066 | -0.534 | 0.016 | MS |
| 2256-53859-455 | 0.205 | 18.576 | 0.014 | -0.245 | 0.033 | -0.022 | -0.564 | 0.017 | MS |
| 2256-53859-485 | 0.191 | 19.103 | 0.018 | -0.253 | 0.057 | -0.018 | -0.544 | 0.023 | MS |
| 2256-53859-489 | 0.182 | 18.749 | 0.011 | -0.310 | 0.059 | -0.084 | -0.544 | 0.026 | MS |
| 2256-53859-501 | 0.189 | 18.751 | 0.010 | -0.329 | 0.042 | -0.102 | -0.523 | 0.016 | MS |
| 2256-53859-506 | 0.207 | 18.794 | 0.016 | -0.230 | 0.044 | -0.003 | -0.565 | 0.020 | MS |
| 2256-53859-530 | 0.200 | 18.682 | 0.008 | -0.180 | 0.039 | 0.045 | -0.518 | 0.020 | MS |
| 2256-53859-537 | 0.211 | 19.293 | 0.012 | -0.277 | 0.043 | -0.038 | -0.563 | 0.021 | MS |
| 2256-53859-539 | 0.210 | 18.874 | 0.009 | -0.174 | 0.041 | 0.056 | -0.511 | 0.019 | MS |
| 2256-53859-546 | 0.196 | 18.505 | 0.017 | -0.229 | 0.042 | -0.008 | -0.528 | 0.019 | MS |
| 2256-53859-566 | 0.231 | 18.824 | 0.012 | -0.249 | 0.045 | -0.021 | -0.522 | 0.021 | MS |
| 2256-53859-571 | 0.199 | 18.654 | 0.008 | -0.271 | 0.037 | -0.047 | -0.506 | 0.015 | MS |
| 2256-53859-575 | 0.162 | 18.591 | 0.009 | -0.246 | 0.041 | -0.023 | -0.570 | 0.019 | MS |
| 2256-53859-576 | 0.190 | 18.548 | 0.009 | -0.196 | 0.033 | 0.026 | -0.557 | 0.016 | MS |
| 2256-53859-579 | 0.210 | 18.810 | 0.014 | -0.303 | 0.040 | -0.075 | -0.532 | 0.020 | MS |
| 2256-53859-612 | 0.185 | 18.499 | 0.008 | -0.242 | 0.041 | -0.022 | -0.528 | 0.019 | MS |
| M15 | | | | | | | | | |
| 1960-53289-441 | 0.399 | 17.582 | 0.011 | -0.203 | 0.033 | -0.009 | -0.465 | 0.013 | RGB |
| 1960-53289-457 | 0.372 | 17.913 | 0.011 | -0.206 | 0.034 | -0.009 | -0.472 | 0.013 | RGB |
| 1960-53289-500 | 0.450 | 17.169 | 0.012 | -0.093 | 0.017 | 0.097 | -0.481 | 0.008 | RGB |
| 1960-53289-522 | 0.416 | 16.909 | 0.011 | -0.228 | 0.022 | -0.041 | -0.494 | 0.012 | RGB |

Table 3—Continued

| spSpec name | $(g-r)_0$ | g | σ_g | S(3839) | $\sigma_{S(3839)}$ | $\delta S(3839)$ | CH(4300) _L | $\sigma_{CH(4300)}$ | Type |
|----------------|-----------|--------|------------|---------|--------------------|------------------|-----------------------|---------------------|------|
| (1) | (2) | (3) | (4) | (5) | (6) | (7) | (8) | (9) | (10) |
| 1960-53289-530 | 0.445 | 17.485 | 0.015 | -0.211 | 0.025 | -0.018 | -0.393 | 0.010 | RGB |
| 1962-53321-364 | 0.392 | 17.583 | 0.014 | -0.167 | 0.014 | 0.027 | -0.489 | 0.007 | RGB |
| 1962-53321-375 | 0.393 | 17.758 | 0.008 | -0.193 | 0.016 | 0.003 | -0.497 | 0.007 | RGB |
| 1962-53321-376 | 0.396 | 17.515 | 0.009 | -0.221 | 0.014 | -0.027 | -0.473 | 0.007 | RGB |
| 1962-53321-402 | 0.372 | 17.913 | 0.011 | -0.264 | 0.021 | -0.067 | -0.481 | 0.008 | RGB |
| 1962-53321-403 | 0.383 | 17.887 | 0.011 | -0.184 | 0.022 | 0.013 | -0.488 | 0.009 | RGB |
| 1962-53321-406 | 0.383 | 17.944 | 0.014 | -0.210 | 0.018 | -0.012 | -0.523 | 0.009 | RGB |
| 1962-53321-413 | 0.384 | 17.556 | 0.011 | -0.183 | 0.015 | 0.010 | -0.489 | 0.007 | RGB |
| 1962-53321-415 | 0.394 | 17.419 | 0.014 | -0.155 | 0.012 | 0.038 | -0.511 | 0.006 | RGB |
| 1962-53321-427 | 0.394 | 17.643 | 0.013 | -0.179 | 0.014 | 0.016 | -0.484 | 0.007 | RGB |
| 1962-53321-438 | 0.422 | 17.546 | 0.015 | -0.186 | 0.014 | 0.008 | -0.483 | 0.006 | RGB |
| 1962-53321-454 | 0.399 | 17.582 | 0.011 | -0.196 | 0.016 | -0.001 | -0.485 | 0.007 | RGB |
| 1962-53321-466 | 0.416 | 17.520 | 0.010 | -0.198 | 0.014 | -0.005 | -0.480 | 0.005 | RGB |
| 1962-53321-474 | 0.391 | 17.449 | 0.015 | -0.194 | 0.014 | -0.002 | -0.485 | 0.006 | RGB |
| 1962-53321-506 | 0.416 | 17.378 | 0.009 | -0.207 | 0.011 | -0.015 | -0.448 | 0.006 | RGB |
| 1962-53321-515 | 0.443 | 17.568 | 0.010 | -0.219 | 0.014 | -0.025 | -0.474 | 0.006 | RGB |
| 1962-53321-532 | 0.382 | 17.487 | 0.012 | -0.191 | 0.013 | 0.002 | -0.510 | 0.005 | RGB |
| 1960-53289-401 | 0.485 | 16.078 | 0.008 | -0.207 | 0.009 | -0.028 | -0.442 | 0.005 | RGB |
| 1960-53289-402 | 0.552 | 15.391 | 0.008 | -0.113 | 0.008 | 0.059 | -0.411 | 0.004 | RGB |
| 1960-53289-406 | 0.552 | 15.393 | 0.007 | -0.153 | 0.007 | 0.020 | -0.446 | 0.004 | RGB |
| 1960-53289-413 | 0.508 | 15.687 | 0.007 | -0.186 | 0.009 | -0.011 | -0.464 | 0.005 | RGB |
| 1960-53289-419 | 0.542 | 15.433 | 0.008 | -0.208 | 0.007 | -0.035 | -0.434 | 0.004 | RGB |
| 1960-53289-442 | 0.487 | 16.342 | 0.008 | -0.238 | 0.015 | -0.056 | -0.437 | 0.006 | RGB |
| 1960-53289-459 | 0.515 | 15.076 | 0.009 | -0.208 | 0.006 | -0.039 | -0.515 | 0.003 | RGB |
| 1960-53289-460 | 0.465 | 16.431 | 0.009 | -0.221 | 0.012 | -0.038 | -0.471 | 0.007 | RGB |
| 1960-53289-511 | 0.509 | 16.568 | 0.009 | -0.189 | 0.014 | -0.005 | -0.505 | 0.007 | RGB |
| 1960-53289-523 | 0.643 | 14.624 | 0.009 | -0.159 | 0.008 | 0.005 | -0.426 | 0.004 | RGB |
| 1960-53289-529 | 0.521 | 15.513 | 0.010 | -0.130 | 0.007 | 0.043 | -0.483 | 0.004 | RGB |
| 1960-53289-420 | 0.362 | 18.421 | 0.011 | -0.201 | 0.040 | 0.002 | -0.525 | 0.017 | SGB |
| 1960-53289-501 | 0.398 | 18.283 | 0.011 | -0.215 | 0.039 | -0.013 | -0.553 | 0.016 | SGB |
| 1962-53321-323 | 0.269 | 18.400 | 0.016 | -0.272 | 0.023 | -0.070 | -0.523 | 0.009 | SGB |

Table 3—Continued

| spSpec name | $(g-r)_0$ | g | σ_g | S(3839) | $\sigma_{S(3839)}$ | $\delta S(3839)$ | CH(4300) _L | $\sigma_{CH(4300)}$ | Type |
|----------------|-----------|--------|------------|---------|--------------------|------------------|-----------------------|---------------------|------|
| (1) | (2) | (3) | (4) | (5) | (6) | (7) | (8) | (9) | (10) |
| 1962-53321-328 | 0.205 | 18.655 | 0.014 | -0.271 | 0.026 | -0.067 | -0.530 | 0.013 | SGB |
| 1962-53321-329 | 0.269 | 18.522 | 0.011 | -0.250 | 0.025 | -0.047 | -0.551 | 0.012 | SGB |
| 1962-53321-335 | 0.301 | 18.411 | 0.014 | -0.274 | 0.024 | -0.072 | -0.516 | 0.009 | SGB |
| 1962-53321-368 | 0.227 | 18.553 | 0.014 | -0.247 | 0.026 | -0.043 | -0.515 | 0.012 | SGB |
| 1962-53321-369 | 0.241 | 18.589 | 0.016 | -0.300 | 0.031 | -0.096 | -0.543 | 0.012 | SGB |
| 1962-53321-370 | 0.279 | 18.453 | 0.015 | -0.274 | 0.022 | -0.071 | -0.542 | 0.011 | SGB |
| 1962-53321-371 | 0.254 | 18.507 | 0.017 | -0.234 | 0.029 | -0.031 | -0.522 | 0.012 | SGB |
| 1962-53321-372 | 0.285 | 18.371 | 0.012 | -0.229 | 0.022 | -0.027 | -0.511 | 0.011 | SGB |
| 1962-53321-407 | 0.226 | 18.444 | 0.013 | -0.260 | 0.029 | -0.057 | -0.526 | 0.013 | SGB |
| 1962-53321-414 | 0.275 | 18.472 | 0.017 | -0.287 | 0.025 | -0.084 | -0.519 | 0.011 | SGB |
| 1962-53321-421 | 0.338 | 18.371 | 0.015 | -0.266 | 0.027 | -0.064 | -0.473 | 0.012 | SGB |
| 1962-53321-423 | 0.363 | 18.205 | 0.013 | -0.125 | 0.022 | 0.076 | -0.466 | 0.009 | SGB |
| 1962-53321-442 | 0.178 | 18.727 | 0.015 | -0.226 | 0.034 | -0.020 | -0.550 | 0.013 | SGB |
| 1962-53321-469 | 0.189 | 18.634 | 0.013 | -0.258 | 0.024 | -0.054 | -0.531 | 0.012 | SGB |
| 1962-53321-470 | 0.235 | 18.633 | 0.017 | -0.248 | 0.022 | -0.044 | -0.536 | 0.011 | SGB |
| 1962-53321-488 | 0.283 | 18.642 | 0.020 | -0.256 | 0.029 | -0.051 | -0.530 | 0.012 | SGB |
| 1962-53321-493 | 0.367 | 18.324 | 0.013 | -0.218 | 0.020 | -0.016 | -0.517 | 0.009 | SGB |
| 1962-53321-495 | 0.254 | 18.787 | 0.015 | -0.300 | 0.030 | -0.094 | -0.523 | 0.011 | SGB |
| 1962-53321-496 | 0.237 | 18.773 | 0.015 | -0.258 | 0.026 | -0.052 | -0.512 | 0.014 | SGB |
| 1962-53321-497 | 0.181 | 18.769 | 0.015 | -0.248 | 0.030 | -0.042 | -0.539 | 0.013 | SGB |
| 1962-53321-500 | 0.256 | 18.396 | 0.013 | -0.253 | 0.020 | -0.051 | -0.525 | 0.009 | SGB |
| 1962-53321-510 | 0.291 | 18.529 | 0.012 | -0.246 | 0.023 | -0.042 | -0.522 | 0.010 | SGB |
| 1962-53321-516 | 0.398 | 18.283 | 0.011 | -0.253 | 0.022 | -0.052 | -0.526 | 0.009 | SGB |
| 1962-53321-518 | 0.361 | 18.253 | 0.011 | -0.239 | 0.019 | -0.039 | -0.504 | 0.008 | SGB |
| 1962-53321-520 | 0.276 | 18.619 | 0.013 | -0.282 | 0.023 | -0.077 | -0.530 | 0.010 | SGB |
| 1962-53321-533 | 0.275 | 18.638 | 0.012 | -0.279 | 0.023 | -0.074 | -0.517 | 0.010 | SGB |
| 1962-53321-549 | 0.296 | 18.326 | 0.028 | -0.285 | 0.022 | -0.083 | -0.528 | 0.010 | SGB |
| 1962-53321-550 | 0.362 | 18.421 | 0.011 | -0.282 | 0.021 | -0.079 | -0.530 | 0.009 | SGB |
| 1962-53321-558 | 0.289 | 18.344 | 0.010 | -0.257 | 0.020 | -0.056 | -0.530 | 0.009 | SGB |
| 1962-53321-339 | 0.138 | 19.041 | 0.019 | -0.330 | 0.036 | -0.122 | -0.550 | 0.015 | MS |
| 1962-53321-363 | 0.211 | 19.252 | 0.021 | -0.204 | 0.048 | 0.007 | -0.505 | 0.020 | MS |

Table 3—Continued

| spSpec name | $(g-r)_0$ | g | σ_g | S(3839) | $\sigma_{S(3839)}$ | $\delta S(3839)$ | CH(4300) _L | $\sigma_{CH(4300)}$ | Type |
|----------------|-----------|--------|------------|---------|--------------------|------------------|-----------------------|---------------------|------|
| (1) | (2) | (3) | (4) | (5) | (6) | (7) | (8) | (9) | (10) |
| 1962-53321-378 | 0.191 | 19.052 | 0.016 | -0.242 | 0.038 | -0.033 | -0.539 | 0.016 | MS |
| 1962-53321-399 | 0.196 | 18.831 | 0.017 | -0.307 | 0.032 | -0.100 | -0.537 | 0.014 | MS |
| 1962-53321-409 | 0.154 | 19.145 | 0.015 | -0.340 | 0.043 | -0.130 | -0.536 | 0.020 | MS |
| 1962-53321-412 | 0.174 | 18.872 | 0.016 | -0.315 | 0.044 | -0.108 | -0.514 | 0.017 | MS |
| 1962-53321-416 | 0.160 | 19.081 | 0.018 | -0.279 | 0.043 | -0.070 | -0.498 | 0.017 | MS |
| 1962-53321-419 | 0.181 | 19.268 | 0.017 | -0.288 | 0.048 | -0.077 | -0.540 | 0.022 | MS |
| 1962-53321-422 | 0.228 | 19.094 | 0.021 | -0.212 | 0.043 | -0.003 | -0.522 | 0.017 | MS |
| 1962-53321-424 | 0.170 | 18.952 | 0.018 | -0.348 | 0.034 | -0.140 | -0.515 | 0.017 | MS |
| 1962-53321-428 | 0.165 | 18.951 | 0.015 | -0.285 | 0.035 | -0.077 | -0.542 | 0.017 | MS |
| 1962-53321-430 | 0.204 | 19.211 | 0.019 | -0.279 | 0.042 | -0.068 | -0.521 | 0.020 | MS |
| 1962-53321-445 | 0.148 | 19.341 | 0.017 | -0.201 | 0.048 | 0.011 | -0.534 | 0.023 | MS |
| 1962-53321-449 | 0.196 | 19.374 | 0.023 | -0.315 | 0.056 | -0.103 | -0.518 | 0.022 | MS |
| 1962-53321-460 | 0.224 | 19.363 | 0.026 | -0.281 | 0.043 | -0.069 | -0.510 | 0.022 | MS |
| 1962-53321-465 | 0.145 | 18.942 | 0.015 | -0.273 | 0.032 | -0.066 | -0.527 | 0.015 | MS |
| 1962-53321-471 | 0.153 | 18.829 | 0.013 | -0.303 | 0.026 | -0.096 | -0.535 | 0.013 | MS |
| 1962-53321-478 | 0.224 | 19.724 | 0.024 | -0.265 | 0.067 | -0.049 | -0.497 | 0.025 | MS |
| 1962-53321-480 | 0.211 | 18.991 | 0.018 | -0.234 | 0.031 | -0.026 | -0.520 | 0.014 | MS |
| 1962-53321-483 | 0.206 | 19.211 | 0.016 | -0.297 | 0.050 | -0.086 | -0.515 | 0.021 | MS |
| 1962-53321-484 | 0.210 | 19.188 | 0.016 | -0.270 | 0.035 | -0.060 | -0.507 | 0.016 | MS |
| 1962-53321-490 | 0.258 | 18.893 | 0.015 | -0.257 | 0.030 | -0.050 | -0.520 | 0.012 | MS |
| 1962-53321-503 | 0.197 | 18.961 | 0.014 | -0.246 | 0.032 | -0.038 | -0.547 | 0.014 | MS |
| 1962-53321-505 | 0.161 | 19.488 | 0.016 | -0.240 | 0.047 | -0.027 | -0.520 | 0.020 | MS |
| 1962-53321-509 | 0.254 | 19.260 | 0.015 | -0.228 | 0.042 | -0.017 | -0.504 | 0.018 | MS |
| 1962-53321-512 | 0.248 | 19.508 | 0.017 | -0.322 | 0.051 | -0.108 | -0.493 | 0.021 | MS |
| 1962-53321-519 | 0.162 | 19.058 | 0.016 | -0.261 | 0.034 | -0.052 | -0.548 | 0.015 | MS |
| 1962-53321-522 | 0.155 | 19.128 | 0.016 | -0.209 | 0.051 | 0.001 | -0.568 | 0.020 | MS |
| 1962-53321-539 | 0.194 | 18.815 | 0.013 | -0.289 | 0.028 | -0.082 | -0.516 | 0.010 | MS |
| 1962-53321-540 | 0.194 | 19.401 | 0.016 | -0.281 | 0.040 | -0.068 | -0.520 | 0.018 | MS |
| 1962-53321-543 | 0.274 | 18.916 | 0.013 | -0.216 | 0.031 | -0.009 | -0.532 | 0.013 | MS |
| 1962-53321-545 | 0.299 | 19.107 | 0.014 | -0.332 | 0.032 | -0.122 | -0.530 | 0.014 | MS |
| 1962-53321-554 | 0.174 | 19.385 | 0.016 | -0.236 | 0.037 | -0.024 | -0.482 | 0.018 | MS |

Table 3—Continued

| spSpec name | $(g-r)_0$ | g | σ_g | S(3839) | $\sigma_{S(3839)}$ | $\delta S(3839)$ | CH(4300) _L | $\sigma_{CH(4300)}$ | Type |
|----------------|-----------|--------|------------|---------|--------------------|------------------|-----------------------|---------------------|------|
| (1) | (2) | (3) | (4) | (5) | (6) | (7) | (8) | (9) | (10) |
| 1962-53321-555 | 0.258 | 19.532 | 0.017 | −0.334 | 0.052 | −0.120 | −0.519 | 0.020 | MS |
| NGC 5053 | | | | | | | | | |
| 2476-53826-486 | 0.462 | 17.746 | 0.009 | −0.126 | 0.043 | 0.058 | −0.429 | 0.019 | RGB |
| 2476-53826-497 | 0.451 | 18.201 | 0.011 | −0.098 | 0.064 | 0.098 | −0.442 | 0.025 | RGB |
| 2476-53826-488 | 0.686 | 15.780 | 0.017 | −0.119 | 0.015 | 0.017 | −0.432 | 0.006 | RGB |
| 2476-53826-501 | 0.632 | 15.988 | 0.008 | −0.182 | 0.012 | −0.042 | −0.443 | 0.006 | RGB |
| 2476-53826-505 | 0.485 | 16.302 | 0.009 | −0.221 | 0.016 | −0.072 | −0.523 | 0.007 | RGB |
| 2476-53826-507 | 0.530 | 16.939 | 0.009 | −0.101 | 0.020 | 0.063 | −0.450 | 0.009 | RGB |
| 2476-53826-508 | 0.532 | 16.803 | 0.009 | −0.131 | 0.022 | 0.030 | −0.447 | 0.010 | RGB |
| 2476-53826-519 | 0.787 | 15.223 | 0.011 | −0.104 | 0.010 | 0.018 | −0.450 | 0.005 | RGB |
| 2476-53826-527 | 0.651 | 15.862 | 0.023 | −0.115 | 0.013 | 0.023 | −0.467 | 0.007 | RGB |
| 2476-53826-573 | 0.529 | 17.197 | 0.012 | −0.169 | 0.024 | 0.002 | −0.447 | 0.011 | RGB |
| 2476-53826-575 | 0.724 | 15.518 | 0.007 | −0.160 | 0.013 | −0.031 | −0.432 | 0.006 | RGB |
| 2476-53826-577 | 0.546 | 16.942 | 0.028 | −0.214 | 0.023 | −0.050 | −0.428 | 0.010 | RGB |
| 2476-53826-578 | 0.698 | 15.602 | 0.015 | −0.111 | 0.012 | 0.020 | −0.450 | 0.006 | RGB |
| M53 | | | | | | | | | |
| 2476-53826-329 | 0.503 | 17.999 | 0.027 | −0.258 | 0.068 | −0.036 | −0.429 | 0.025 | RGB |
| 2476-53826-405 | 0.494 | 18.055 | 0.017 | −0.049 | 0.078 | 0.175 | −0.377 | 0.032 | RGB |
| 2476-53826-413 | 0.535 | 17.791 | 0.017 | −0.188 | 0.062 | 0.029 | −0.444 | 0.019 | RGB |
| 2476-53826-418 | 0.504 | 18.063 | 0.017 | −0.032 | 0.079 | 0.192 | −0.465 | 0.028 | RGB |
| 2476-53826-361 | 0.638 | 16.908 | 0.018 | −0.166 | 0.037 | 0.026 | −0.359 | 0.014 | RGB |
| 2476-53826-372 | 0.546 | 16.868 | 0.018 | −0.209 | 0.025 | −0.017 | −0.450 | 0.013 | RGB |
| 2476-53826-375 | 0.544 | 17.094 | 0.018 | 0.041 | 0.041 | 0.239 | −0.435 | 0.014 | RGB |
| 2476-53826-378 | 0.618 | 16.225 | 0.018 | −0.159 | 0.018 | 0.016 | −0.457 | 0.006 | RGB |
| 2476-53826-401 | 0.531 | 17.438 | 0.017 | −0.154 | 0.039 | 0.053 | −0.369 | 0.017 | RGB |
| 2476-53826-404 | 0.749 | 15.836 | 0.018 | −0.011 | 0.018 | 0.153 | −0.431 | 0.007 | RGB |
| 2476-53826-409 | 0.508 | 17.321 | 0.017 | −0.052 | 0.044 | 0.152 | −0.419 | 0.017 | RGB |
| 2476-53826-451 | 0.602 | 16.775 | 0.019 | −0.257 | 0.029 | −0.068 | −0.367 | 0.014 | RGB |
| 2476-53826-452 | 0.503 | 17.369 | 0.017 | −0.192 | 0.042 | 0.013 | −0.387 | 0.017 | RGB |
| M2 | | | | | | | | | |
| 1961-53299-140 | 0.471 | 17.276 | 0.019 | −0.037 | 0.020 | 0.207 | −0.462 | 0.008 | RGB |

Table 3—Continued

| spSpec name | $(g - r)_0$ | g | σ_g | S(3839) | $\sigma_{S(3839)}$ | $\delta S(3839)$ | CH(4300) _L | $\sigma_{CH(4300)}$ | Type |
|----------------|-------------|--------|------------|---------|--------------------|------------------|-----------------------|---------------------|------|
| (1) | (2) | (3) | (4) | (5) | (6) | (7) | (8) | (9) | (10) |
| 1961-53299-213 | 0.467 | 17.182 | 0.008 | -0.032 | 0.019 | 0.206 | -0.463 | 0.008 | RGB |
| 1963-54331-098 | 0.495 | 17.576 | 0.015 | -0.065 | 0.021 | 0.199 | -0.438 | 0.007 | RGB |
| 1963-54331-121 | 0.487 | 17.536 | 0.013 | 0.018 | 0.018 | 0.280 | -0.453 | 0.006 | RGB |
| 1963-54331-126 | 0.451 | 18.287 | 0.023 | -0.063 | 0.033 | 0.247 | -0.449 | 0.013 | RGB |
| 1963-54331-128 | 0.470 | 18.253 | 0.022 | -0.006 | 0.032 | 0.302 | -0.422 | 0.012 | RGB |
| 1963-54331-131 | 0.457 | 18.210 | 0.012 | -0.011 | 0.032 | 0.294 | -0.441 | 0.011 | RGB |
| 1963-54331-137 | 0.475 | 17.895 | 0.008 | -0.172 | 0.022 | 0.113 | -0.413 | 0.010 | RGB |
| 1963-54331-139 | 0.483 | 17.919 | 0.008 | -0.147 | 0.025 | 0.139 | -0.414 | 0.010 | RGB |
| 1963-54331-144 | 0.471 | 17.663 | 0.016 | -0.211 | 0.020 | 0.059 | -0.393 | 0.008 | RGB |
| 1963-54331-164 | 0.434 | 18.434 | 0.022 | -0.178 | 0.029 | 0.142 | -0.432 | 0.013 | RGB |
| 1963-54331-178 | 0.423 | 18.477 | 0.016 | -0.164 | 0.037 | 0.158 | -0.408 | 0.014 | RGB |
| 1963-54331-204 | 0.488 | 17.953 | 0.011 | -0.255 | 0.023 | 0.033 | -0.394 | 0.009 | RGB |
| 1963-54331-208 | 0.461 | 17.815 | 0.009 | -0.245 | 0.022 | 0.034 | -0.418 | 0.009 | RGB |
| 1963-54331-209 | 0.412 | 18.339 | 0.012 | -0.106 | 0.027 | 0.207 | -0.450 | 0.012 | RGB |
| 1963-54331-211 | 0.463 | 18.346 | 0.011 | -0.116 | 0.028 | 0.198 | -0.430 | 0.011 | RGB |
| 1963-54331-217 | 0.461 | 17.824 | 0.009 | -0.059 | 0.019 | 0.221 | -0.456 | 0.010 | RGB |
| 1963-54331-218 | 0.451 | 17.963 | 0.008 | -0.158 | 0.023 | 0.131 | -0.444 | 0.011 | RGB |
| 1961-53299-124 | 0.598 | 16.087 | 0.020 | -0.184 | 0.013 | -0.017 | -0.358 | 0.005 | RGB |
| 1961-53299-125 | 0.592 | 15.997 | 0.006 | 0.175 | 0.011 | 0.336 | -0.378 | 0.005 | RGB |
| 1961-53299-131 | 0.555 | 16.680 | 0.008 | -0.219 | 0.013 | -0.014 | -0.372 | 0.008 | RGB |
| 1961-53299-134 | 0.701 | 15.105 | 0.015 | 0.174 | 0.008 | 0.277 | -0.397 | 0.004 | RGB |
| 1961-53299-136 | 0.529 | 16.913 | 0.011 | -0.243 | 0.019 | -0.022 | -0.378 | 0.008 | RGB |
| 1961-53299-144 | 0.470 | 16.940 | 0.008 | -0.003 | 0.017 | 0.219 | -0.464 | 0.008 | RGB |
| 1961-53299-152 | 0.570 | 16.618 | 0.022 | -0.037 | 0.014 | 0.164 | -0.415 | 0.006 | RGB |
| 1961-53299-159 | 0.492 | 16.866 | 0.009 | -0.028 | 0.018 | 0.189 | -0.452 | 0.007 | RGB |
| 1961-53299-215 | 0.581 | 16.353 | 0.009 | 0.026 | 0.013 | 0.211 | -0.392 | 0.005 | RGB |
| 1963-54331-043 | 0.394 | 18.766 | 0.027 | -0.128 | 0.043 | 0.213 | -0.496 | 0.015 | SGB |
| 1963-54331-083 | 0.342 | 18.907 | 0.015 | -0.204 | 0.041 | 0.147 | -0.514 | 0.019 | SGB |
| 1963-54331-090 | 0.354 | 18.869 | 0.014 | -0.167 | 0.035 | 0.181 | -0.466 | 0.016 | SGB |
| 1963-54331-091 | 0.496 | 18.520 | 0.026 | -0.287 | 0.040 | 0.038 | -0.422 | 0.014 | SGB |
| 1963-54331-096 | 0.326 | 18.954 | 0.013 | -0.087 | 0.040 | 0.267 | -0.504 | 0.017 | SGB |

Table 3—Continued

| spSpec name | $(g-r)_0$ | g | σ_g | S(3839) | $\sigma_{S(3839)}$ | $\delta S(3839)$ | CH(4300) _L | $\sigma_{CH(4300)}$ | Type |
|----------------|-----------|--------|------------|---------|--------------------|------------------|-----------------------|---------------------|------|
| (1) | (2) | (3) | (4) | (5) | (6) | (7) | (8) | (9) | (10) |
| 1963-54331-100 | 0.340 | 18.929 | 0.012 | -0.286 | 0.044 | 0.065 | -0.441 | 0.015 | SGB |
| 1963-54331-102 | 0.294 | 18.951 | 0.017 | -0.190 | 0.052 | 0.163 | -0.506 | 0.017 | SGB |
| 1963-54331-114 | 0.244 | 19.245 | 0.019 | -0.195 | 0.054 | 0.177 | -0.543 | 0.018 | SGB |
| 1963-54331-123 | 0.415 | 18.695 | 0.009 | -0.132 | 0.043 | 0.205 | -0.452 | 0.018 | SGB |
| 1963-54331-124 | 0.263 | 19.069 | 0.016 | -0.280 | 0.049 | 0.081 | -0.571 | 0.017 | SGB |
| 1963-54331-143 | 0.352 | 18.808 | 0.016 | -0.182 | 0.040 | 0.162 | -0.473 | 0.017 | SGB |
| 1963-54331-145 | 0.375 | 18.911 | 0.015 | -0.200 | 0.047 | 0.150 | -0.453 | 0.018 | SGB |
| 1963-54331-146 | 0.231 | 19.186 | 0.013 | -0.241 | 0.053 | 0.127 | -0.518 | 0.020 | SGB |
| 1963-54331-147 | 0.211 | 19.252 | 0.017 | -0.225 | 0.049 | 0.147 | -0.516 | 0.020 | SGB |
| 1963-54331-148 | 0.380 | 18.896 | 0.014 | -0.122 | 0.046 | 0.228 | -0.459 | 0.020 | SGB |
| 1963-54331-150 | 0.302 | 18.980 | 0.015 | -0.222 | 0.068 | 0.133 | -0.555 | 0.029 | SGB |
| 1963-54331-179 | 0.234 | 19.219 | 0.016 | -0.167 | 0.050 | 0.203 | -0.494 | 0.018 | SGB |
| 1963-54331-180 | 0.415 | 18.721 | 0.013 | -0.144 | 0.037 | 0.195 | -0.490 | 0.013 | SGB |
| 1963-54331-181 | 0.201 | 19.174 | 0.015 | -0.329 | 0.038 | 0.039 | -0.511 | 0.016 | SGB |
| 1963-54331-184 | 0.414 | 18.640 | 0.012 | -0.185 | 0.037 | 0.148 | -0.478 | 0.013 | SGB |
| 1963-54331-189 | 0.215 | 19.273 | 0.017 | -0.243 | 0.047 | 0.131 | -0.535 | 0.018 | SGB |
| 1963-54331-194 | 0.272 | 19.216 | 0.015 | -0.207 | 0.047 | 0.164 | -0.552 | 0.019 | SGB |
| 1963-54331-196 | 0.157 | 19.245 | 0.015 | -0.283 | 0.046 | 0.089 | -0.528 | 0.020 | SGB |
| 1963-54331-201 | 0.390 | 18.658 | 0.011 | -0.116 | 0.033 | 0.218 | -0.481 | 0.015 | SGB |
| 1963-54331-206 | 0.218 | 19.258 | 0.012 | -0.329 | 0.048 | 0.044 | -0.523 | 0.023 | SGB |
| 1963-54331-212 | 0.423 | 18.636 | 0.012 | -0.315 | 0.038 | 0.018 | -0.441 | 0.013 | SGB |
| 1963-54331-223 | 0.273 | 19.280 | 0.019 | -0.263 | 0.045 | 0.112 | -0.508 | 0.022 | SGB |
| 1963-54331-254 | 0.237 | 19.273 | 0.019 | -0.362 | 0.055 | 0.012 | -0.536 | 0.021 | SGB |
| 1963-54331-041 | 0.246 | 19.492 | 0.028 | -0.258 | 0.070 | -0.126 | -0.514 | 0.024 | MS |
| 1963-54331-045 | 0.214 | 19.350 | 0.027 | -0.144 | 0.055 | -0.022 | -0.562 | 0.019 | MS |
| 1963-54331-082 | 0.271 | 19.536 | 0.028 | -0.156 | 0.067 | -0.022 | -0.485 | 0.023 | MS |
| 1963-54331-154 | 0.224 | 19.588 | 0.023 | -0.226 | 0.067 | -0.088 | -0.554 | 0.025 | MS |
| 1963-54331-156 | 0.211 | 19.443 | 0.020 | -0.239 | 0.059 | -0.111 | -0.564 | 0.024 | MS |
| 1963-54331-162 | 0.200 | 19.585 | 0.022 | -0.161 | 0.069 | -0.023 | -0.537 | 0.025 | MS |
| 1963-54331-169 | 0.233 | 19.599 | 0.018 | -0.181 | 0.061 | -0.043 | -0.558 | 0.024 | MS |
| 1963-54331-170 | 0.166 | 19.483 | 0.017 | -0.252 | 0.059 | -0.121 | -0.563 | 0.022 | MS |

Table 3—Continued

| spSpec name | $(g-r)_0$ | g | σ_g | S(3839) | $\sigma_{S(3839)}$ | $\delta S(3839)$ | CH(4300) _L | $\sigma_{CH(4300)}$ | Type |
|----------------|-----------|--------|------------|---------|--------------------|------------------|-----------------------|---------------------|------|
| (1) | (2) | (3) | (4) | (5) | (6) | (7) | (8) | (9) | (10) |
| 1963-54331-185 | 0.201 | 19.507 | 0.018 | -0.329 | 0.059 | -0.197 | -0.527 | 0.022 | MS |
| 1963-54331-186 | 0.188 | 19.654 | 0.022 | -0.238 | 0.061 | -0.096 | -0.509 | 0.024 | MS |
| 1963-54331-197 | 0.203 | 19.581 | 0.019 | -0.183 | 0.061 | -0.046 | -0.553 | 0.022 | MS |
| 1963-54331-200 | 0.221 | 19.563 | 0.020 | -0.274 | 0.056 | -0.138 | -0.537 | 0.025 | MS |
| 1963-54331-207 | 0.230 | 19.495 | 0.015 | -0.187 | 0.067 | -0.055 | -0.558 | 0.022 | MS |
| 1963-54331-220 | 0.227 | 19.336 | 0.014 | -0.287 | 0.048 | -0.166 | -0.506 | 0.018 | MS |
| 1963-54331-222 | 0.199 | 19.344 | 0.017 | -0.233 | 0.049 | -0.111 | -0.508 | 0.021 | MS |
| M13 | | | | | | | | | |
| 2174-53521-087 | 0.462 | 17.258 | 0.016 | -0.117 | 0.026 | 0.100 | -0.431 | 0.010 | RGB |
| 2174-53521-094 | 0.464 | 17.245 | 0.016 | -0.270 | 0.022 | -0.053 | -0.409 | 0.008 | RGB |
| 2174-53521-121 | 0.543 | 16.227 | 0.011 | -0.031 | 0.013 | 0.167 | -0.437 | 0.006 | RGB |
| 2174-53521-126 | 0.478 | 17.014 | 0.013 | -0.048 | 0.019 | 0.164 | -0.487 | 0.009 | RGB |
| 2174-53521-128 | 0.458 | 17.480 | 0.008 | 0.181 | 0.041 | 0.402 | -0.445 | 0.013 | RGB |
| 2174-53521-133 | 0.495 | 16.876 | 0.008 | -0.075 | 0.017 | 0.135 | -0.424 | 0.007 | RGB |
| 2174-53521-134 | 0.452 | 17.284 | 0.011 | -0.190 | 0.019 | 0.028 | -0.422 | 0.010 | RGB |
| 2174-53521-155 | 0.514 | 16.521 | 0.007 | -0.008 | 0.016 | 0.196 | -0.431 | 0.007 | RGB |
| 2174-53521-407 | 0.518 | 16.612 | 0.009 | -0.215 | 0.011 | -0.010 | -0.394 | 0.006 | RGB |
| 2174-53521-412 | 0.506 | 17.467 | 0.016 | -0.051 | 0.023 | 0.169 | -0.489 | 0.009 | RGB |
| 2174-53521-414 | 0.547 | 17.456 | 0.016 | -0.091 | 0.018 | 0.129 | -0.442 | 0.009 | RGB |
| 2174-53521-456 | 0.463 | 17.371 | 0.014 | -0.075 | 0.019 | 0.144 | -0.473 | 0.008 | RGB |
| 2174-53521-461 | 0.465 | 17.359 | 0.009 | -0.216 | 0.020 | 0.003 | -0.408 | 0.010 | RGB |
| 2174-53521-471 | 0.538 | 16.278 | 0.006 | -0.113 | 0.011 | 0.086 | -0.406 | 0.006 | RGB |
| 2174-53521-480 | 0.489 | 16.899 | 0.009 | -0.124 | 0.016 | 0.086 | -0.415 | 0.007 | RGB |
| 2174-53521-529 | 0.520 | 16.474 | 0.020 | -0.216 | 0.011 | -0.013 | -0.381 | 0.006 | RGB |
| 2174-53521-563 | 0.516 | 16.408 | 0.015 | -0.119 | 0.013 | 0.083 | -0.397 | 0.006 | RGB |
| 2255-53565-114 | 0.466 | 17.080 | 0.012 | -0.097 | 0.019 | 0.117 | -0.467 | 0.009 | RGB |
| 2255-53565-116 | 0.540 | 16.291 | 0.009 | -0.132 | 0.013 | 0.068 | -0.396 | 0.005 | RGB |
| 2255-53565-437 | 0.454 | 17.471 | 0.009 | -0.122 | 0.025 | 0.099 | -0.467 | 0.010 | RGB |
| 2255-53565-476 | 0.469 | 17.172 | 0.009 | -0.082 | 0.021 | 0.133 | -0.426 | 0.009 | RGB |
| 2255-53565-490 | 0.514 | 16.279 | 0.007 | -0.049 | 0.009 | 0.151 | -0.429 | 0.005 | RGB |
| 2255-53565-556 | 0.464 | 17.253 | 0.007 | -0.076 | 0.018 | 0.141 | -0.462 | 0.007 | RGB |

Table 3—Continued

| spSpec name | $(g-r)_0$ | g | σ_g | S(3839) | $\sigma_{S(3839)}$ | $\delta S(3839)$ | CH(4300) _L | $\sigma_{CH(4300)}$ | Type |
|----------------|-----------|--------|------------|---------|--------------------|------------------|-----------------------|---------------------|------|
| (1) | (2) | (3) | (4) | (5) | (6) | (7) | (8) | (9) | (10) |
| 2255-53565-597 | 0.523 | 16.411 | 0.006 | -0.133 | 0.011 | 0.069 | -0.391 | 0.006 | RGB |
| 2174-53521-082 | 0.579 | 15.424 | 0.013 | 0.066 | 0.010 | 0.250 | -0.387 | 0.004 | RGB |
| 2174-53521-093 | 0.636 | 15.225 | 0.012 | -0.167 | 0.008 | 0.014 | -0.352 | 0.004 | RGB |
| 2174-53521-098 | 0.586 | 15.525 | 0.009 | -0.191 | 0.008 | -0.005 | -0.372 | 0.004 | RGB |
| 2174-53521-137 | 0.560 | 15.567 | 0.006 | 0.054 | 0.009 | 0.241 | -0.438 | 0.004 | RGB |
| 2174-53521-145 | 0.655 | 14.969 | 0.012 | -0.011 | 0.007 | 0.165 | -0.361 | 0.004 | RGB |
| 2174-53521-154 | 0.609 | 15.058 | 0.005 | 0.121 | 0.009 | 0.299 | -0.386 | 0.004 | RGB |
| 2174-53521-156 | 0.589 | 15.656 | 0.006 | 0.029 | 0.010 | 0.217 | -0.399 | 0.005 | RGB |
| 2174-53521-158 | 0.523 | 15.567 | 0.015 | 0.041 | 0.010 | 0.228 | -0.395 | 0.006 | RGB |
| 2174-53521-159 | 0.619 | 15.025 | 0.008 | 0.132 | 0.008 | 0.309 | -0.438 | 0.004 | RGB |
| 2174-53521-160 | 0.589 | 15.354 | 0.007 | 0.073 | 0.008 | 0.256 | -0.434 | 0.004 | RGB |
| 2174-53521-166 | 0.585 | 15.623 | 0.005 | -0.185 | 0.009 | 0.003 | -0.361 | 0.005 | RGB |
| 2174-53521-167 | 0.626 | 14.817 | 0.010 | 0.144 | 0.008 | 0.317 | -0.427 | 0.005 | RGB |
| 2174-53521-168 | 0.579 | 15.244 | 0.012 | 0.120 | 0.009 | 0.301 | -0.420 | 0.005 | RGB |
| 2174-53521-171 | 0.660 | 14.958 | 0.011 | -0.041 | 0.007 | 0.135 | -0.353 | 0.004 | RGB |
| 2174-53521-172 | 0.609 | 15.298 | 0.010 | 0.088 | 0.009 | 0.269 | -0.371 | 0.004 | RGB |
| 2174-53521-176 | 0.565 | 15.730 | 0.005 | -0.079 | 0.011 | 0.110 | -0.359 | 0.005 | RGB |
| 2174-53521-215 | 0.564 | 15.346 | 0.016 | -0.059 | 0.008 | 0.124 | -0.377 | 0.005 | RGB |
| 2174-53521-376 | 0.571 | 15.783 | 0.015 | 0.007 | 0.008 | 0.198 | -0.429 | 0.004 | RGB |
| 2174-53521-410 | 0.635 | 15.329 | 0.008 | 0.053 | 0.007 | 0.235 | -0.384 | 0.005 | RGB |
| 2174-53521-413 | 0.571 | 15.535 | 0.012 | 0.051 | 0.008 | 0.237 | -0.452 | 0.005 | RGB |
| 2174-53521-443 | 0.587 | 15.333 | 0.015 | 0.087 | 0.007 | 0.269 | -0.438 | 0.004 | RGB |
| 2174-53521-449 | 0.584 | 15.349 | 0.014 | 0.081 | 0.007 | 0.264 | -0.406 | 0.004 | RGB |
| 2174-53521-452 | 0.608 | 15.112 | 0.013 | -0.193 | 0.007 | -0.015 | -0.358 | 0.003 | RGB |
| 2174-53521-453 | 0.609 | 15.286 | 0.021 | -0.155 | 0.007 | 0.027 | -0.372 | 0.004 | RGB |
| 2174-53521-455 | 0.599 | 15.378 | 0.009 | 0.086 | 0.007 | 0.270 | -0.388 | 0.005 | RGB |
| 2174-53521-457 | 0.617 | 15.178 | 0.011 | 0.065 | 0.006 | 0.245 | -0.390 | 0.004 | RGB |
| 2174-53521-458 | 0.611 | 15.068 | 0.014 | 0.130 | 0.006 | 0.307 | -0.414 | 0.004 | RGB |
| 2174-53521-459 | 0.558 | 15.201 | 0.016 | 0.047 | 0.007 | 0.227 | -0.363 | 0.004 | RGB |
| 2174-53521-460 | 0.621 | 14.823 | 0.012 | 0.138 | 0.006 | 0.311 | -0.443 | 0.004 | RGB |
| 2174-53521-462 | 0.617 | 15.126 | 0.014 | -0.194 | 0.006 | -0.016 | -0.351 | 0.004 | RGB |

Table 3—Continued

| spSpec name | $(g-r)_0$ | g | σ_g | S(3839) | $\sigma_{S(3839)}$ | $\delta S(3839)$ | CH(4300) _L | $\sigma_{CH(4300)}$ | Type |
|----------------|-----------|--------|------------|---------|--------------------|------------------|-----------------------|---------------------|------|
| (1) | (2) | (3) | (4) | (5) | (6) | (7) | (8) | (9) | (10) |
| 2174-53521-463 | 0.576 | 15.630 | 0.005 | 0.076 | 0.010 | 0.264 | -0.420 | 0.004 | RGB |
| 2174-53521-470 | 0.624 | 14.850 | 0.007 | 0.138 | 0.006 | 0.312 | -0.403 | 0.004 | RGB |
| 2174-53521-476 | 0.544 | 15.727 | 0.008 | 0.334 | 0.008 | 0.523 | -0.367 | 0.005 | RGB |
| 2174-53521-477 | 0.634 | 15.217 | 0.006 | -0.153 | 0.008 | 0.027 | -0.352 | 0.005 | RGB |
| 2174-53521-478 | 0.580 | 15.422 | 0.008 | 0.069 | 0.008 | 0.253 | -0.430 | 0.005 | RGB |
| 2174-53521-483 | 0.609 | 15.141 | 0.013 | 0.077 | 0.007 | 0.256 | -0.382 | 0.004 | RGB |
| 2174-53521-484 | 0.629 | 15.187 | 0.015 | -0.018 | 0.007 | 0.162 | -0.365 | 0.004 | RGB |
| 2174-53521-485 | 0.549 | 15.489 | 0.016 | 0.044 | 0.007 | 0.229 | -0.449 | 0.004 | RGB |
| 2174-53521-488 | 0.573 | 15.725 | 0.013 | -0.060 | 0.008 | 0.129 | -0.373 | 0.005 | RGB |
| 2174-53521-489 | 0.604 | 15.576 | 0.009 | 0.083 | 0.009 | 0.270 | -0.435 | 0.004 | RGB |
| 2174-53521-493 | 0.604 | 15.088 | 0.024 | 0.042 | 0.006 | 0.220 | -0.407 | 0.003 | RGB |
| 2174-53521-494 | 0.620 | 15.143 | 0.019 | 0.092 | 0.007 | 0.271 | -0.435 | 0.004 | RGB |
| 2174-53521-495 | 0.573 | 15.998 | 0.015 | -0.110 | 0.009 | 0.085 | -0.396 | 0.005 | RGB |
| 2174-53521-497 | 0.628 | 15.410 | 0.009 | 0.100 | 0.008 | 0.283 | -0.422 | 0.004 | RGB |
| 2174-53521-498 | 0.600 | 15.122 | 0.006 | 0.023 | 0.007 | 0.202 | -0.376 | 0.004 | RGB |
| 2174-53521-499 | 0.607 | 15.089 | 0.014 | 0.135 | 0.007 | 0.313 | -0.416 | 0.004 | RGB |
| 2174-53521-500 | 0.602 | 15.302 | 0.011 | -0.169 | 0.006 | 0.013 | -0.365 | 0.004 | RGB |
| 2174-53521-522 | 0.584 | 15.503 | 0.010 | 0.083 | 0.008 | 0.269 | -0.417 | 0.004 | RGB |
| 2174-53521-530 | 0.620 | 15.287 | 0.004 | 0.112 | 0.007 | 0.294 | -0.393 | 0.004 | RGB |
| 2174-53521-531 | 0.615 | 15.229 | 0.006 | -0.196 | 0.008 | -0.016 | -0.354 | 0.004 | RGB |
| 2174-53521-537 | 0.532 | 15.965 | 0.007 | -0.033 | 0.007 | 0.161 | -0.396 | 0.004 | RGB |
| 2174-53521-538 | 0.630 | 15.042 | 0.003 | 0.079 | 0.006 | 0.256 | -0.382 | 0.005 | RGB |
| 2174-53521-542 | 0.616 | 15.276 | 0.010 | 0.092 | 0.007 | 0.273 | -0.383 | 0.004 | RGB |
| 2174-53521-554 | 0.562 | 15.843 | 0.009 | -0.022 | 0.008 | 0.169 | -0.409 | 0.004 | RGB |
| 2255-53565-112 | 0.636 | 15.225 | 0.012 | -0.184 | 0.045 | -0.003 | -0.347 | 0.021 | RGB |
| 2255-53565-120 | 0.586 | 15.525 | 0.009 | -0.175 | 0.008 | 0.010 | -0.374 | 0.005 | RGB |
| 2255-53565-143 | 0.544 | 15.959 | 0.011 | 0.006 | 0.010 | 0.199 | -0.415 | 0.005 | RGB |
| 2255-53565-144 | 0.523 | 15.567 | 0.015 | 0.019 | 0.009 | 0.206 | -0.397 | 0.004 | RGB |
| 2255-53565-148 | 0.557 | 15.819 | 0.007 | 0.096 | 0.010 | 0.287 | -0.412 | 0.005 | RGB |
| 2255-53565-153 | 0.564 | 15.684 | 0.008 | 0.050 | 0.010 | 0.238 | -0.415 | 0.004 | RGB |
| 2255-53565-157 | 0.623 | 15.107 | 0.007 | -0.188 | 0.007 | -0.010 | -0.347 | 0.003 | RGB |

Table 3—Continued

| spSpec name | $(g-r)_0$ | g | σ_g | S(3839) | $\sigma_{S(3839)}$ | $\delta S(3839)$ | CH(4300) _L | $\sigma_{CH(4300)}$ | Type |
|----------------|-----------|--------|------------|---------|--------------------|------------------|-----------------------|---------------------|------|
| (1) | (2) | (3) | (4) | (5) | (6) | (7) | (8) | (9) | (10) |
| 2255-53565-171 | 0.589 | 15.354 | 0.007 | 0.074 | 0.007 | 0.257 | -0.439 | 0.004 | RGB |
| 2255-53565-175 | 0.565 | 15.730 | 0.005 | -0.065 | 0.009 | 0.124 | -0.370 | 0.005 | RGB |
| 2255-53565-426 | 0.571 | 15.535 | 0.012 | 0.071 | 0.007 | 0.257 | -0.444 | 0.004 | RGB |
| 2255-53565-483 | 0.617 | 15.126 | 0.014 | -0.188 | 0.007 | -0.010 | -0.349 | 0.004 | RGB |
| 2255-53565-485 | 0.561 | 15.581 | 0.009 | 0.060 | 0.010 | 0.247 | -0.430 | 0.005 | RGB |
| 2255-53565-486 | 0.603 | 15.229 | 0.004 | 0.104 | 0.056 | 0.284 | -0.358 | 0.018 | RGB |
| 2255-53565-495 | 0.630 | 14.660 | 0.022 | -0.160 | 0.039 | 0.010 | -0.352 | 0.012 | RGB |
| 2255-53565-496 | 0.624 | 14.850 | 0.007 | 0.091 | 0.034 | 0.265 | -0.400 | 0.011 | RGB |
| 2255-53565-504 | 0.637 | 14.477 | 0.005 | -0.011 | 0.036 | 0.156 | -0.378 | 0.011 | RGB |
| 2255-53565-510 | 0.576 | 15.630 | 0.005 | 0.065 | 0.008 | 0.253 | -0.415 | 0.005 | RGB |
| 2255-53565-512 | 0.600 | 15.122 | 0.006 | 0.060 | 0.046 | 0.238 | -0.382 | 0.017 | RGB |
| 2255-53565-515 | 0.544 | 15.727 | 0.008 | 0.314 | 0.011 | 0.504 | -0.350 | 0.004 | RGB |
| 2255-53565-520 | 0.602 | 14.930 | 0.015 | 0.019 | 0.042 | 0.194 | -0.454 | 0.014 | RGB |
| 2255-53565-542 | 0.584 | 15.503 | 0.010 | 0.084 | 0.007 | 0.269 | -0.418 | 0.004 | RGB |
| 2255-53565-543 | 0.604 | 15.576 | 0.009 | 0.069 | 0.008 | 0.256 | -0.427 | 0.004 | RGB |
| 2255-53565-544 | 0.606 | 15.131 | 0.015 | 0.048 | 0.044 | 0.227 | -0.427 | 0.017 | RGB |
| 2255-53565-545 | 0.591 | 15.473 | 0.007 | 0.073 | 0.008 | 0.258 | -0.442 | 0.004 | RGB |
| 2255-53565-548 | 0.628 | 15.410 | 0.009 | 0.099 | 0.008 | 0.283 | -0.421 | 0.005 | RGB |
| 2255-53565-550 | 0.573 | 15.725 | 0.013 | -0.074 | 0.007 | 0.116 | -0.372 | 0.004 | RGB |
| 2255-53565-551 | 0.615 | 15.229 | 0.006 | -0.197 | 0.007 | -0.016 | -0.346 | 0.004 | RGB |
| 2255-53565-552 | 0.639 | 14.555 | 0.005 | 0.155 | 0.034 | 0.323 | -0.412 | 0.010 | RGB |
| 2255-53565-553 | 0.585 | 15.382 | 0.007 | 0.091 | 0.006 | 0.274 | -0.430 | 0.003 | RGB |
| 2255-53565-557 | 0.630 | 15.042 | 0.003 | 0.091 | 0.039 | 0.268 | -0.389 | 0.016 | RGB |
| 2255-53565-559 | 0.644 | 14.741 | 0.014 | 0.037 | 0.028 | 0.209 | -0.427 | 0.009 | RGB |
| 2255-53565-586 | 0.636 | 14.521 | 0.009 | -0.173 | 0.025 | -0.005 | -0.453 | 0.011 | RGB |
| 2255-53565-589 | 0.620 | 15.287 | 0.004 | 0.104 | 0.007 | 0.286 | -0.395 | 0.004 | RGB |
| 2174-53521-054 | 0.423 | 17.814 | 0.014 | -0.249 | 0.031 | -0.022 | -0.515 | 0.012 | SGB |
| 2174-53521-131 | 0.267 | 18.175 | 0.010 | -0.219 | 0.008 | 0.015 | -0.347 | 0.004 | SGB |
| 2174-53521-146 | 0.427 | 17.680 | 0.013 | -0.144 | 0.033 | 0.080 | -0.479 | 0.012 | SGB |
| 2174-53521-149 | 0.422 | 17.781 | 0.013 | -0.159 | 0.035 | 0.067 | -0.466 | 0.015 | SGB |
| 2174-53521-174 | 0.426 | 17.904 | 0.017 | -0.001 | 0.039 | 0.228 | -0.474 | 0.016 | SGB |

Table 3—Continued

| spSpec name | $(g-r)_0$ | g | σ_g | S(3839) | $\sigma_{S(3839)}$ | $\delta S(3839)$ | CH(4300) _L | $\sigma_{CH(4300)}$ | Type |
|----------------|-----------|--------|------------|---------|--------------------|------------------|-----------------------|---------------------|------|
| (1) | (2) | (3) | (4) | (5) | (6) | (7) | (8) | (9) | (10) |
| 2174-53521-368 | 0.461 | 17.507 | 0.016 | -0.230 | 0.023 | -0.009 | -0.433 | 0.011 | SGB |
| 2174-53521-402 | 0.412 | 17.810 | 0.009 | -0.193 | 0.027 | 0.034 | -0.441 | 0.012 | SGB |
| 2174-53521-403 | 0.373 | 17.981 | 0.010 | -0.142 | 0.028 | 0.088 | -0.492 | 0.012 | SGB |
| 2174-53521-406 | 0.406 | 17.893 | 0.008 | -0.157 | 0.022 | 0.072 | -0.465 | 0.012 | SGB |
| 2174-53521-445 | 0.403 | 17.893 | 0.011 | -0.131 | 0.026 | 0.098 | -0.500 | 0.011 | SGB |
| 2174-53521-447 | 0.443 | 17.683 | 0.011 | -0.123 | 0.025 | 0.101 | -0.477 | 0.011 | SGB |
| 2174-53521-474 | 0.459 | 17.612 | 0.008 | -0.128 | 0.022 | 0.096 | -0.452 | 0.010 | SGB |
| 2174-53521-481 | 0.408 | 17.867 | 0.010 | -0.129 | 0.039 | 0.099 | -0.462 | 0.014 | SGB |
| 2174-53521-533 | 0.437 | 17.797 | 0.009 | -0.181 | 0.030 | 0.046 | -0.465 | 0.012 | SGB |
| 2174-53521-539 | 0.473 | 17.657 | 0.007 | -0.203 | 0.021 | 0.022 | -0.399 | 0.012 | SGB |
| 2174-53521-560 | 0.528 | 17.547 | 0.008 | -0.150 | 0.019 | 0.072 | -0.445 | 0.009 | SGB |
| 2174-53521-565 | 0.422 | 17.915 | 0.008 | -0.255 | 0.020 | -0.026 | -0.451 | 0.013 | SGB |
| 2174-53521-573 | 0.369 | 17.961 | 0.014 | -0.254 | 0.026 | -0.025 | -0.427 | 0.012 | SGB |
| 2174-53521-576 | 0.449 | 17.672 | 0.007 | -0.120 | 0.022 | 0.105 | -0.428 | 0.011 | SGB |
| 2174-53521-577 | 0.421 | 17.902 | 0.009 | -0.172 | 0.024 | 0.056 | -0.447 | 0.012 | SGB |
| 2185-53532-141 | 0.227 | 18.392 | 0.019 | -0.249 | 0.020 | -0.012 | -0.525 | 0.008 | SGB |
| 2185-53532-153 | 0.379 | 18.098 | 0.015 | -0.241 | 0.015 | -0.009 | -0.494 | 0.006 | SGB |
| 2185-53532-237 | 0.286 | 18.063 | 0.017 | -0.243 | 0.018 | -0.011 | -0.523 | 0.007 | SGB |
| 2185-53532-388 | 0.240 | 18.283 | 0.016 | -0.270 | 0.015 | -0.035 | -0.524 | 0.007 | SGB |
| 2185-53532-425 | 0.262 | 18.304 | 0.022 | -0.241 | 0.014 | -0.005 | -0.539 | 0.007 | SGB |
| 2185-53532-426 | 0.336 | 18.012 | 0.016 | -0.192 | 0.013 | 0.038 | -0.509 | 0.006 | SGB |
| 2185-53532-427 | 0.350 | 18.001 | 0.016 | -0.178 | 0.013 | 0.052 | -0.522 | 0.006 | SGB |
| 2185-53532-439 | 0.278 | 18.125 | 0.016 | -0.232 | 0.012 | 0.001 | -0.520 | 0.006 | SGB |
| 2185-53532-461 | 0.234 | 18.368 | 0.010 | -0.241 | 0.014 | -0.005 | -0.546 | 0.006 | SGB |
| 2185-53532-462 | 0.273 | 18.194 | 0.018 | -0.232 | 0.014 | 0.001 | -0.519 | 0.006 | SGB |
| 2185-53532-481 | 0.270 | 18.195 | 0.008 | -0.262 | 0.014 | -0.028 | -0.523 | 0.006 | SGB |
| 2185-53532-482 | 0.311 | 18.100 | 0.008 | -0.236 | 0.015 | -0.004 | -0.514 | 0.007 | SGB |
| 2185-53532-487 | 0.271 | 18.319 | 0.010 | -0.255 | 0.016 | -0.019 | -0.529 | 0.007 | SGB |
| 2185-53532-492 | 0.285 | 18.167 | 0.015 | -0.263 | 0.011 | -0.030 | -0.520 | 0.006 | SGB |
| 2185-53532-493 | 0.219 | 18.347 | 0.013 | -0.248 | 0.013 | -0.011 | -0.522 | 0.007 | SGB |
| 2185-53532-506 | 0.372 | 18.036 | 0.012 | -0.184 | 0.012 | 0.047 | -0.502 | 0.006 | SGB |

Table 3—Continued

| spSpec name | $(g-r)_0$ | g | σ_g | S(3839) | $\sigma_{S(3839)}$ | $\delta S(3839)$ | CH(4300) _L | $\sigma_{CH(4300)}$ | Type |
|----------------|-----------|--------|------------|---------|--------------------|------------------|-----------------------|---------------------|------|
| (1) | (2) | (3) | (4) | (5) | (6) | (7) | (8) | (9) | (10) |
| 2185-53532-512 | 0.252 | 18.258 | 0.010 | -0.254 | 0.012 | -0.019 | -0.515 | 0.006 | SGB |
| 2185-53532-520 | 0.261 | 18.398 | 0.013 | -0.254 | 0.013 | -0.016 | -0.528 | 0.007 | SGB |
| 2185-53532-543 | 0.266 | 18.284 | 0.010 | -0.216 | 0.014 | 0.020 | -0.527 | 0.007 | SGB |
| 2185-53532-553 | 0.334 | 18.065 | 0.011 | -0.214 | 0.012 | 0.018 | -0.486 | 0.006 | SGB |
| 2185-53532-554 | 0.269 | 18.347 | 0.012 | -0.249 | 0.015 | -0.012 | -0.533 | 0.006 | SGB |
| 2255-53565-103 | 0.383 | 17.974 | 0.014 | -0.155 | 0.030 | 0.075 | -0.509 | 0.013 | SGB |
| 2255-53565-115 | 0.394 | 17.934 | 0.014 | -0.169 | 0.030 | 0.060 | -0.506 | 0.012 | SGB |
| 2255-53565-173 | 0.453 | 17.636 | 0.012 | -0.131 | 0.041 | 0.093 | -0.428 | 0.016 | SGB |
| 2255-53565-424 | 0.424 | 17.789 | 0.011 | -0.130 | 0.032 | 0.096 | -0.429 | 0.015 | SGB |
| 2255-53565-425 | 0.396 | 17.915 | 0.010 | -0.152 | 0.030 | 0.077 | -0.433 | 0.012 | SGB |
| 2255-53565-432 | 0.389 | 17.981 | 0.011 | -0.190 | 0.032 | 0.040 | -0.451 | 0.014 | SGB |
| 2255-53565-466 | 0.391 | 17.856 | 0.020 | -0.142 | 0.027 | 0.085 | -0.482 | 0.013 | SGB |
| 2185-53532-106 | 0.275 | 19.687 | 0.019 | -0.197 | 0.048 | 0.064 | -0.494 | 0.020 | MS |
| 2185-53532-111 | 0.242 | 18.572 | 0.016 | -0.259 | 0.028 | -0.018 | -0.541 | 0.011 | MS |
| 2185-53532-113 | 0.333 | 19.812 | 0.020 | -0.193 | 0.072 | 0.070 | -0.569 | 0.027 | MS |
| 2185-53532-116 | 0.258 | 19.363 | 0.018 | -0.252 | 0.041 | 0.003 | -0.506 | 0.016 | MS |
| 2185-53532-120 | 0.282 | 19.189 | 0.018 | -0.280 | 0.036 | -0.028 | -0.534 | 0.015 | MS |
| 2185-53532-143 | 0.245 | 18.517 | 0.018 | -0.186 | 0.022 | 0.053 | -0.520 | 0.010 | MS |
| 2185-53532-146 | 0.294 | 19.753 | 0.021 | -0.386 | 0.051 | -0.124 | -0.544 | 0.021 | MS |
| 2185-53532-148 | 0.251 | 18.997 | 0.016 | -0.262 | 0.024 | -0.013 | -0.538 | 0.011 | MS |
| 2185-53532-150 | 0.238 | 18.782 | 0.021 | -0.260 | 0.025 | -0.015 | -0.537 | 0.010 | MS |
| 2185-53532-151 | 0.279 | 19.422 | 0.018 | -0.158 | 0.038 | 0.098 | -0.535 | 0.016 | MS |
| 2185-53532-152 | 0.216 | 18.796 | 0.016 | -0.268 | 0.024 | -0.023 | -0.542 | 0.011 | MS |
| 2185-53532-154 | 0.267 | 19.689 | 0.020 | -0.238 | 0.052 | 0.023 | -0.510 | 0.018 | MS |
| 2185-53532-156 | 0.267 | 19.033 | 0.012 | -0.250 | 0.027 | -0.001 | -0.527 | 0.011 | MS |
| 2185-53532-158 | 0.252 | 18.930 | 0.013 | -0.257 | 0.024 | -0.010 | -0.558 | 0.012 | MS |
| 2185-53532-160 | 0.236 | 19.196 | 0.014 | -0.259 | 0.032 | -0.007 | -0.545 | 0.013 | MS |
| 2185-53532-161 | 0.260 | 19.647 | 0.015 | -0.286 | 0.048 | -0.026 | -0.471 | 0.024 | MS |
| 2185-53532-167 | 0.224 | 18.742 | 0.015 | -0.251 | 0.022 | -0.008 | -0.531 | 0.011 | MS |
| 2185-53532-169 | 0.251 | 19.007 | 0.016 | -0.305 | 0.027 | -0.056 | -0.541 | 0.012 | MS |
| 2185-53532-171 | 0.293 | 19.837 | 0.015 | -0.017 | 0.055 | 0.246 | -0.516 | 0.020 | MS |

Table 3—Continued

| spSpec name | $(g-r)_0$ | g | σ_g | S(3839) | $\sigma_{S(3839)}$ | $\delta S(3839)$ | CH(4300) _L | $\sigma_{CH(4300)}$ | Type |
|----------------|-----------|--------|------------|---------|--------------------|------------------|-----------------------|---------------------|------|
| (1) | (2) | (3) | (4) | (5) | (6) | (7) | (8) | (9) | (10) |
| 2185-53532-172 | 0.238 | 18.769 | 0.018 | -0.278 | 0.021 | -0.034 | -0.522 | 0.011 | MS |
| 2185-53532-175 | 0.187 | 18.804 | 0.011 | -0.277 | 0.026 | -0.032 | -0.529 | 0.010 | MS |
| 2185-53532-176 | 0.240 | 18.810 | 0.011 | -0.300 | 0.024 | -0.055 | -0.514 | 0.009 | MS |
| 2185-53532-177 | 0.217 | 18.859 | 0.010 | -0.294 | 0.024 | -0.048 | -0.522 | 0.010 | MS |
| 2185-53532-178 | 0.250 | 19.076 | 0.017 | -0.268 | 0.028 | -0.019 | -0.547 | 0.010 | MS |
| 2185-53532-179 | 0.229 | 18.436 | 0.018 | -0.262 | 0.018 | -0.024 | -0.527 | 0.008 | MS |
| 2185-53532-181 | 0.236 | 18.742 | 0.018 | -0.324 | 0.024 | -0.080 | -0.520 | 0.012 | MS |
| 2185-53532-196 | 0.270 | 19.028 | 0.018 | -0.258 | 0.033 | -0.009 | -0.522 | 0.013 | MS |
| 2185-53532-197 | 0.259 | 19.108 | 0.019 | -0.282 | 0.035 | -0.032 | -0.534 | 0.015 | MS |
| 2185-53532-198 | 0.262 | 18.883 | 0.018 | -0.276 | 0.025 | -0.029 | -0.523 | 0.009 | MS |
| 2185-53532-200 | 0.286 | 19.754 | 0.022 | -0.174 | 0.047 | 0.088 | -0.535 | 0.024 | MS |
| 2185-53532-390 | 0.263 | 19.372 | 0.018 | -0.263 | 0.045 | -0.008 | -0.517 | 0.019 | MS |
| 2185-53532-393 | 0.375 | 19.913 | 0.025 | -0.256 | 0.057 | 0.009 | -0.514 | 0.023 | MS |
| 2185-53532-423 | 0.243 | 18.879 | 0.017 | -0.278 | 0.018 | -0.032 | -0.534 | 0.010 | MS |
| 2185-53532-424 | 0.265 | 19.227 | 0.106 | -0.259 | 0.022 | -0.006 | -0.540 | 0.009 | MS |
| 2185-53532-428 | 0.276 | 19.180 | 0.018 | -0.235 | 0.028 | 0.016 | -0.513 | 0.011 | MS |
| 2185-53532-430 | 0.296 | 19.686 | 0.020 | -0.279 | 0.047 | -0.019 | -0.513 | 0.020 | MS |
| 2185-53532-431 | 0.288 | 19.867 | 0.018 | -0.244 | 0.052 | 0.020 | -0.505 | 0.020 | MS |
| 2185-53532-433 | 0.376 | 19.927 | 0.023 | -0.260 | 0.050 | 0.005 | -0.483 | 0.023 | MS |
| 2185-53532-435 | 0.245 | 19.031 | 0.011 | -0.242 | 0.027 | 0.007 | -0.519 | 0.013 | MS |
| 2185-53532-440 | 0.280 | 19.727 | 0.015 | -0.269 | 0.045 | -0.008 | -0.507 | 0.018 | MS |
| 2185-53532-464 | 0.276 | 19.434 | 0.018 | -0.261 | 0.036 | -0.005 | -0.523 | 0.015 | MS |
| 2185-53532-466 | 0.197 | 18.790 | 0.019 | -0.219 | 0.025 | 0.025 | -0.528 | 0.010 | MS |
| 2185-53532-469 | 0.233 | 18.983 | 0.010 | -0.283 | 0.031 | -0.035 | -0.523 | 0.014 | MS |
| 2185-53532-473 | 0.266 | 19.259 | 0.015 | -0.238 | 0.030 | 0.015 | -0.535 | 0.012 | MS |
| 2185-53532-475 | 0.292 | 18.585 | 0.017 | -0.257 | 0.020 | -0.016 | -0.515 | 0.008 | MS |
| 2185-53532-476 | 0.324 | 19.062 | 0.018 | -0.210 | 0.026 | 0.040 | -0.527 | 0.012 | MS |
| 2185-53532-477 | 0.311 | 19.570 | 0.019 | -0.203 | 0.043 | 0.056 | -0.503 | 0.016 | MS |
| 2185-53532-478 | 0.311 | 19.009 | 0.019 | -0.193 | 0.024 | 0.056 | -0.522 | 0.010 | MS |
| 2185-53532-479 | 0.331 | 19.447 | 0.018 | -0.259 | 0.037 | -0.003 | -0.535 | 0.014 | MS |
| 2185-53532-480 | 0.300 | 19.678 | 0.020 | -0.170 | 0.041 | 0.091 | -0.500 | 0.018 | MS |

Table 3—Continued

| spSpec name | $(g-r)_0$ | g | σ_g | S(3839) | $\sigma_{S(3839)}$ | $\delta S(3839)$ | CH(4300) _L | $\sigma_{CH(4300)}$ | Type |
|----------------|-----------|--------|------------|---------|--------------------|------------------|-----------------------|---------------------|------|
| (1) | (2) | (3) | (4) | (5) | (6) | (7) | (8) | (9) | (10) |
| 2185-53532-483 | 0.265 | 19.130 | 0.014 | -0.226 | 0.030 | 0.025 | -0.526 | 0.012 | MS |
| 2185-53532-485 | 0.230 | 18.446 | 0.011 | -0.284 | 0.012 | -0.046 | -0.528 | 0.007 | MS |
| 2185-53532-486 | 0.232 | 19.404 | 0.018 | -0.242 | 0.035 | 0.013 | -0.521 | 0.014 | MS |
| 2185-53532-488 | 0.270 | 19.547 | 0.019 | -0.214 | 0.040 | 0.044 | -0.535 | 0.017 | MS |
| 2185-53532-489 | 0.217 | 19.029 | 0.013 | -0.214 | 0.025 | 0.034 | -0.497 | 0.011 | MS |
| 2185-53532-490 | 0.270 | 19.343 | 0.016 | -0.202 | 0.029 | 0.053 | -0.520 | 0.015 | MS |
| 2185-53532-494 | 0.287 | 19.210 | 0.013 | -0.247 | 0.025 | 0.005 | -0.521 | 0.011 | MS |
| 2185-53532-495 | 0.230 | 18.657 | 0.012 | -0.261 | 0.018 | -0.019 | -0.534 | 0.009 | MS |
| 2185-53532-496 | 0.332 | 19.899 | 0.020 | -0.254 | 0.049 | 0.010 | -0.485 | 0.020 | MS |
| 2185-53532-497 | 0.320 | 19.585 | 0.025 | -0.193 | 0.037 | 0.066 | -0.486 | 0.017 | MS |
| 2185-53532-498 | 0.267 | 18.689 | 0.010 | -0.257 | 0.017 | -0.015 | -0.537 | 0.008 | MS |
| 2185-53532-499 | 0.229 | 18.733 | 0.015 | -0.253 | 0.021 | -0.009 | -0.540 | 0.009 | MS |
| 2185-53532-500 | 0.194 | 19.108 | 0.027 | -0.252 | 0.012 | -0.002 | -0.518 | 0.007 | MS |
| 2185-53532-504 | 0.225 | 18.726 | 0.021 | -0.258 | 0.017 | -0.014 | -0.508 | 0.008 | MS |
| 2185-53532-507 | 0.301 | 19.165 | 0.015 | -0.170 | 0.024 | 0.082 | -0.533 | 0.011 | MS |
| 2185-53532-508 | 0.167 | 18.999 | 0.014 | -0.190 | 0.022 | 0.058 | -0.522 | 0.010 | MS |
| 2185-53532-511 | 0.292 | 19.856 | 0.022 | -0.243 | 0.040 | 0.021 | -0.456 | 0.015 | MS |
| 2185-53532-513 | 0.272 | 18.920 | 0.012 | -0.252 | 0.020 | -0.005 | -0.508 | 0.010 | MS |
| 2185-53532-514 | 0.254 | 19.263 | 0.016 | -0.250 | 0.026 | 0.003 | -0.521 | 0.012 | MS |
| 2185-53532-515 | 0.236 | 18.936 | 0.013 | -0.250 | 0.021 | -0.003 | -0.540 | 0.011 | MS |
| 2185-53532-516 | 0.298 | 19.869 | 0.017 | -0.226 | 0.051 | 0.038 | -0.491 | 0.022 | MS |
| 2185-53532-517 | 0.315 | 19.904 | 0.019 | -0.187 | 0.043 | 0.078 | -0.469 | 0.020 | MS |
| 2185-53532-519 | 0.231 | 18.973 | 0.012 | -0.203 | 0.019 | 0.045 | -0.536 | 0.011 | MS |
| 2185-53532-534 | 0.281 | 18.601 | 0.019 | -0.241 | 0.015 | 0.000 | -0.525 | 0.008 | MS |
| 2185-53532-537 | 0.258 | 18.767 | 0.016 | -0.228 | 0.019 | 0.016 | -0.533 | 0.010 | MS |
| 2185-53532-539 | 0.278 | 19.508 | 0.021 | -0.217 | 0.038 | 0.040 | -0.494 | 0.014 | MS |
| 2185-53532-540 | 0.253 | 19.204 | 0.020 | -0.257 | 0.030 | -0.005 | -0.518 | 0.014 | MS |
| 2185-53532-541 | 0.323 | 19.867 | 0.024 | -0.196 | 0.051 | 0.068 | -0.530 | 0.019 | MS |
| 2185-53532-542 | 0.312 | 19.432 | 0.017 | -0.263 | 0.034 | -0.007 | -0.530 | 0.013 | MS |
| 2185-53532-544 | 0.243 | 18.847 | 0.011 | -0.249 | 0.022 | -0.003 | -0.526 | 0.010 | MS |
| 2185-53532-545 | 0.292 | 19.061 | 0.021 | -0.230 | 0.023 | 0.019 | -0.513 | 0.010 | MS |

Table 3—Continued

| spSpec name | $(g-r)_0$ | g | σ_g | S(3839) | $\sigma_{S(3839)}$ | $\delta S(3839)$ | CH(4300) _L | $\sigma_{CH(4300)}$ | Type |
|----------------|-----------|--------|------------|---------|--------------------|------------------|-----------------------|---------------------|------|
| (1) | (2) | (3) | (4) | (5) | (6) | (7) | (8) | (9) | (10) |
| 2185-53532-546 | 0.320 | 19.915 | 0.017 | -0.247 | 0.043 | 0.018 | -0.464 | 0.021 | MS |
| 2185-53532-547 | 0.360 | 19.909 | 0.024 | -0.259 | 0.042 | 0.006 | -0.483 | 0.015 | MS |
| 2185-53532-548 | 0.361 | 19.959 | 0.023 | -0.124 | 0.044 | 0.142 | -0.545 | 0.025 | MS |
| 2185-53532-549 | 0.382 | 19.507 | 0.018 | -0.276 | 0.034 | -0.018 | -0.460 | 0.017 | MS |
| 2185-53532-550 | 0.286 | 19.738 | 0.019 | -0.189 | 0.042 | 0.073 | -0.486 | 0.017 | MS |
| 2185-53532-551 | 0.310 | 19.909 | 0.022 | -0.143 | 0.045 | 0.122 | -0.465 | 0.020 | MS |
| 2185-53532-552 | 0.251 | 18.899 | 0.012 | -0.252 | 0.024 | -0.005 | -0.522 | 0.011 | MS |
| 2185-53532-555 | 0.303 | 19.342 | 0.019 | -0.224 | 0.029 | 0.031 | -0.515 | 0.012 | MS |
| 2185-53532-556 | 0.281 | 19.376 | 0.018 | -0.238 | 0.029 | 0.017 | -0.547 | 0.013 | MS |
| 2185-53532-557 | 0.266 | 18.690 | 0.014 | -0.291 | 0.018 | -0.048 | -0.529 | 0.009 | MS |
| 2185-53532-558 | 0.264 | 18.577 | 0.009 | -0.262 | 0.016 | -0.022 | -0.516 | 0.008 | MS |
| 2185-53532-559 | 0.254 | 18.915 | 0.011 | -0.277 | 0.024 | -0.030 | -0.518 | 0.009 | MS |
| 2185-53532-560 | 0.261 | 18.421 | 0.013 | -0.256 | 0.014 | -0.018 | -0.535 | 0.007 | MS |
| 2185-53532-575 | 0.349 | 19.769 | 0.024 | -0.209 | 0.050 | 0.053 | -0.542 | 0.018 | MS |
| 2185-53532-577 | 0.260 | 19.163 | 0.017 | -0.253 | 0.023 | -0.002 | -0.515 | 0.011 | MS |
| 2185-53532-581 | 0.296 | 19.299 | 0.018 | -0.228 | 0.030 | 0.026 | -0.515 | 0.012 | MS |
| 2185-53532-584 | 0.199 | 19.257 | 0.014 | -0.196 | 0.029 | 0.057 | -0.522 | 0.012 | MS |
| 2185-53532-585 | 0.290 | 19.137 | 0.014 | -0.245 | 0.026 | 0.006 | -0.501 | 0.012 | MS |
| 2185-53532-587 | 0.293 | 19.806 | 0.023 | -0.163 | 0.051 | 0.100 | -0.498 | 0.021 | MS |
| 2185-53532-589 | 0.241 | 18.974 | 0.012 | -0.238 | 0.022 | 0.010 | -0.529 | 0.012 | MS |
| 2185-53532-591 | 0.228 | 18.773 | 0.013 | -0.245 | 0.020 | -0.001 | -0.526 | 0.010 | MS |
| 2185-53532-592 | 0.247 | 19.454 | 0.015 | -0.284 | 0.032 | -0.028 | -0.515 | 0.016 | MS |
| 2185-53532-593 | 0.229 | 18.893 | 0.012 | -0.248 | 0.023 | -0.001 | -0.525 | 0.009 | MS |
| 2185-53532-594 | 0.293 | 19.523 | 0.023 | -0.188 | 0.033 | 0.070 | -0.517 | 0.017 | MS |
| 2185-53532-596 | 0.357 | 19.876 | 0.020 | -0.301 | 0.042 | -0.036 | -0.494 | 0.022 | MS |
| 2185-53532-598 | 0.262 | 19.415 | 0.020 | -0.201 | 0.032 | 0.055 | -0.528 | 0.016 | MS |
| 2185-53532-599 | 0.263 | 19.391 | 0.017 | -0.180 | 0.036 | 0.075 | -0.508 | 0.015 | MS |
| 2185-53532-600 | 0.303 | 19.845 | 0.019 | -0.234 | 0.051 | 0.030 | -0.471 | 0.019 | MS |
| 2255-53565-436 | 0.369 | 20.193 | 0.022 | -0.018 | 0.050 | 0.251 | -0.423 | 0.016 | MS |
| 2255-53565-518 | 0.456 | 20.561 | 0.035 | -0.159 | 0.038 | 0.117 | -0.370 | 0.014 | MS |

Table 3—Continued

| spSpec name | $(g-r)_0$ | g | σ_g | S(3839) | $\sigma_{S(3839)}$ | $\delta S(3839)$ | CH(4300) _L | $\sigma_{CH(4300)}$ | Type |
|----------------|-----------|--------|------------|---------|--------------------|------------------|-----------------------|---------------------|------|
| (1) | (2) | (3) | (4) | (5) | (6) | (7) | (8) | (9) | (10) |
| 2475-53845-145 | 0.567 | 15.116 | 0.006 | -0.096 | 0.015 | -0.032 | -0.468 | 0.006 | AGB |
| 2475-53845-150 | 0.635 | 14.933 | 0.006 | -0.156 | 0.013 | -0.115 | -0.425 | 0.005 | AGB |
| 2475-53845-162 | 0.590 | 15.176 | 0.022 | -0.113 | 0.016 | -0.042 | -0.425 | 0.007 | AGB |
| 2475-53845-173 | 0.636 | 15.115 | 0.007 | -0.125 | 0.014 | -0.061 | -0.409 | 0.005 | AGB |
| 2475-53845-199 | 0.633 | 14.936 | 0.010 | -0.024 | 0.015 | 0.017 | -0.434 | 0.006 | AGB |
| 2475-53845-463 | 0.578 | 15.139 | 0.008 | -0.150 | 0.012 | -0.083 | -0.455 | 0.006 | AGB |
| 2475-53845-471 | 0.576 | 15.103 | 0.005 | -0.071 | 0.012 | -0.009 | -0.471 | 0.005 | AGB |
| 2475-53845-479 | 0.603 | 14.984 | 0.012 | -0.138 | 0.010 | -0.091 | -0.439 | 0.005 | AGB |
| 2475-53845-486 | 0.569 | 14.507 | 0.014 | 0.168 | 0.011 | 0.155 | -0.349 | 0.004 | AGB |
| 2475-53845-506 | 0.658 | 14.816 | 0.005 | -0.082 | 0.008 | -0.056 | -0.398 | 0.004 | AGB |
| 2475-53845-511 | 0.613 | 15.134 | 0.005 | -0.136 | 0.012 | -0.069 | -0.408 | 0.005 | AGB |
| 2475-53845-118 | 0.485 | 17.492 | 0.015 | -0.229 | 0.092 | 0.134 | -0.443 | 0.030 | RGB |
| 2475-53845-183 | 0.575 | 16.382 | 0.011 | -0.244 | 0.032 | -0.021 | -0.371 | 0.013 | RGB |
| 2475-53845-185 | 0.508 | 17.131 | 0.011 | -0.101 | 0.067 | 0.217 | -0.398 | 0.023 | RGB |
| 2475-53845-192 | 0.574 | 16.891 | 0.024 | -0.162 | 0.052 | 0.126 | -0.394 | 0.021 | RGB |
| 2475-53845-200 | 0.508 | 17.238 | 0.009 | 0.034 | 0.069 | 0.365 | -0.385 | 0.021 | RGB |
| 2475-53845-430 | 0.523 | 17.342 | 0.024 | 0.003 | 0.071 | 0.347 | -0.443 | 0.021 | RGB |
| 2475-53845-469 | 0.528 | 16.634 | 0.007 | -0.017 | 0.032 | 0.238 | -0.387 | 0.013 | RGB |
| 2475-53845-487 | 0.486 | 17.760 | 0.006 | -0.256 | 0.098 | 0.141 | -0.438 | 0.030 | RGB |
| 2475-53845-501 | 0.550 | 16.335 | 0.007 | -0.063 | 0.028 | 0.154 | -0.375 | 0.010 | RGB |
| 2475-53845-507 | 0.491 | 17.033 | 0.005 | -0.129 | 0.052 | 0.177 | -0.401 | 0.018 | RGB |
| 2475-53845-550 | 0.461 | 17.683 | 0.017 | -0.163 | 0.076 | 0.224 | -0.395 | 0.026 | RGB |
| 2475-53845-557 | 0.545 | 16.703 | 0.006 | 0.077 | 0.042 | 0.340 | -0.397 | 0.012 | RGB |
| 2475-53845-116 | 0.714 | 15.109 | 0.014 | -0.014 | 0.015 | 0.049 | -0.331 | 0.006 | RGB |
| 2475-53845-119 | 0.608 | 16.003 | 0.004 | -0.177 | 0.031 | -0.002 | -0.350 | 0.009 | RGB |
| 2475-53845-120 | 0.575 | 16.254 | 0.005 | -0.221 | 0.033 | -0.013 | -0.361 | 0.011 | RGB |
| 2475-53845-141 | 0.676 | 15.471 | 0.022 | -0.099 | 0.028 | 0.009 | -0.332 | 0.010 | RGB |
| 2475-53845-142 | 0.672 | 15.427 | 0.014 | -0.058 | 0.022 | 0.045 | -0.335 | 0.009 | RGB |
| 2475-53845-143 | 0.631 | 15.621 | 0.010 | -0.166 | 0.024 | -0.038 | -0.336 | 0.009 | RGB |
| 2475-53845-144 | 0.624 | 15.915 | 0.005 | -0.169 | 0.030 | -0.004 | -0.339 | 0.011 | RGB |
| 2475-53845-160 | 0.602 | 15.631 | 0.020 | -0.200 | 0.022 | -0.071 | -0.349 | 0.009 | RGB |

Table 3—Continued

| spSpec name | $(g-r)_0$ | g | σ_g | S(3839) | $\sigma_{S(3839)}$ | $\delta S(3839)$ | CH(4300) _L | $\sigma_{CH(4300)}$ | Type |
|----------------|-----------|--------|------------|---------|--------------------|------------------|-----------------------|---------------------|------|
| (1) | (2) | (3) | (4) | (5) | (6) | (7) | (8) | (9) | (10) |
| 2475-53845-171 | 0.684 | 15.421 | 0.005 | -0.076 | 0.028 | 0.027 | -0.331 | 0.010 | RGB |
| 2475-53845-176 | 0.740 | 14.720 | 0.013 | -0.089 | 0.013 | -0.075 | -0.353 | 0.006 | RGB |
| 2475-53845-177 | 0.596 | 15.806 | 0.005 | 0.129 | 0.027 | 0.280 | -0.338 | 0.009 | RGB |
| 2475-53845-178 | 0.624 | 15.715 | 0.013 | -0.191 | 0.025 | -0.052 | -0.347 | 0.009 | RGB |
| 2475-53845-186 | 0.688 | 15.265 | 0.006 | -0.108 | 0.021 | -0.025 | -0.331 | 0.008 | RGB |
| 2475-53845-196 | 0.645 | 15.513 | 0.011 | -0.125 | 0.019 | -0.011 | -0.342 | 0.007 | RGB |
| 2475-53845-198 | 0.711 | 15.040 | 0.016 | 0.270 | 0.016 | 0.324 | -0.389 | 0.006 | RGB |
| 2475-53845-421 | 0.755 | 14.656 | 0.014 | 0.007 | 0.012 | 0.013 | -0.348 | 0.005 | RGB |
| 2475-53845-436 | 0.724 | 14.956 | 0.011 | 0.314 | 0.018 | 0.357 | -0.346 | 0.007 | RGB |
| 2475-53845-440 | 0.686 | 15.039 | 0.010 | 0.245 | 0.018 | 0.299 | -0.380 | 0.006 | RGB |
| 2475-53845-461 | 0.641 | 15.477 | 0.009 | -0.147 | 0.018 | -0.037 | -0.373 | 0.007 | RGB |
| 2475-53845-466 | 0.650 | 15.360 | 0.012 | -0.127 | 0.018 | -0.033 | -0.379 | 0.006 | RGB |
| 2475-53845-473 | 0.681 | 14.981 | 0.005 | 0.202 | 0.013 | 0.249 | -0.373 | 0.005 | RGB |
| 2475-53845-475 | 0.636 | 15.547 | 0.004 | -0.085 | 0.016 | 0.033 | -0.374 | 0.006 | RGB |
| 2475-53845-480 | 0.638 | 15.350 | 0.007 | 0.204 | 0.020 | 0.297 | -0.393 | 0.006 | RGB |
| 2475-53845-483 | 0.753 | 14.470 | 0.010 | 0.300 | 0.013 | 0.282 | -0.389 | 0.005 | RGB |
| 2475-53845-488 | 0.602 | 15.680 | 0.005 | -0.138 | 0.020 | -0.003 | -0.360 | 0.009 | RGB |
| 2475-53845-489 | 0.685 | 15.342 | 0.011 | 0.274 | 0.018 | 0.366 | -0.368 | 0.006 | RGB |
| 2475-53845-496 | 0.677 | 15.134 | 0.005 | -0.075 | 0.015 | -0.009 | -0.362 | 0.005 | RGB |
| 2475-53845-497 | 0.677 | 15.078 | 0.013 | -0.043 | 0.014 | 0.016 | -0.345 | 0.006 | RGB |
| 2475-53845-498 | 0.667 | 15.368 | 0.005 | 0.178 | 0.018 | 0.273 | -0.377 | 0.006 | RGB |
| 2475-53845-509 | 0.640 | 15.615 | 0.006 | -0.119 | 0.015 | 0.008 | -0.345 | 0.007 | RGB |
| 2475-53845-514 | 0.570 | 16.109 | 0.005 | 0.017 | 0.025 | 0.206 | -0.350 | 0.009 | RGB |
| 2475-53845-515 | 0.649 | 15.384 | 0.005 | 0.216 | 0.020 | 0.313 | -0.394 | 0.006 | RGB |
| 2475-53845-518 | 0.728 | 15.058 | 0.004 | 0.020 | 0.015 | 0.076 | -0.334 | 0.005 | RGB |
| 2475-53845-519 | 0.604 | 15.947 | 0.007 | -0.186 | 0.019 | -0.017 | -0.354 | 0.009 | RGB |
| 2475-53845-520 | 0.599 | 16.177 | 0.008 | -0.184 | 0.024 | 0.014 | -0.344 | 0.009 | RGB |
| 2475-53845-551 | 0.686 | 15.296 | 0.007 | -0.082 | 0.016 | 0.005 | -0.351 | 0.006 | RGB |
| 2475-53845-558 | 0.602 | 16.075 | 0.004 | -0.155 | 0.024 | 0.030 | -0.368 | 0.008 | RGB |
| 2475-53845-559 | 0.627 | 15.713 | 0.006 | -0.128 | 0.018 | 0.011 | -0.353 | 0.007 | RGB |

Table 3—Continued

| spSpec name | $(g-r)_0$ | g | σ_g | S(3839) | $\sigma_{S(3839)}$ | $\delta S(3839)$ | CH(4300) _L | $\sigma_{CH(4300)}$ | Type |
|----------------|-----------|--------|------------|---------|--------------------|------------------|-----------------------|---------------------|------|
| (1) | (2) | (3) | (4) | (5) | (6) | (7) | (8) | (9) | (10) |
| 2338-53683-186 | 0.628 | 15.236 | 0.005 | −0.206 | 0.024 | −0.018 | −0.307 | 0.010 | RGB |
| 2338-53683-199 | 0.628 | 15.533 | 0.005 | −0.062 | 0.040 | 0.191 | −0.312 | 0.012 | RGB |
| 2333-53682-191 | 0.770 | 14.282 | 0.007 | −0.046 | 0.030 | −0.067 | −0.302 | 0.007 | RGB |
| 2333-53682-193 | 0.614 | 14.170 | 0.006 | 0.198 | 0.020 | 0.152 | −0.380 | 0.006 | RGB |
| 2333-53682-198 | 0.644 | 14.494 | 0.006 | 0.376 | 0.035 | 0.401 | −0.334 | 0.009 | RGB |
| 2333-53682-228 | 0.658 | 14.357 | 0.007 | 0.200 | 0.025 | 0.196 | −0.354 | 0.007 | RGB |
| 2333-53682-229 | 0.657 | 14.488 | 0.004 | 0.160 | 0.023 | 0.184 | −0.338 | 0.007 | RGB |
| 2338-53683-200 | 0.649 | 14.561 | 0.013 | −0.003 | 0.019 | 0.037 | −0.319 | 0.006 | RGB |

Note. — Line index values derived from adopted cluster member stars. Column 1 lists the spSpec name, which identifies the star on the spectral plate in the form of spectroscopic plug-plate number (four digits), Modified Julian Date (five digits), and fiber used (three digits), while Columns 2, 3, and 4 list the $(g-r)_0$ and g_0 photometry. Column 5 lists the raw S(3839) CN index, which for AGB, RGB, and SGB stars was calculated using the definition from Norris et al. (1981) and for MS stars was calculated using the definition from Harbeck et al. (2003a), and column 6 lists the corresponding uncertainties. Column 7 gives the temperature-corrected CN index, and columns 8 and 9 list the CH indices and corresponding uncertainties. Column 10 indicates the luminosity class.

(This table is available in its entirety in machine-readable and Virtual Observatory (VO) forms in the online journal. A portion is shown here for guidance regarding its form and content.)

Table 4. Individual Cluster RGB CN Number Ratios

| Cluster | N_s | N_w | r |
|----------|--------|---------|-------------|
| M92 | 0 (12) | 24 (12) | 0.00 (1.00) |
| M15 | 0 (23) | 32 (9) | 0.00 (2.56) |
| NGC 5053 | 0 (9) | 13 (4) | 0.00 (2.25) |
| M53 | 5 | 8 | 0.62 |
| M2 | 21 | 6 | 3.50 |
| M13 | 90 | 21 | 4.29 |
| M3 | 22 | 28 | 0.79 |
| M71 | 5 | 3 | 1.67 |

Note. — Number of CN-strong (N_s) and CN-weak (N_w) stars, and CN number ratios, for RGB stars from individual GCs in our sample. Values in parentheses for M92 and M15 represent the groupings based on the proposed divisions described in the text.

Table 5. Literature CN Number Ratios

| Sample | N | $\langle M_V \rangle$ | $\langle r \rangle$ |
|-----------------------|----|-----------------------|---------------------|
| Kayser et al. (2008) | 8 | –6.19 | 0.61 |
| Pancino et al. (2010) | 12 | –7.84 | 0.82 |
| This study | 8 | –8.12 | 1.36 |
| Smith & Mateo (1990) | 16 | –8.21 | 1.72 |

Note. — Mean CN number ratios from four samples of GCs as a function of absolute integrated magnitude. N indicates the number of clusters included in each sample.

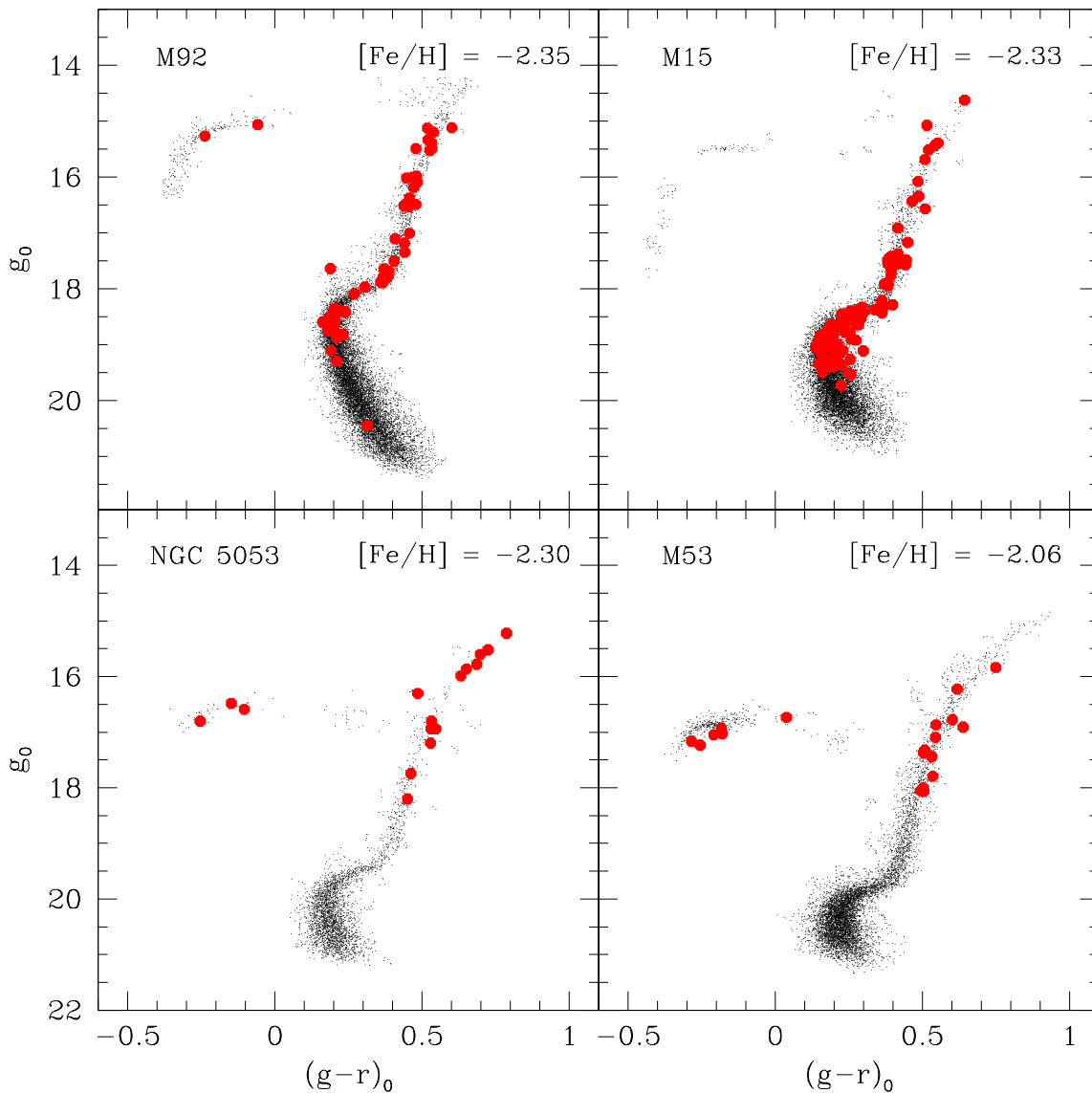


Fig. 1.— Color-magnitude diagrams for the four globular clusters in our sample with $[Fe/H] < -2.0$: M92, M15, NGC 5053, and M53. The black points represent photometric data for likely cluster members that passed the tidal radius and CMD mask algorithm cuts. The red points correspond to spectroscopic data for our selected true cluster members.

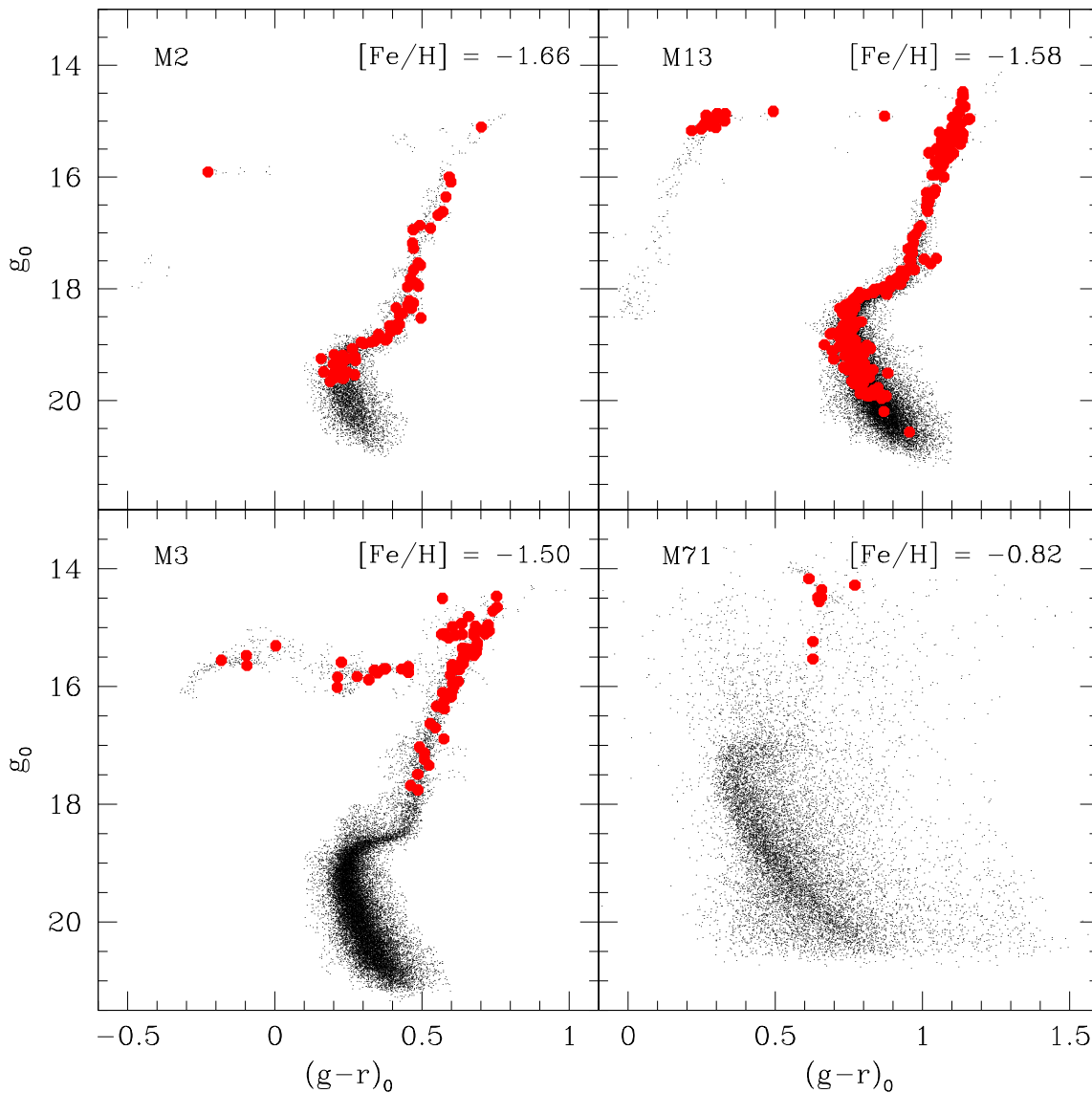


Fig. 2.— Same as Figure 1, but for the four globular clusters in our sample with $[Fe/H] > -2.0$: M2, M13, M3, and M71. Membership selection for M71 was slightly different, as described in Section 2, thus more photometric data is present in the CMD for this cluster. The black points for this cluster do not all represent likely cluster members.

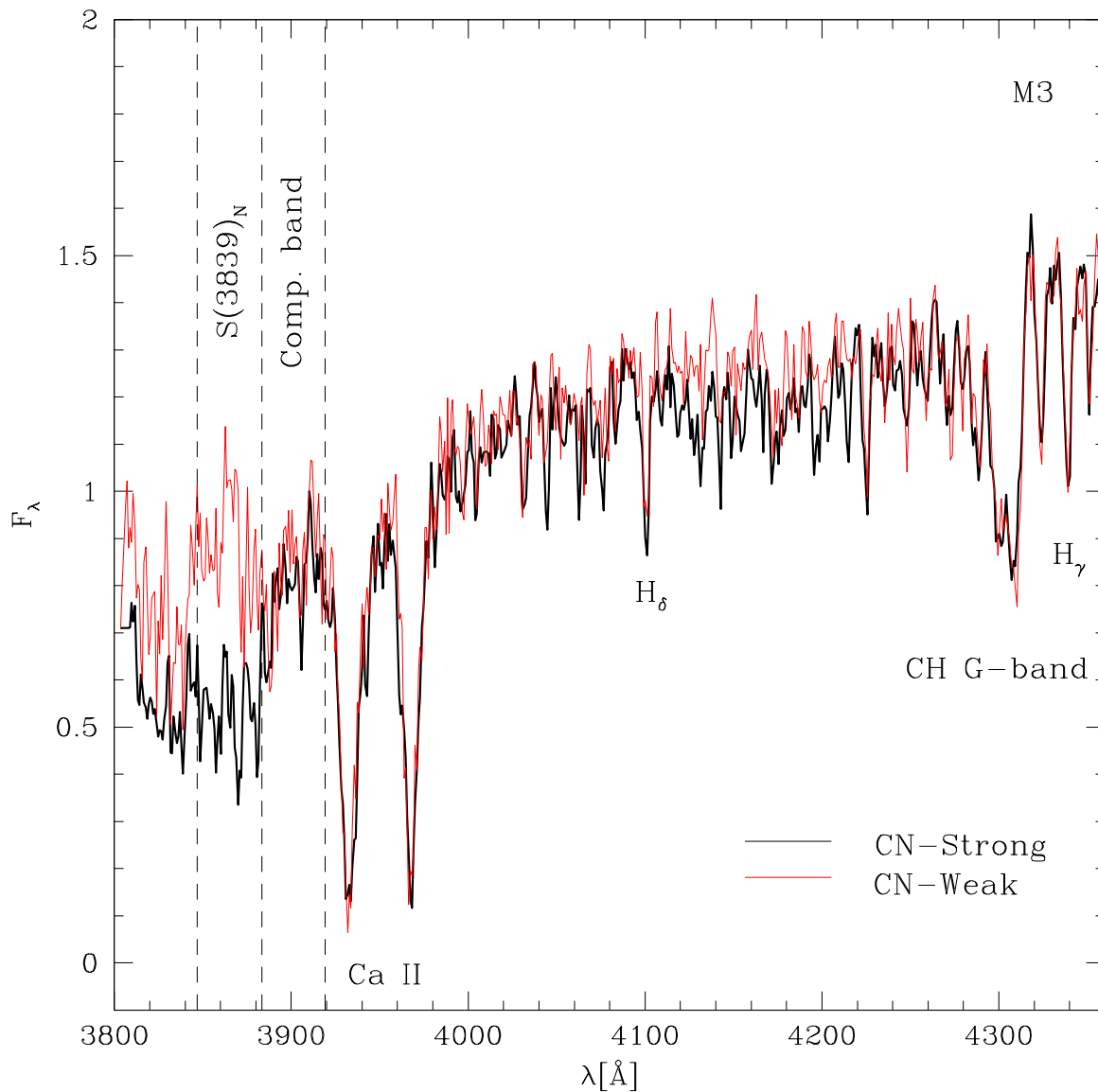


Fig. 3.— Representative blue SDSS spectra of CN-weak (red thin line; fiber 2475-53845-160) and CN-strong (black thick line; fiber 2475-53845-489) RGB stars in M3. The areas between the dashed vertical lines indicate the portions of the spectrum used in measuring $S(3839)_N$. Other prominent spectral features are labeled.

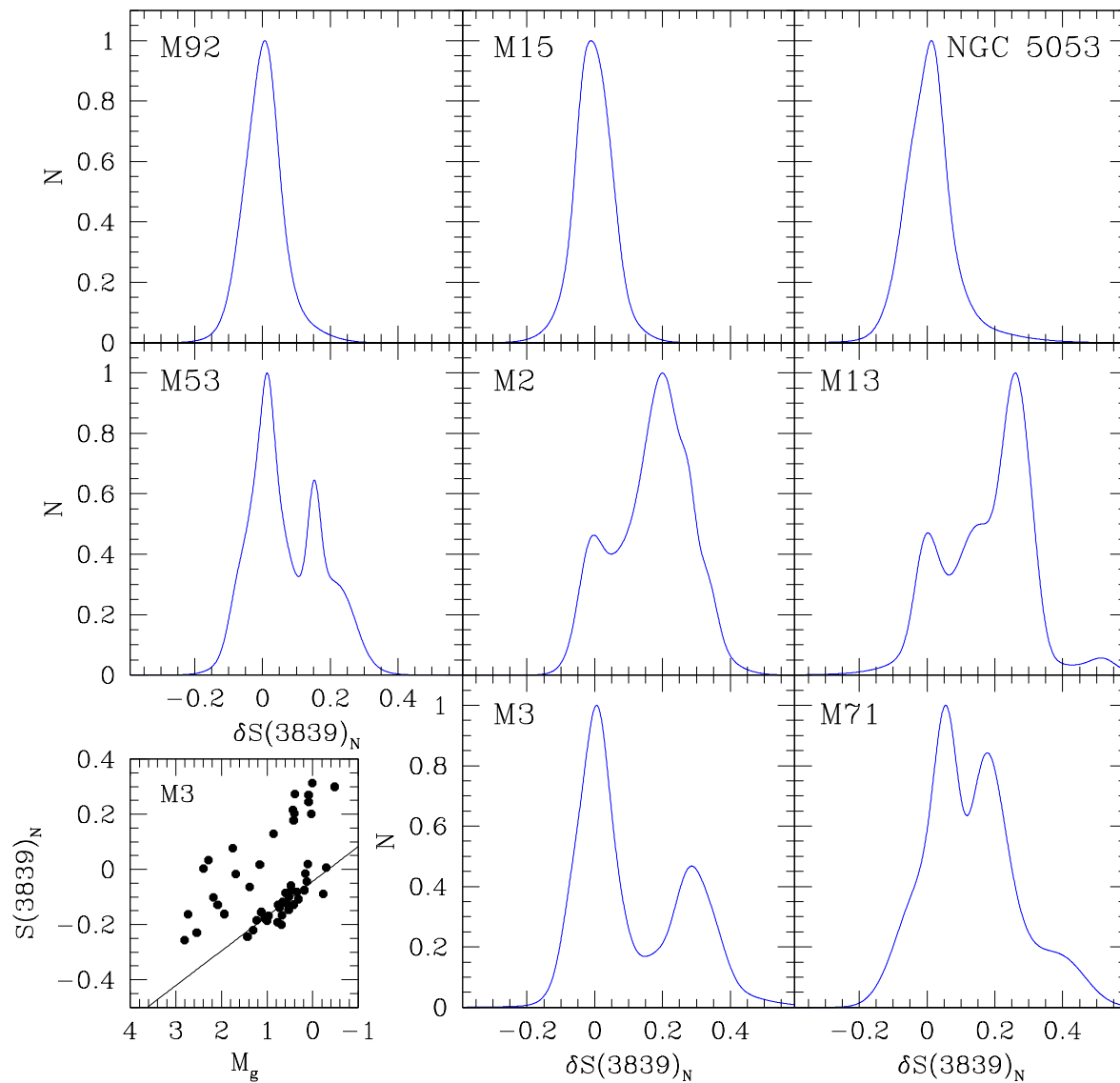


Fig. 4.— Generalized histograms for the $\delta S(3839)_N$ distributions of RGB stars within each globular cluster. The bottom-left panel shows an example of the way $\delta S(3839)_N$ was determined, as described in Section 3, where the baseline against which $\delta S(3839)_N$ was measured is shown as a solid line.

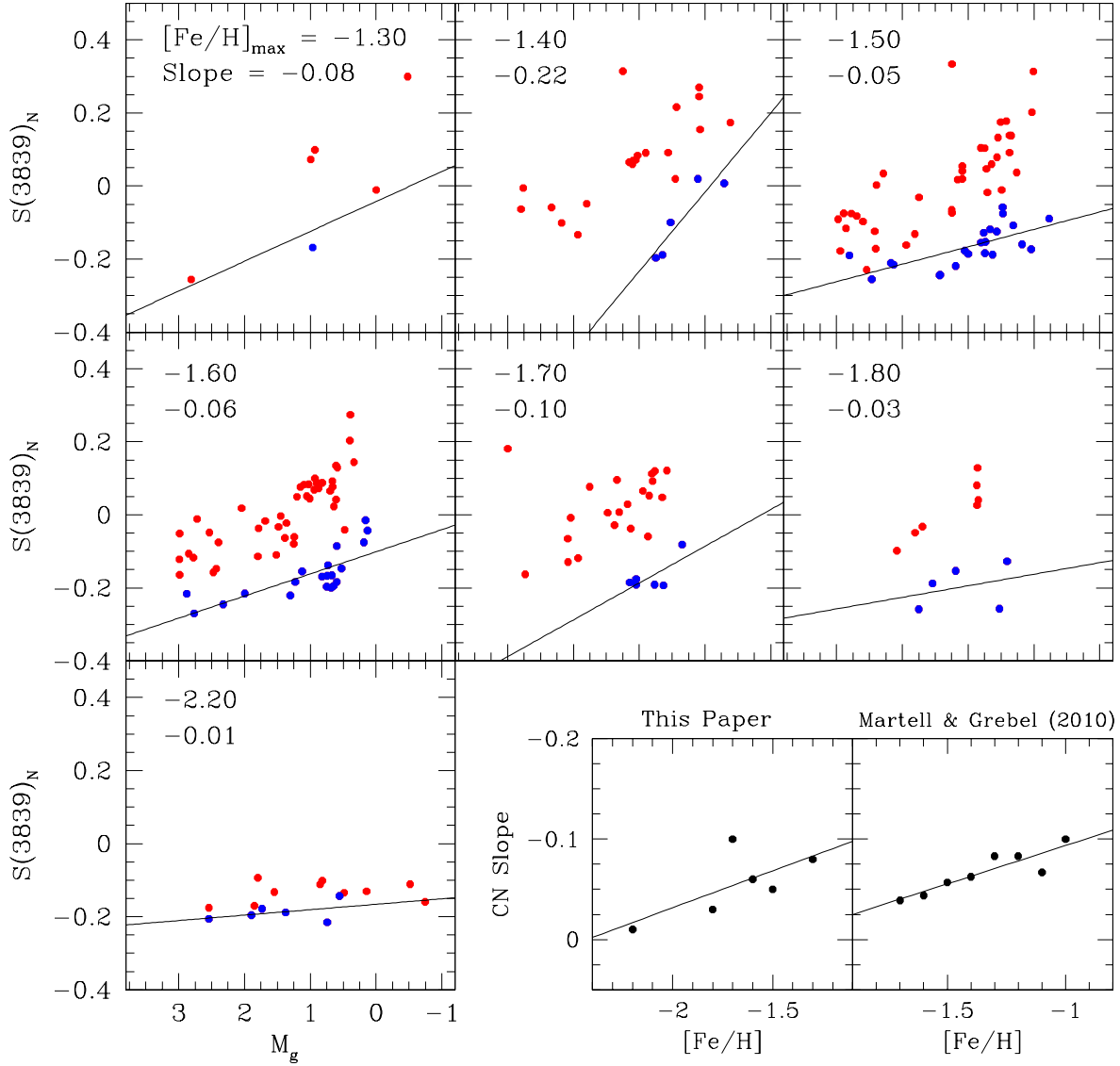


Fig. 5.— Raw $S(3839)_N$ values versus absolute g -magnitude for seven 0.1-dex-wide metallicity bins for the cluster RGB stars in our sample. The top number in the upper-left corner of each panel indicates the maximum metallicity for each bin, while the bottom number indicates the slope of the fit to the CN-strong locus. Red points indicate stars that were identified as CN-strong within their respective clusters, while blue points indicate stars identified as CN-weak.

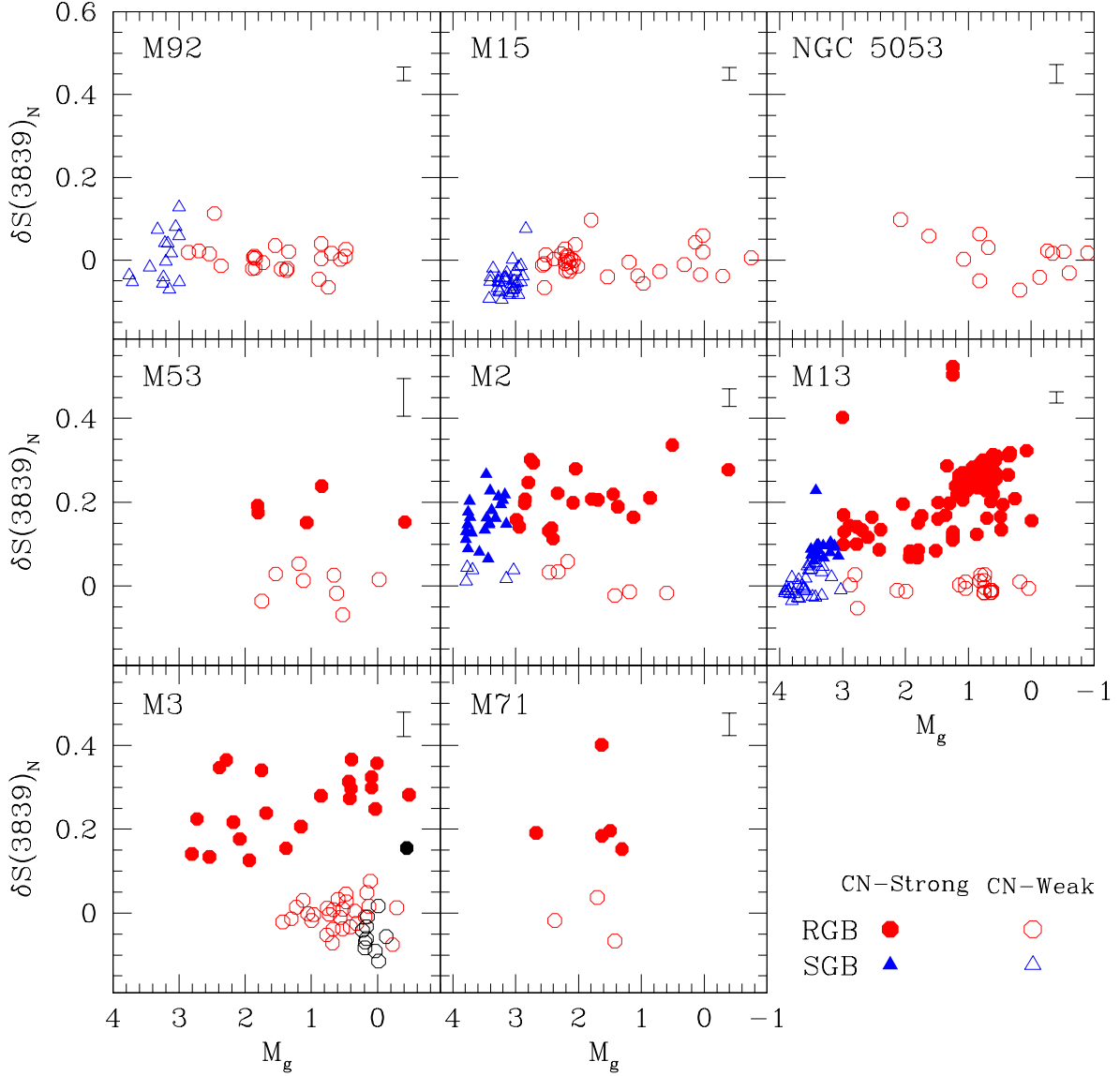


Fig. 6.— The distributions of $\delta S(3839)_N$ as a function of absolute g -magnitude for RGB and SGB stars, using the CN index definition from Norris et al. (1981). Blue triangles represent SGB stars and red circles indicate RGB stars. CN strong stars are shown using filled symbols, while the open symbols represent CN weak stars. The black points in M3 are AGB stars. Typical uncertainties are indicated by the vertical line in the upper right corner. Clusters are arranged in order of increasing $[\text{Fe}/\text{H}]$.

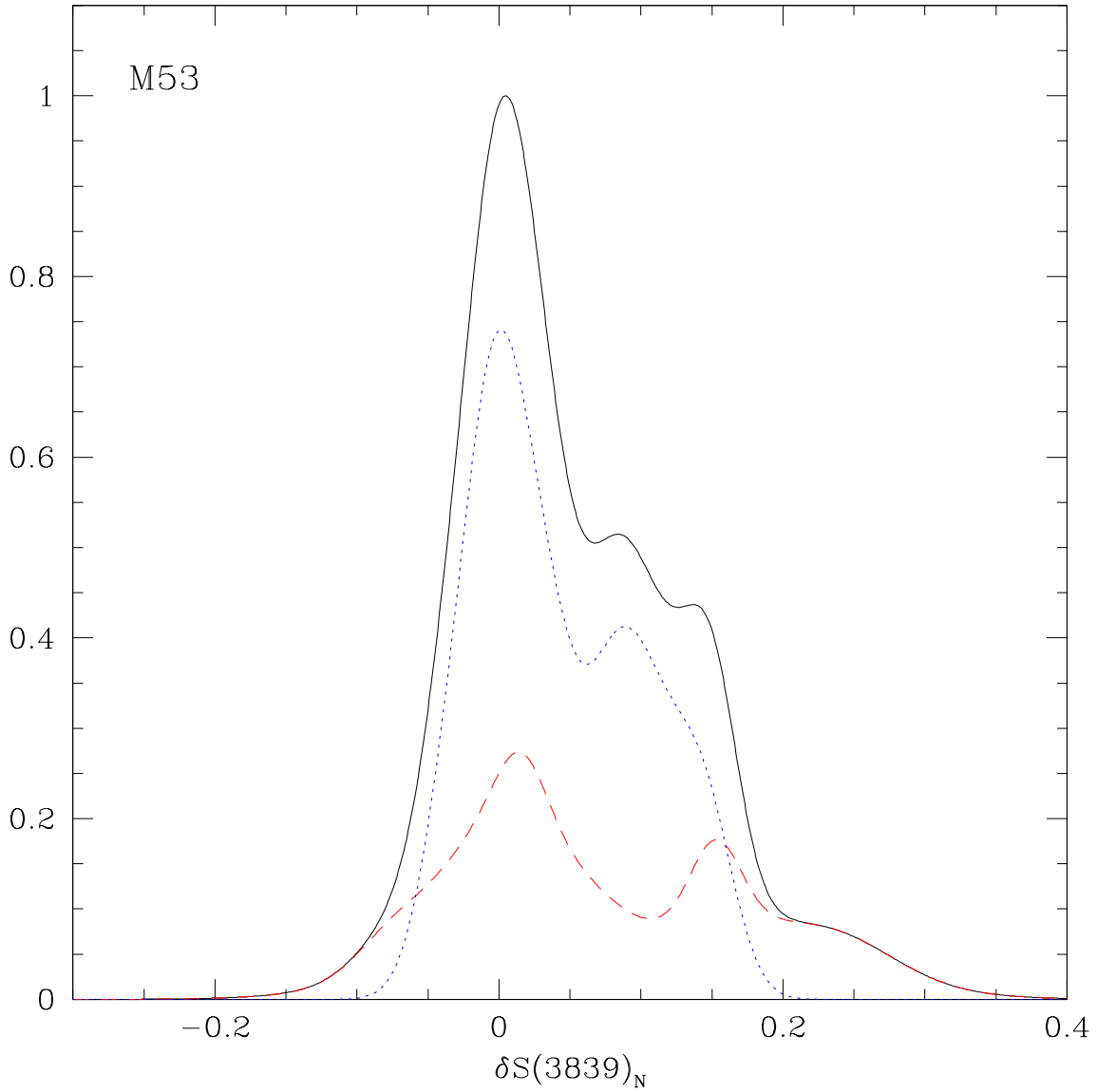


Fig. 7.— Generalized histogram for the combined (solid black line) $\delta S(3839)_N$ data sets for RGB stars in M53 from our sample (red dashed line) and that of Martell et al. (2008b) (blue dotted line). This distribution suggests that while there is a prominent CN-weak group, a group of CN-strong stars also exists in this cluster.

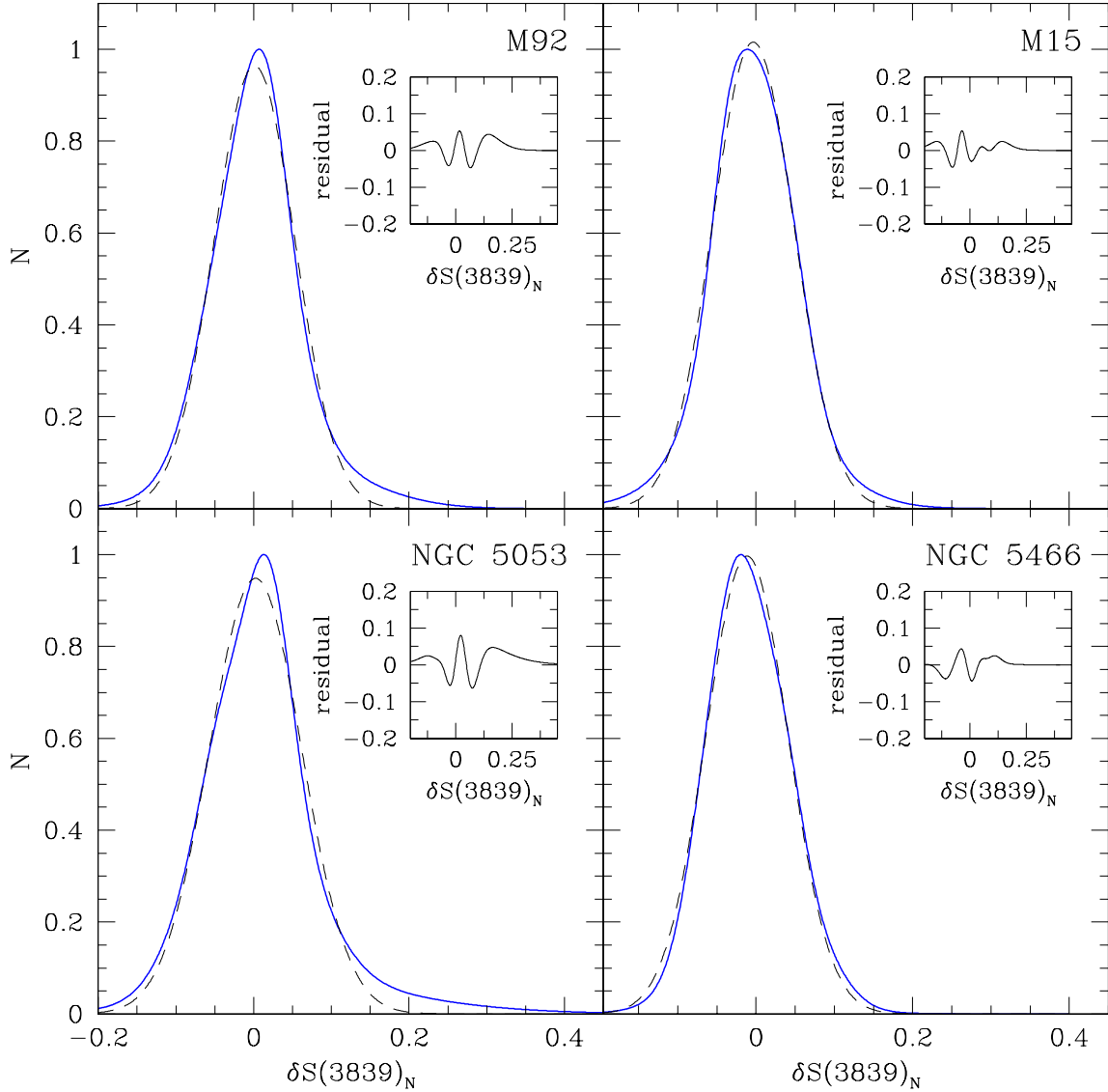


Fig. 8.— Generalized histograms for RGB stars in the very metal-poor clusters M92, M15, and NGC 5053, along with NGC 5466 ($[\text{Fe}/\text{H}] = -2.2$), taken from Shetrone et al. (2010). The blue solid line is the data, while the black dashed line represents the single Gaussian that best fit the distribution. The inset shows the residual between this best-fit curve and the data; the double-peaked nature of the residual may suggest that the data may be best represented by two overlapping Gaussian distributions.

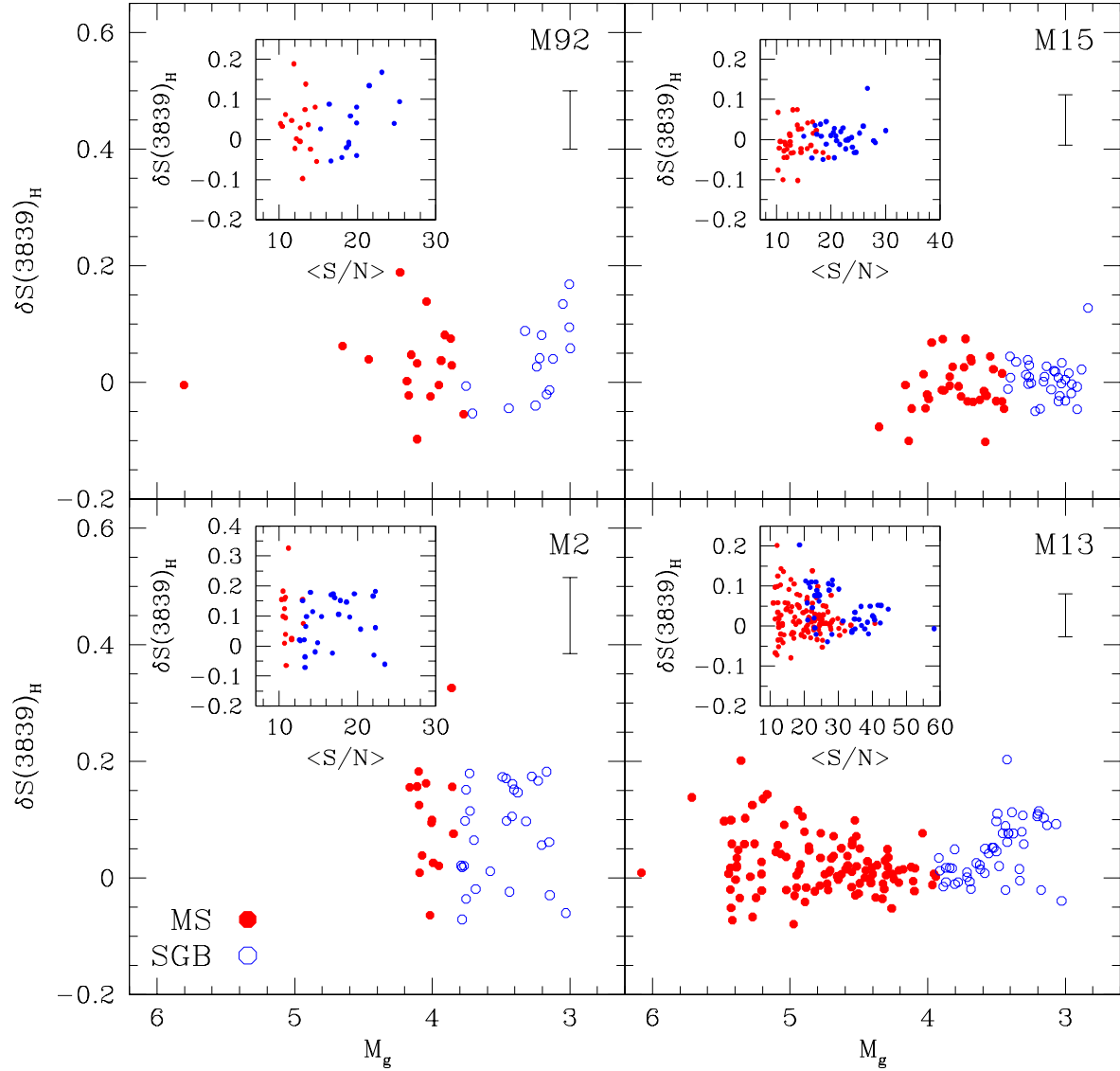


Fig. 9.— Distribution of $\delta S(3839)_H$ as a function of absolute g -magnitude for MS and SGB stars from clusters with SEGUE spectra on the MS, using the CN index definition from Harbeck et al. (2003a). Blue open circles represent SGB stars and red filled circles represent MS stars. Plotted as insets for each cluster are the distributions of $\delta S(3839)_H$ as a function of $\langle S/N \rangle$. This is done to demonstrate that the large scatter of CN absorption strength on the MS may simply be due to low S/N. Typical uncertainties are indicated by the vertical line in the upper right corner. Clusters are arranged in order of increasing $[\text{Fe}/\text{H}]$.

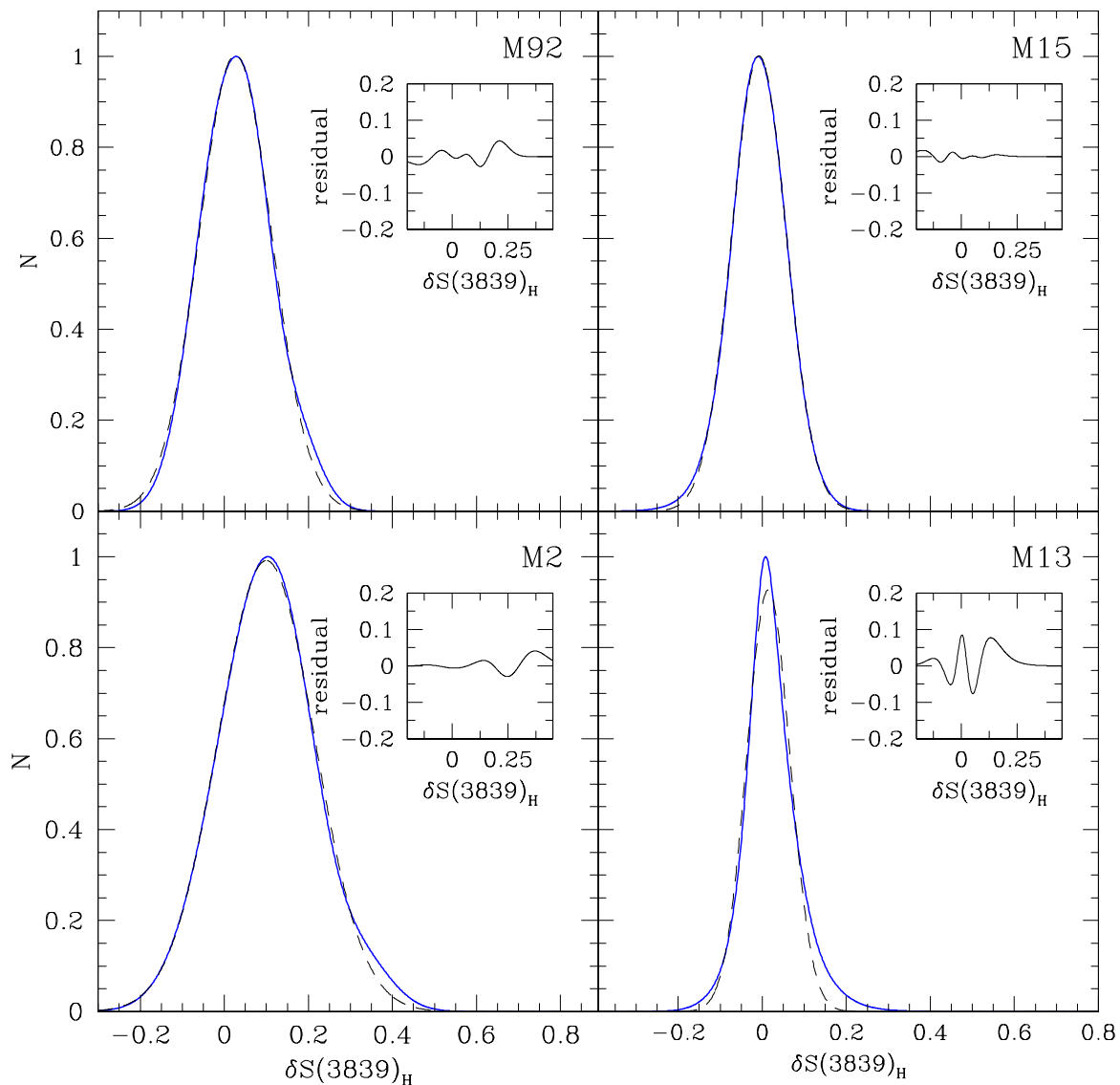


Fig. 10.— Generalized histograms for the $\delta S(3839)_H$ distributions of MS stars within each globular cluster for which SEGUE spectra exist on the MS. $\delta S(3839)_H$ on the MS is calculated in the same way as for RGB stars. No indication of bimodality is apparent.

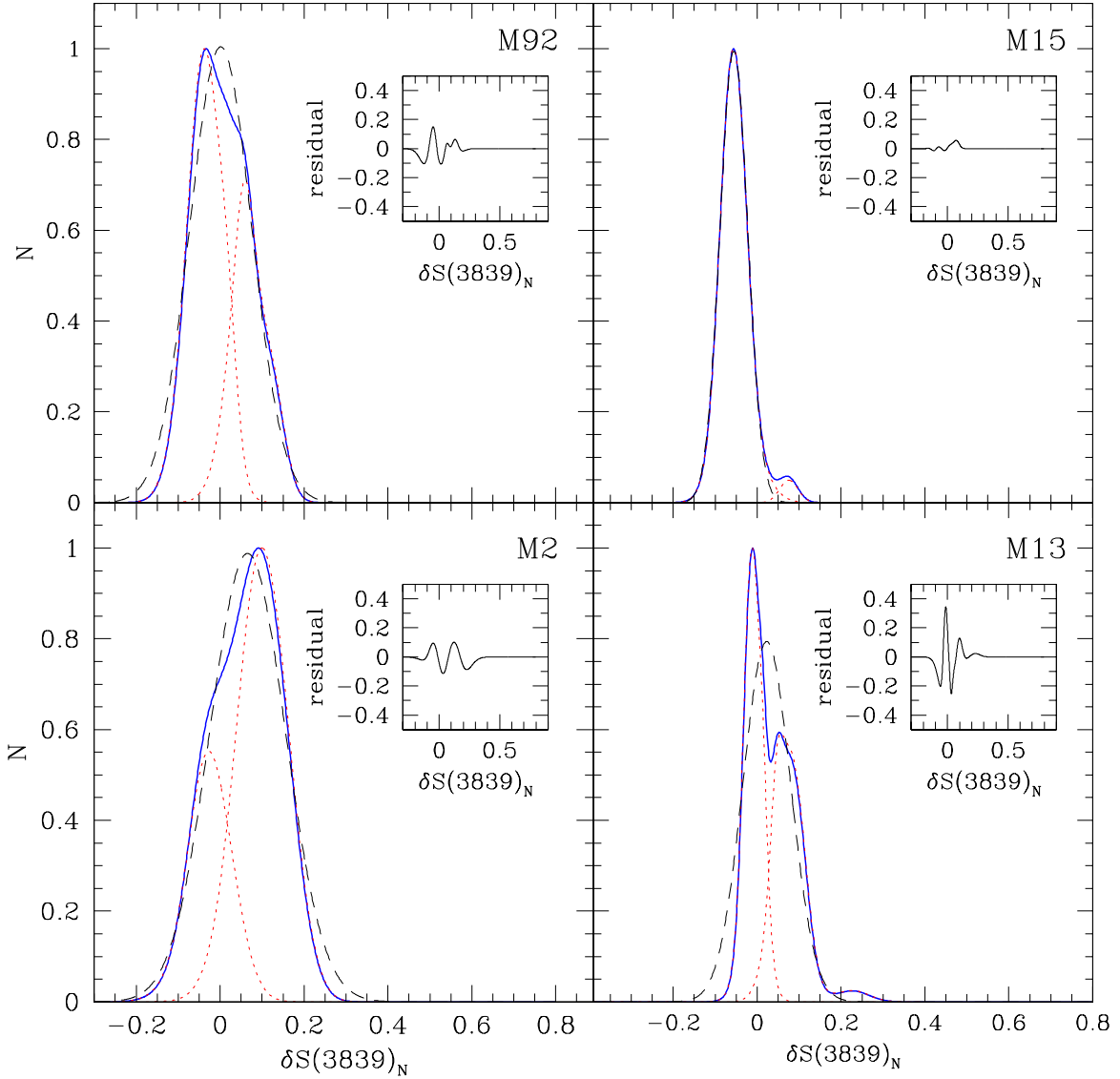


Fig. 11.— Generalized histograms for the $\delta S(3839)_N$ distributions of SGB stars within each globular cluster for which SEGUE spectra exist on the SGB. The solid blue curves are the generalized histograms for each cluster. A simple Gaussian fit to the distribution is overplotted as a dashed black line, and the red dotted curves are generalized histograms for the groups we might presume to be CN-strong and CN-weak, taken separately. The inset box shows the difference between the blue generalized histogram for the entire sample of SGB stars and the simple Gaussian fit. The small bump on the CN-strong side represents one star and cannot be confidently assigned to any presumed CN-strong group.

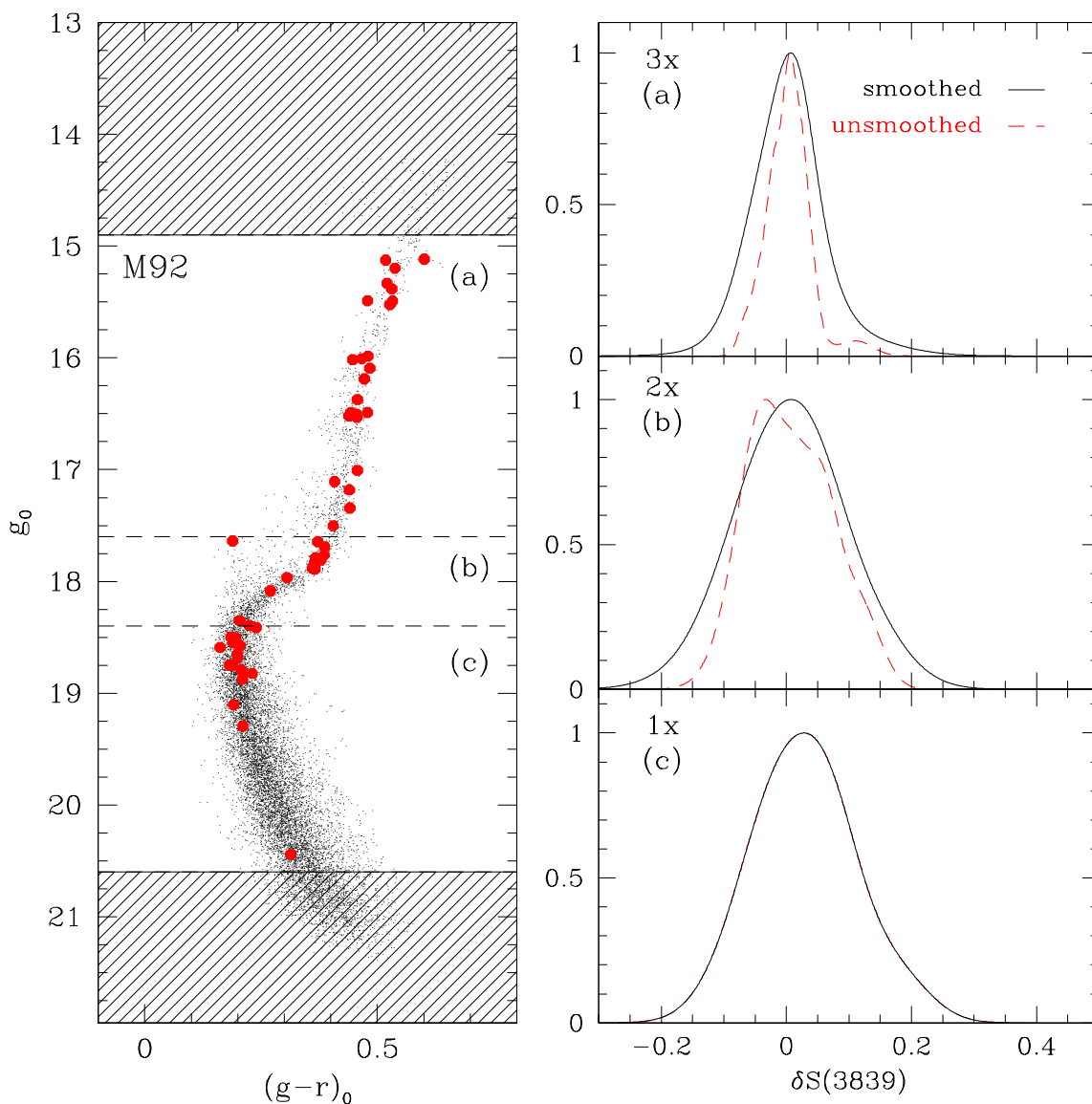


Fig. 12.— Region divisions for the color-magnitude diagram of M92 are shown in the left panel, while the right panel shows the generalized histograms of the $\delta S(3839)$ distribution within each unshaded region. The solid black lines in the histograms represent the smoothed distribution, with the smoothing factor given in the upper-left corner, while the dashed red lines represent the unsmoothed distribution. The multipliers listed in the upper left corner of the right-hand set of panels indicate the amount of smoothing employed (see text). The HB stars were not included in the analysis.

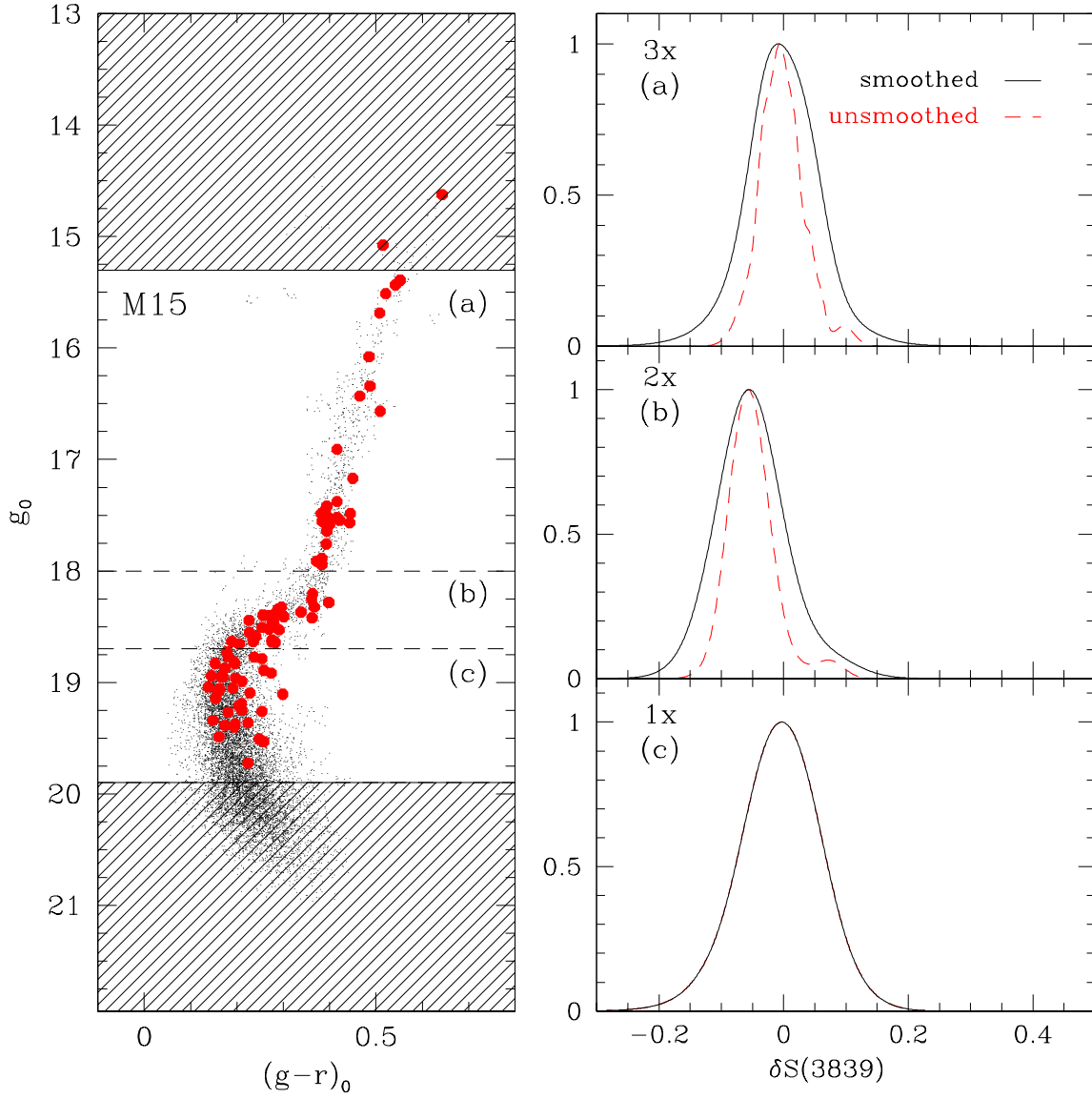


Fig. 13.— Same as Figure 12 but for M15.

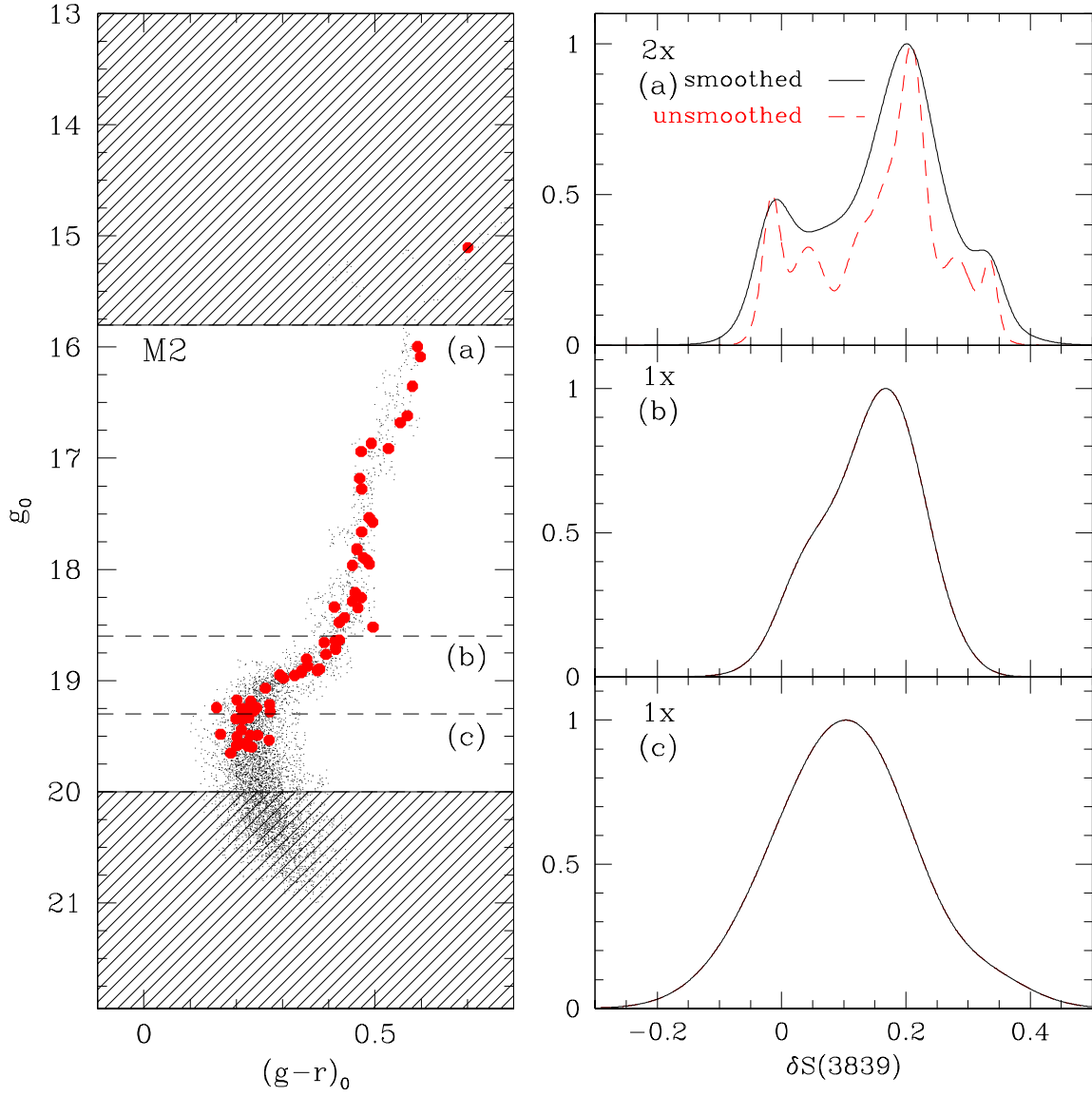


Fig. 14.— Same as Figure 12 but for M2.

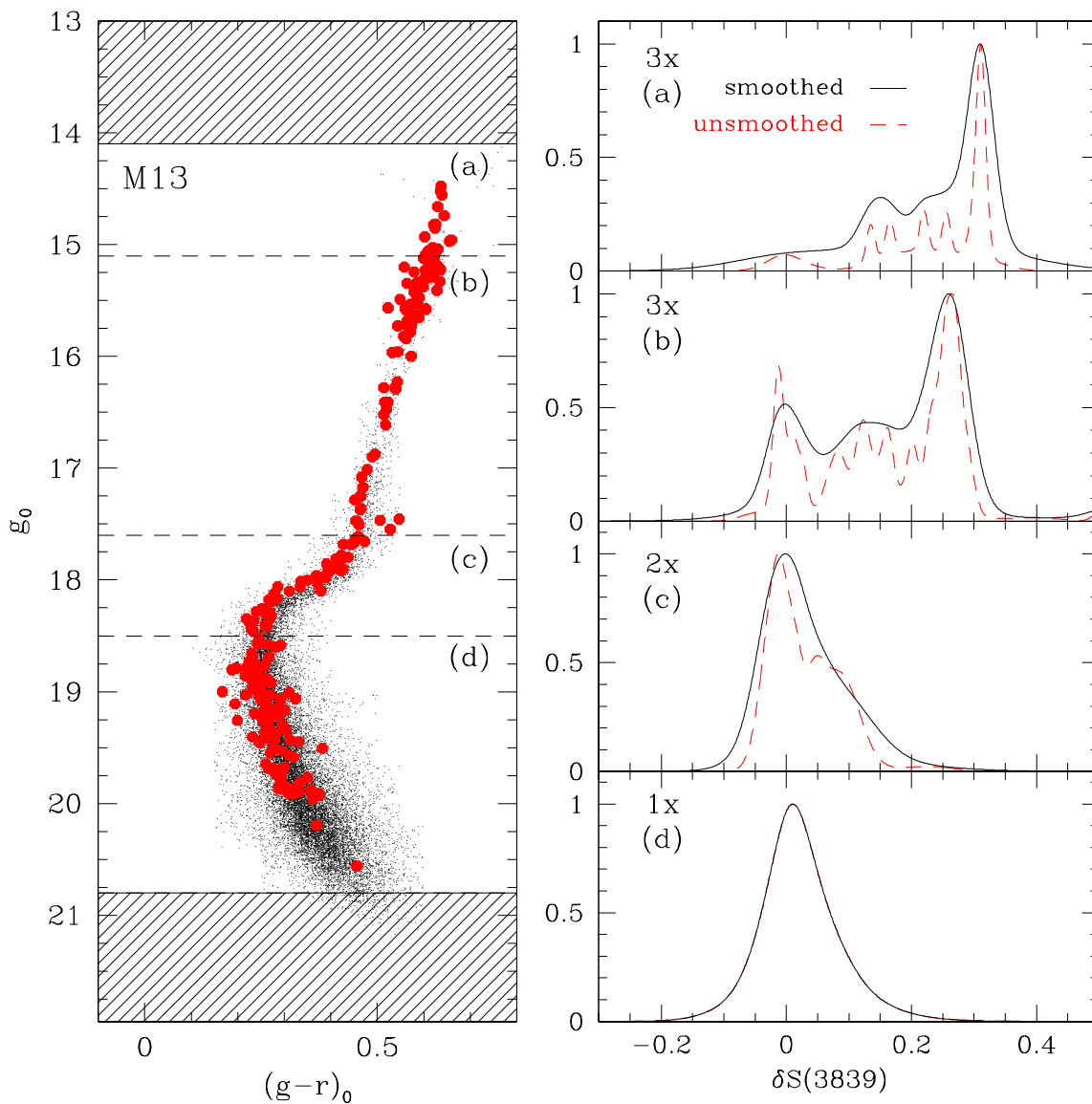


Fig. 15.— Same as Figure 12 but for M13. This cluster had data sampled above the RGB bump, shown in panel (a) of the right-hand set of panels. More than the other clusters, M13 shows a steady progression of increasing CN richness as one moves up the RGB. The small bump at $\delta S(3839) \approx 0.0$ in the top unsmoothed histogram corresponds to an AGB star, identified later as such by its $u - g$ color.

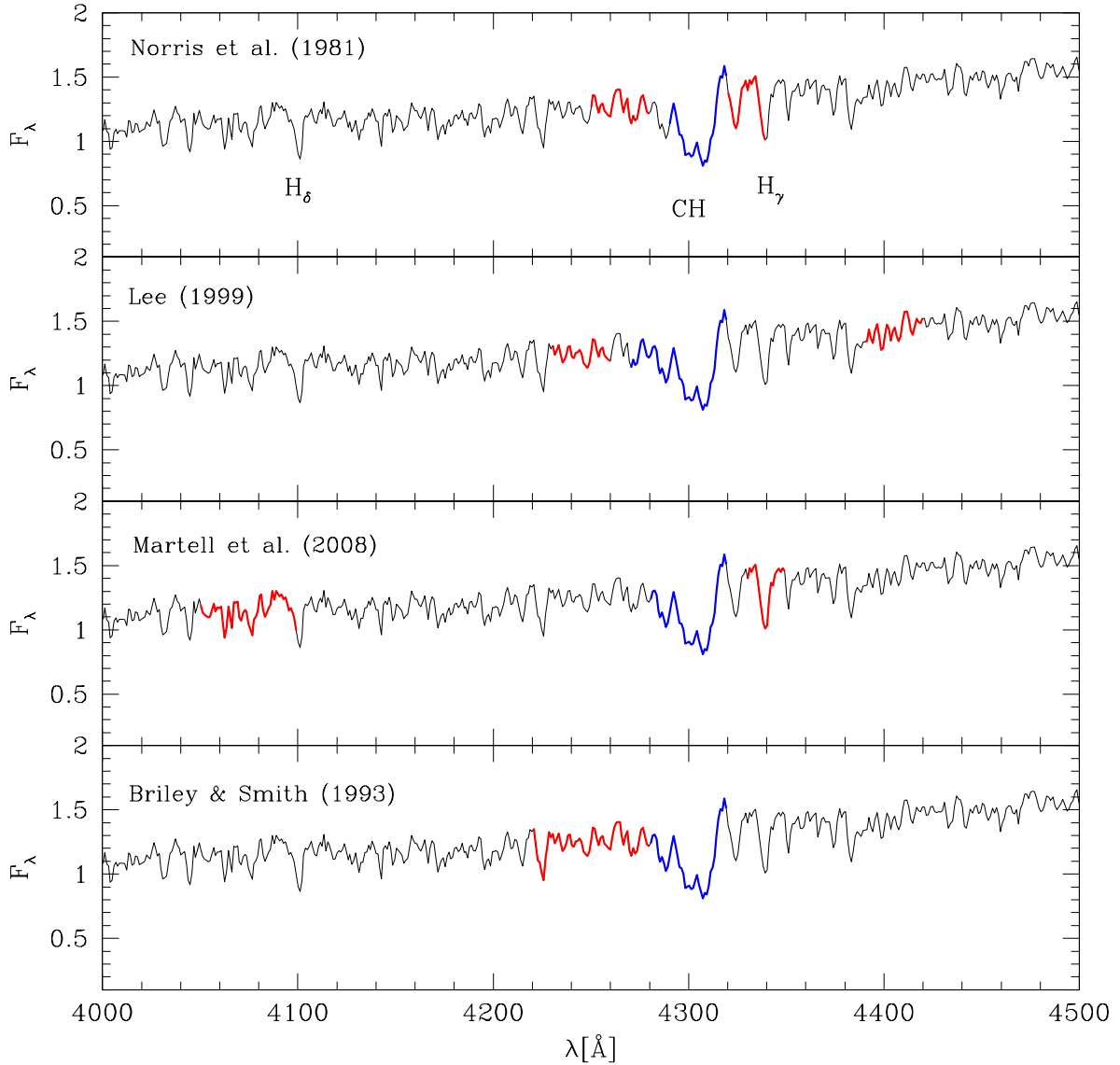


Fig. 16.— CH bandstrength measurement windows for four popular index definitions, shown for a typical M3 red giant spectrum (fiber 2475-53845-489). The blue line on each spectrum indicates the line band while the red lines indicate the continuum windows used for comparison. The CH G-band is indicated, along with two hydrogen Balmer lines for reference.

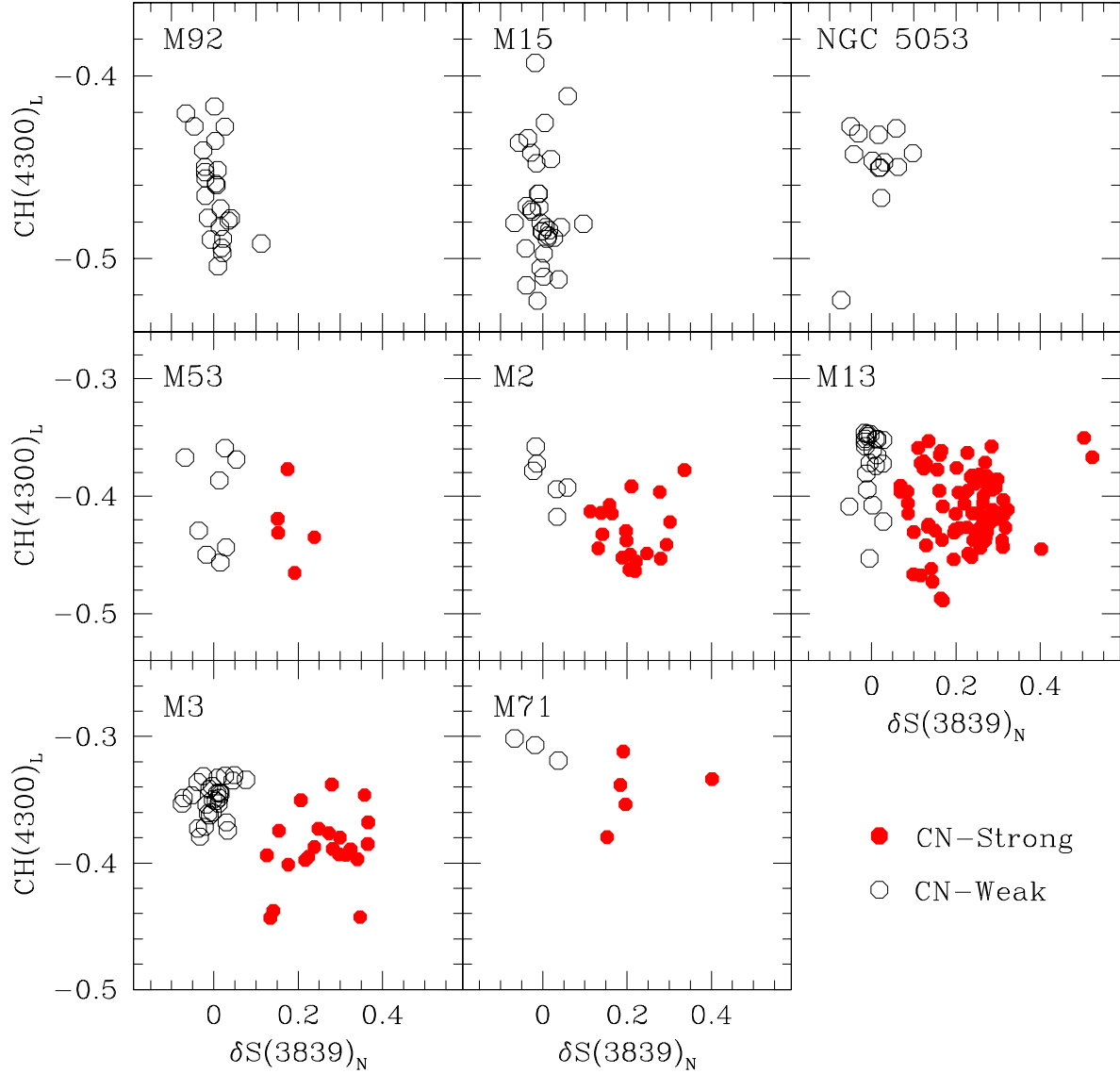


Fig. 17.— CH absorption strength versus $\delta S(3839)_N$ for RGB stars in our sample. Red filled circles are CN-strong stars and black open circles are CN-weak stars. In most clusters, a trend from CH-strong/CN-weak to CH-weak/CN-strong is seen. The subscript ‘L’ indicates the Lee (1999) definition.

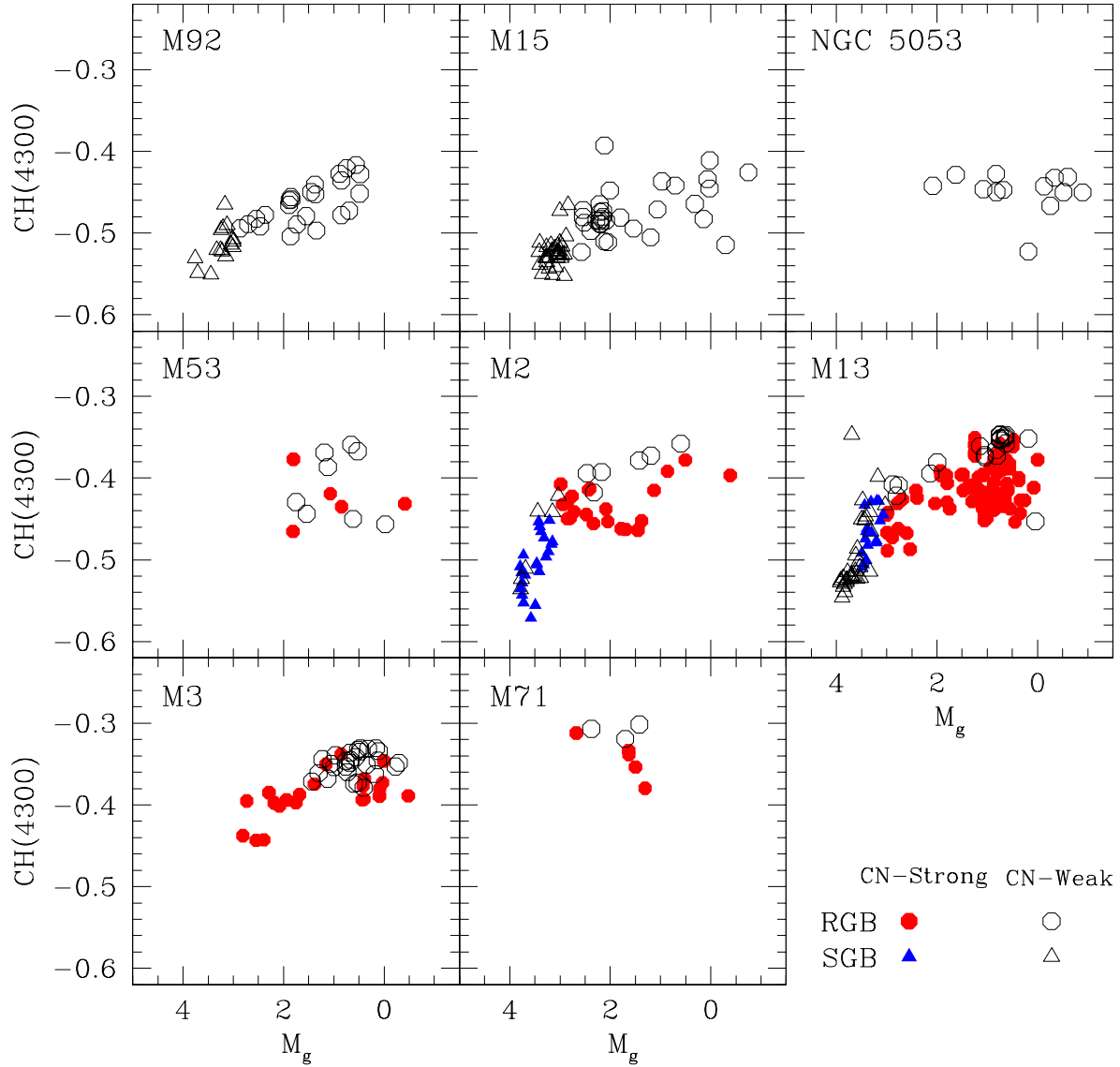


Fig. 18.— CH absorption strength as a function of luminosity, with blue triangles corresponding to SGB stars while red circles are RGB stars. Filled symbols represent CN-strong stars, while open symbols represent CN-weak stars.

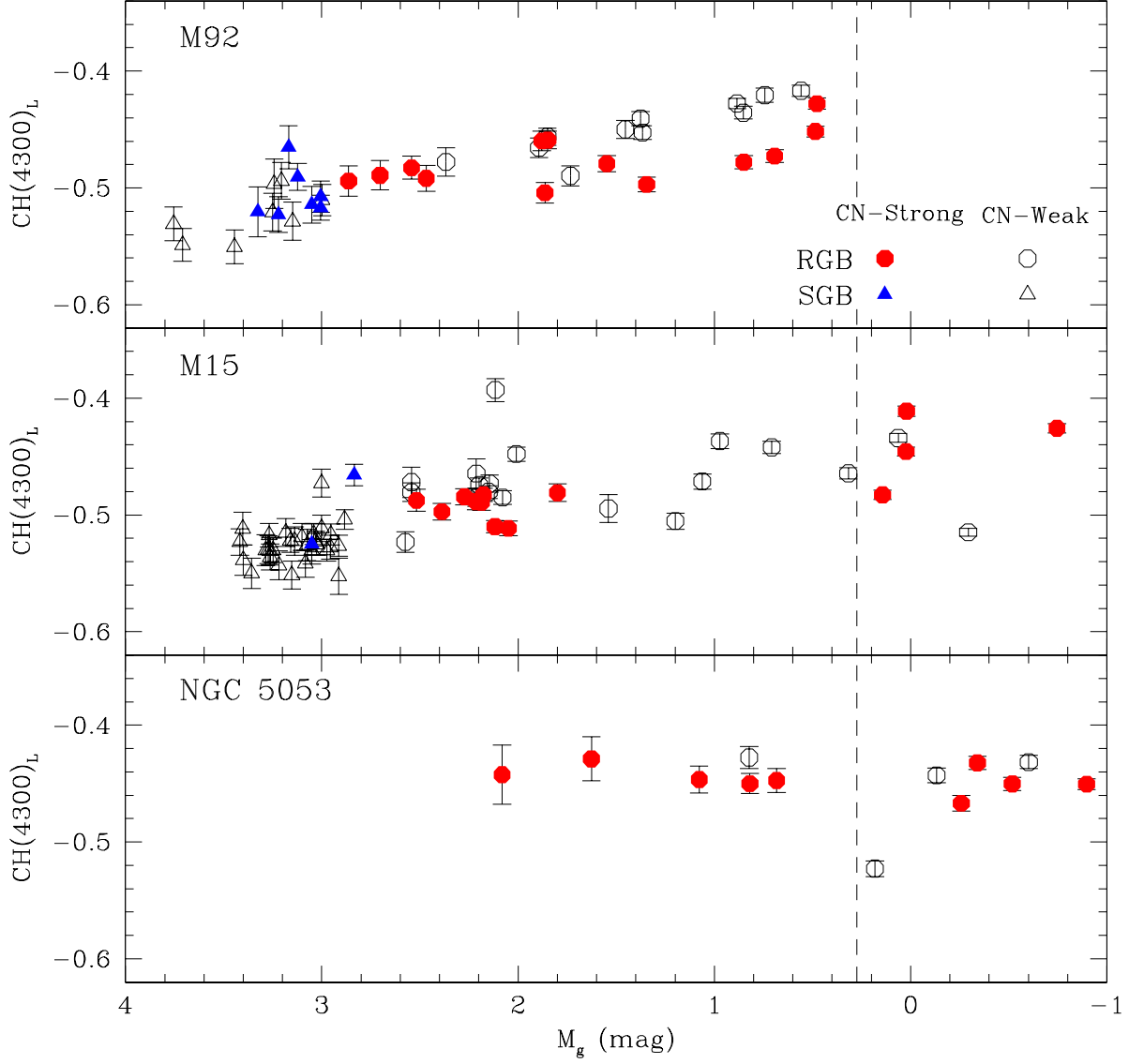


Fig. 19.— Illustration of CH scatter on the RGBs of M92 (top), M15 (middle), and NGC 5053 (bottom). We have made a proposed CN-strong/weak cut at $\delta S(3839)_N=0.0$, based on a simple linear fit to the raw RGB $S(3839)_N$ values, and have plotted the CH abundance of CN-strong (filled circles) and CN-weak (open circles) stars in each panel. The vertical dashed line is the location of the RGB bump, drawn from Fusi Pecci et al. (1990).

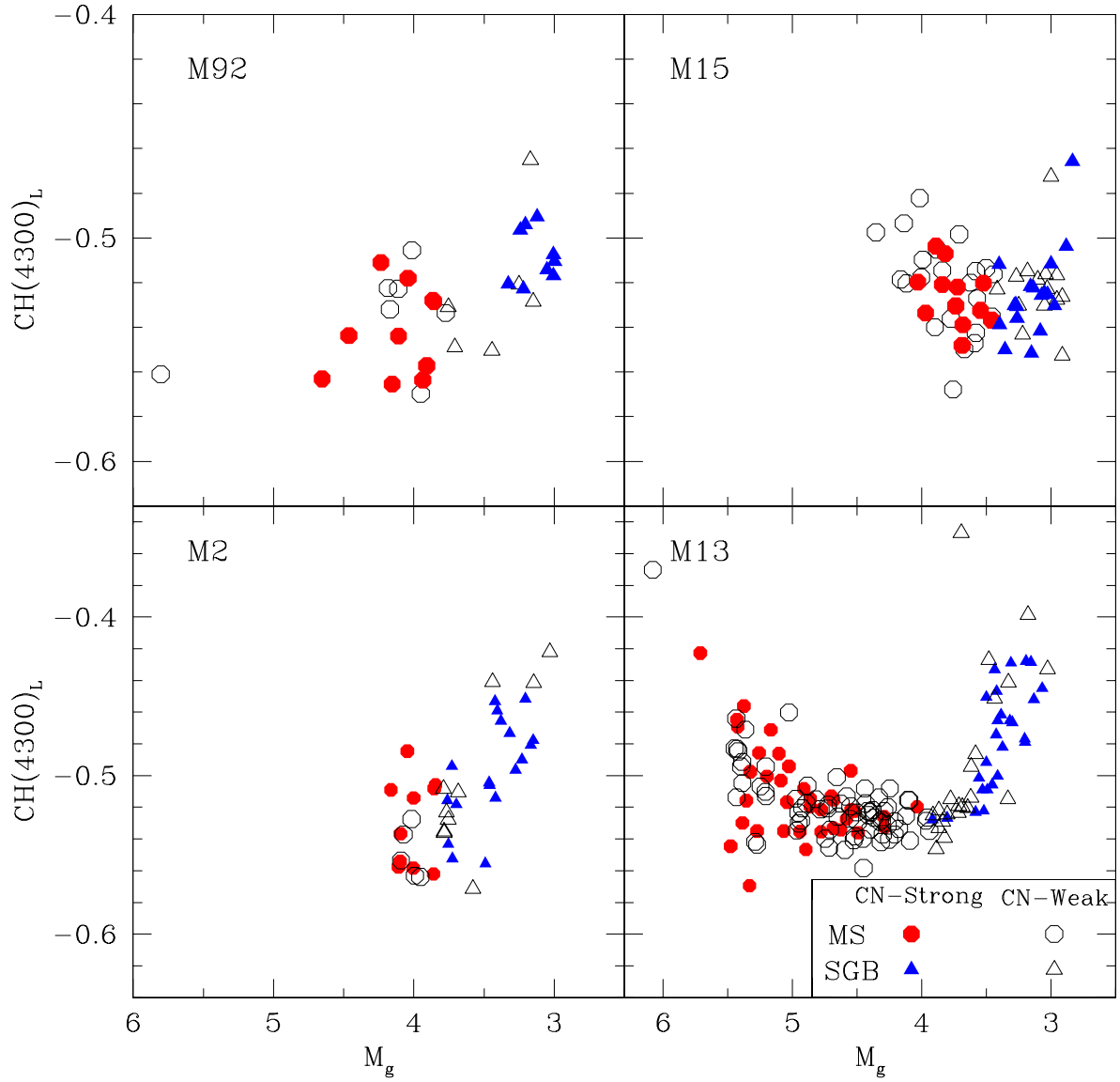


Fig. 20.— CH absorption strength versus M_g for MS and SGB stars. Approximate divisions are made to indicate those stars that are higher (filled symbols) and lower (open symbols) than the mean for CN absorption. No anticorrelation is seen.

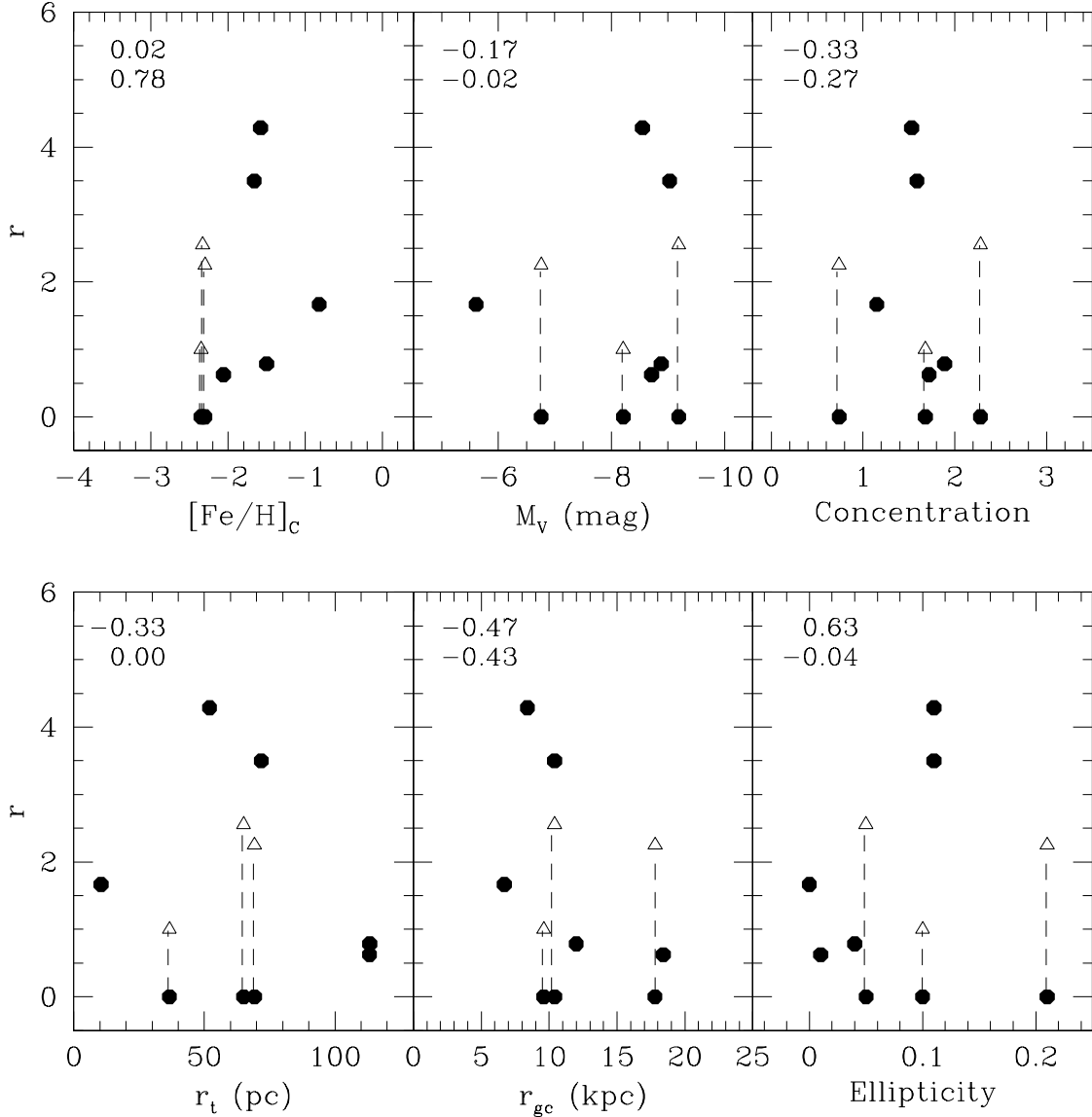


Fig. 21.— The number ratio of CN-strong to CN-weak stars (designated as r) plotted against various cluster parameters. The filled circles represent the adopted ratios for each cluster, while the open triangles representing M92 and M15 if we were to make the proposed divisions and identify relatively CN-strong and CN-weak stars in each. The Spearman rank correlation coefficients are given in the upper-left corners of each panel; the top numbers correspond to the correlation coefficient using the r values from the proposed M92 and M15 divisions (triangles), while the bottom numbers correspond to the distribution using $r = 0$ for M92 and M15.

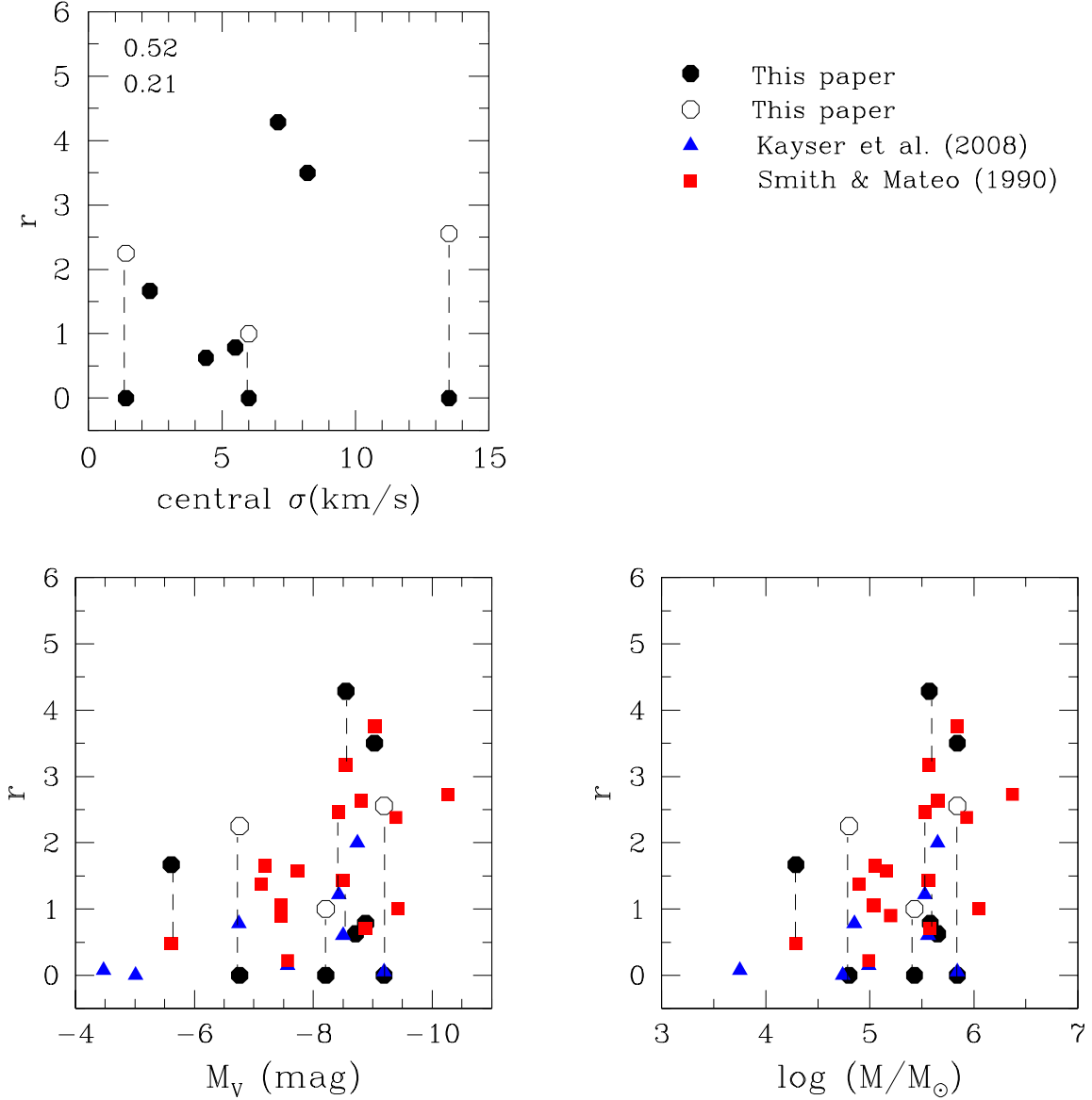


Fig. 22.— The number ratio of CN-strong to CN-weak stars plotted against central velocity dispersion, absolute V magnitude, and total cluster mass, combined with data from Kayser et al. (2008) (blue triangles) and Smith & Mateo (1990) (red squares). The Spearman rank correlation coefficients for the r - σ relation are given in the upper-left corners and correspond the same way as in Figure 21. A correlation is seen when using the CN division in M92 and M15. Absolute magnitudes are drawn from the 2010 revision of the Harris (1996) catalog, while masses are drawn from Mandushev et al. (1991) and McLaughlin & van der Marel (2005). Data points that correspond to the same clusters are connected with a dashed line